Diss. Joh. Gutenberg-Univ. Mainz	135 S.	51 Abb., 8 Taf., 7 Anl.	Mainz, Januar 2006

Climate signatures in corals of the tropical-temperate transition zone (Late Miocene, Crete/Greece)

Klimasignaturen in Korallen der tropisch-temperaten Übergangszone (Ober-Miozän, Kreta/Griechenland)

Dissertation
zur Erlangung des Grades
Doktor der Naturwissenschaften
Dr. rer. nat.

am Fachbereich Chemie, Pharmazie und Geowissenschaften
der Johannes Gutenberg-Universität in Mainz

Markus Reuter
geb. am 22.06.1972 in Neustadt am Rbge.

Mainz 2006

Erklärung

Ich versichere hiermit, die vorliegende Arbeit selbstständig und nur unter Verwendung der angegebenen Quellen und Hilfsmittel verfasst zu haben.

.....

Markus Reuter
Mainz, Januar 2006

Kurzfassung

Der Übergang zwischen tropischer und temperater Karbonatprovinz verläuft in den heutigen Meeren graduell entlang eines E-W gerichteten Längsgürtels, der weite Flächen auf den Schelfen einnimmt. Trotzdem ist das Wissen über die geologischen Merkmale dieser Zone gering.

In dieser Arbeit wird erstmalig ein ober-miozänes Karbonatsystem von der Insel Kreta (Griechenland) beschrieben, das sowohl Merkmale tropischer als auch temperater Karbonatsysteme enthält. Stratale Geometrien und Faziesmuster belegen für das Arbeitsgebiet (Westrand des Heraklion Beckens) ein aktives Halbgrabensystem mit ausgeprägtem submarinen Relief, das durch synsedimentäre Bewegungen zahlreicher Kippschollen kontrolliert wurde. Die übereinstimmenden coastal onlap Muster in den untersuchten Aufschlüssen belegen jedoch, dass die tektonischen Bewegungen zu gering waren, um das eustatische Meeresspiegelsignal (3. und 4. Ordnung) zu überdecken.

Niedrigdiverse Korallenriffe und andere riffartige Strukturen, die von *Porites* und *Tarbellastrea* mit geringer Beteiligung von *Acanthastrea* und *Siderastrea* aufgebaut werden, sind durchgängig über die untersuchte Schichtenfolge des normalmarinen Ober-Miozäns verbreitet. Lang anhaltende Phasen in den das Riffwachstum völlig zusammenbrach, wie für das westliche Mittelmeergebiet nachgewiesen, sind nicht dokumentiert. Die Riffe kommen entlang eines schmalen Küstensaumes in der Umrandung einer „Zentralkretischen Landmasse“ in gemischt karbonatisch-siliziklastischen Sedimenten vor, die auf flach einfallenden, dip-slope Rampen abgelagert wurden. Zeitgleich inkrustierten Korallenriffe außerdem steile Kliffs an footwall scarps von herausgehobenen Halbhorsten, die der Küste vorgelagert und vor klastischem Eintrag geschützt waren. Ihre flach einfallenden dip-slope Rampen nehmen sehr weite Flächen im Becken ein und die auf ihnen abgelagerten Rotalgen-Bryozoen-Foraminiferen-Karbonate sind deshalb im Gelände sehr prominent. In den flacheren Abschnitten dieser Rampen enthalten die Rotalgen-Bryozoen-Foraminiferen level-bottom Gemeinschaften außerdem isolierte *Porites*- und *Tarbellastrea*-Kolonien, die niedrigenergetische Verhältnisse in größerer Wassertiefe (verglichen mit den Riffgemeinschaften) abbilden. Das Faziesmodel legt eine Oberflächenwassertemperatur (SST) am kritischen Schwellenwert für Korallenriffe (~17.5°C) nahe, die mit zunehmender Tiefe rasch unterschritten wurde.

Eine anhaltende Aridisierung, die oligotrophe Verhältnisse förderte ist durch die sukkzessive Abnahme des terrigenen Sedimenteintrags dokumentiert. Dieser Trend ist zeitgleich überall im Mittemeerraum widerzufinden und wird deshalb als mögliche Ursache für die Ausbreitung sowohl tropischer, als auch temperater Flachwasserkarbonate in der Umrandung von aufsteigenden, alpidischen Gebirgszügen vorgeschlagen.

In dem Skelett riffbildender Korallen sind Informationen über die Umweltverhältnisse gespeichert, die während seines Wachstums vorherrschten. Meßreihen von stabilen Isotopen ($\delta^{18}O$, $\delta^{13}C$), die an 10 Mio Jahre alten, massiven *Porites*-Kolonien in aussergewöhnlicher Aragoniterhaltung gemessen wurden, spiegeln saisonale Schwankungen von SST, Salinität und Photoautotrophie wider. Die Spektralanalyse eines 69 Jahre umfassenden $\delta^{18}O$-Datensatzes zeigt außerdem eine signifikante Varianz bei 5-6 Jahren, die auch für das heutige Mittelmeergebiet gilt und durch die Arktische Oszillation/Nordatlantische Oszillation (AO/NAO) verursacht wird. Diese atmosphärische Variabilität dominiert heute das Klima im Nordatlantik und den angrenzenden Gebieten und ist bislang erst ab dem Eem-Interglazial belegt, während das Klima im Mittelmeerraum im Miozän als Monsun-beeinflußt gilt. Die Annahme einer solchen AO/NAO-Beeinflussung des östlichen Mittelmeergebietes bereits im Unter-Torton, wird durch Simulationen mit einem komplexen atmosphärischen Zirkulationsmodel unterstützt.

Im Regelfall sind miozäne Korallen allerdings vollständig rekristallisiert und für geochemische Analysen ungeeignet. Rekristallisierte Korallen zeigen aber fast immer deutliche Geisterstrukturen der ursprünglichen Wachstumsrhytmizität (Hell-/Dunkel-Bänderung). Aus dem Arbeitsgebiet liegen alle Übergänge von *Porites*-Korallen in unveränderter Aragoniterhaltung bis vollständig in Sparit transformiert vor. Die Analyse der diagenetischen Übergangsstadien zeigt, dass die sichtbare Hell-/Dunkel-Bänderung in rekristallisierten Korallen mit massiver Wuchsform auf der bevorzugten Lösung des high density-Bandes beruht und tatsächlich ein primäres Wachstumsmuster abbildet.

Variationen in der Dicke der Wachstumsbänderrelikte spiegeln deshalb auch wechselnde Umweltverhältnisse im Korallenhabitat wider. Systematische Messungen der Dicken transformierter Wachstumsinkremente erfolgten an massiven *Porites*-Stöcken aus verschiedenen Korallenbiotopen und Lokalitäten über die gesamte untersuchte Schichtenfolge. Diese Daten dokumentieren einen gleichmäßig geringen jährlichen Zuwachs von durchschnittlich 2-4 mm/a^{-1} für den Zeitraum Unter-Torton bis Unter-Messin. Das entspricht in etwa den jährlichen Kalzifikationsraten massiver *Porites*-Stöcke in heutigen Riffen, die auf höheren Breitengraden liegen und weist auf eine SST im Winter nicht unterhalb von 19-21°C. Die Geringe Variationsbreite der mit dem „*Porites*-Thermometer“ ermittelten SST-Daten über die Zeit deutet auf einen E-W gerichteten Temperaturgradienten während kühler Phasen, in denen das Korallenwachstum im westlichen Mittelmeergebiet infolge von Einstrom kalten Atlantikwassers aussetzte und lässt auf einen „Eastern Mediterranean Warm Pool“ schließen, der dann als Korallenrefugium diente.

Abstract

In modern oceans, the transition zone between the tropical and temperate carbonate province is gradual and covers a wide latitudinal belt. Little knowledge exists regarding the geological signatures of this zone. The present study describes a Late Miocene (early Tortonian - early Messinian) transitional carbonate system that combines elements of tropical and cool-water carbonate systems (Irakleion Basin, island of Crete, Greece). As documented by stratal geometries, the submarine topography of the basin was controlled by tilting blocks. Coral reefs formed by *Porites* and *Tarbellastrea* occurred in a narrow clastic coastal belt along a „central Cretan landmass“ and steep escarpments formed by faulting. Extensive covers of level-bottom communities existed in a low-energy environment on the gentle dip-slope ramps of the blocks that show the widest geographical distribution within the basin. Isolated colonial corals were present in the shallow segments of the ramps. Consistent patterns of landward and basinward shift of coastal onlap in all outcrop studies reveal an overriding control of 3rd and 4th order sea level changes on sediment dynamics and facies distributions over block movements. An increasingly dry climate and the complex submarine topography of the fault block mosaic kept sediment and nutrient discharge at a minimum. The skeletal limestone facies therefore reflects oligotrophic conditions and a sea surface temperature (SST) near the lower threshold temperature of coral reefs in a climatic position transitional between the tropical coral reef belt and the temperate zone. It is suggested, that the recognition of an overall Late Miocene aridification trend helps to explain the Mediterranean-wide distribution of shallow-marine carbonates, both cool-water and warm-water in settings adjacent to uplifting mountain ranges (intramontane basins).

The environmental information stored in the skeleton of reef corals is a unique source of information that resolves seasonal to interannual climate variability. Stable isotope records ($\delta^{18}O$, $\delta^{13}C$) from massiv, exceptionally preserved Late Miocene aragonite coral skeletons reflect seasonal changes in sea surface temperature and symbiont autotrophy. Spectral analysis of a 69 years coral $\delta^{18}O$ record reveals significant variance at interannual time scales (5-6 years) that matches the present-day eastern Mediterranean climate variability controlled by the Arctic Oscillation/North Atlantic Oscillation (AO/NAO), the Northern Hemisphere's dominant mode of atmospheric variability. Supported by simulations with a complex atmospheric general circulation model coupled to a mixed-layer ocean model, it is suggested, that climate dynamics in the eastern Mediterranean and central Europe reflect atmospheric variability related to the Icelandic Low 10 million years ago.

Usually, Miocene corals are transformed in calcite spar in geological time and isotope values are reset by diagenetic alteration. However, ghost structures of annual growth rhythms have a high potential to be retained in the transformed skeleton.

Annual growth bands in the colonial coral *Porites* in a perfect (aragonite and microstructures retained) and fully recrystallized (sparry calcite mosaic) style of preservation are described from sediments of Late Miocene age (Crete, Greece). Analysis of a continuous spectrum of transitional preservational stages show, that in Miocene *Porites* preservation of the growth banding was controlled by preferential dissolution of the high density band associated with cementation by drusy calcite spar during freshwater diagenesis/shallow burial diagenesis.

It is demonstrated that the relicts of growthbands represent an intriguing source of information for the growth conditions of fossil corals. Recrystallized growth bands were measured systematically in massive *Porites* from Crete that were found in biostromes, patch reefs and level-bottom associations of attached mixed clastic environments as well as in isolated offshore carbonate environments. The Late Miocene corals were growing slowly with 2-4 mm/yr^{-1}, compatible with present-day *Porites* from high latitude reefs, a relationship that fits the position of Crete at the margin of the Miocene tropical reef belt. Over Late Miocene time (Tortonian - early Messinian) growth rates remained remarkably constant, and if the modern growth temperature relationship for massive *Porites* applies to the Neogene, minimum (winter) SST did not exceed 19-21°C. Therefore, the „*Porites*-thermometer“ data supports the idea of an „Eastern Mediterranean Warm Pool“ as a refuge for corals during phases when coral reefs collapsed in the western Mediterranean due to inflow of cold Atlantik water.

Einführung

In der jüngeren, erdgeschichtlichen Vergangenheit führte die schrittweise globale Abkühlung über das Känozoikum zur Umgestaltung der Erde von einer greenhouse Welt ohne Eiskappen an den Polen (Oberkreide, Alttertiär) zu der icehouse Welt, wie wir sie heute kennen (Zachos *et al.*, 2001). Für die Zukunft wird dagegen mit dem zunehmenden Anstieg von Treibhaus-Gasen in der Atmosphäre, infolge der Industralisierung ein gegenläufiger Trend erwartet. Moderne Klimamodelle sagen für die nächsten Jahrhunderte einen Anstieg der globalen Temperatur um 1-2K (IPCC, 2001) und ein mögliches Abschmelzen des Grönlandeisschildes (Gregory *et al.*, 2004) voraus. Dieses Szenario entspricht etwa den Bedingungen während des Tortons, einer Zeit wärmeren Klimas in dem sich im Mittelmeer Korallenriffe ausbreiteten und die nördliche Hemisphäre letztmalig in der Erdgeschichte ohne Eisbedeckung war (Crowley & Zachos, 2000). Die genaue Kenntnis um das Klimageschehen zu dieser Zeit kann daher wichtige Hinweise auf das zukünftige Klima geben und helfen die möglichen Auswirkungen eines globalen Temperaturanstiegs abzuschätzen.

Aufgrund seiner damaligen Lage am Nordrand des tropischen Riffgürtels, ist das Mittelmeer ein geeignetes Gebiet für die Erforschung des Klimas im Ober-Miozän. In kalten Perioden verschob sich die Grenze zwischen tropischen und temperaten Klimasystem nach Süden, während wärmerer Perioden nach Norden. Solche extremen klimatischen Veränderungen haben Einfluß auf die Wasserqualität des Meeres und da die meisten marinen Organismen keine abrupte und/oder drastische Veränderung der Temperatur oder chemischen Zusammensetzung des Meerwassers tolerieren, spiegeln sie sich in der Zusammensetzung von Flachwasserlebensgemeinschaften deutlich wider (Brachert *et al.*, 1996). Wechselnde Assoziationen von Faziesfossilien in Karbonaten, sind insbesondere im westlichen Mittelmeer für die Zeitscheibe Ober-Miozän gut untersucht (Brachert *et al.*, 1998, 2001, 2002; Betzler *et al.*, 1997; Martín *et al.*, 1996). Karbonate mit level-bottom communities (*sensu* Brenchley & Harper, 1998), die durch Bivalven und/oder Bryozoen, Corallinaceen, Foraminiferen, Echinodermen und Balaniden charakterisiert sind (Bryomol-/Foramol-Assoziation *sensu* Lees & Buller, 1972; Nelson *et al.*, 1988) und lockere Bestände von isoliert stehenden zooxanthellaten Korallen enthalten können werden als Bildungen der warm-temperaten oder subtropischen Klimazone interpretiert, während gerüstbildende Korallengemeinschaften und verkalkte Grünalgen (Chlorozoan-Assoziation *sensu* Lees & Buller, 1972) als Anzeiger für tropisches Klima gelten. Der zeitliche Wechsel dieser Biofazies-Typen dokumentiert demnach Klimaschwankungen, aus denen N-S gerichtete Verlagerungen des tropischen/temperaten Klimagürtels verbunden mit der Über- bzw. Unterschreitung der Temperaturschwelle beider Organismenassozia-

tionen resultierten (Brachert *et al.*, 1996). Das Auftreten von Korallenriffen ist aber nicht nur durch die Wassertemperatur, sondern auch durch Nährstoffeintrag und Wassertrübe kontrolliert (Hallock & Schlager, 1986; Halfar *et al.*, 2004). Einige Bearbeiter sehen deshalb im Wechsel von Korallenriffkalken und Kalksteinen mit level-bottom communities Änderungen im Nährstoffgehalt des Mittelmeerwassers, die entweder die Ausbreitung von Suspensionsfressern (Bryozoen, Mollusken) oder photoautotrophen Biota (Korallen, Großforaminiferen) förderten (Pomar *et al.*, 2004).

Für den östlichen Mittelmeerraum existieren nur wenige vergleichbare Untersuchungen (Kroeger, 2004), obwohl auch hier Karbonate mit temperater und tropischer Biofazies vorkommen (Buchbinder, 1996). In den intramontanen Neogenbecken Zentralkretas (Heraklion Becken, Messara Becken) nehmen Flachwasserkarbonate besonders mit Rotalgen-Bryozen-Foraminiferen-Mollusken-Echinodermen level-bottom communities aber in geringerem Umfang auch mit Korallenriffen weite Flächen ein (ten Veen & Postma, 1999; Pomoni-Papaioannou *et al.*, 2002; Kroeger, 2004). In dem stark reliefierten Heraklion Becken kommen Korallenriffe und level-bottom communities parallel sowohl auf küstenahen Rampen in gemischt siliziklastisch-karbonatischen Systemen vor, als auch in rein karbonatischen Ablagerungsräumen auf isolierten Hochgebieten im Beckeninneren, die vor terrigenem Eintrag geschützt waren. Wegen der unterschiedlichen Ausbildung der Korallengemeinschaften in den verschiedenen sedimentären Systemen ist das Heraklion Becken ein geeignetes Studienobjekt, um zu klären inwiefern das Vorhandensein oder Fehlen von Korallen und die Verteilungsmuster von level-bottom communities und Korallenriffen neben der Wassertemperatur auch auf andere Umweltfaktoren, etwa wechselnde Wassertiefe, Nährstoffeintrag oder hohe Sedimentationsraten zurückgeht.

Erschwert werden paläoklimatische Analysen von känozoischen Flachwasserablagerungen im Mittelmeerraum durch unvollständige stratigraphische Überlieferung und ungenaue Altersmodelle (Schlager, 1992, 1999). Für Kreta liegen hochauflösende biostratigraphische und astronomische Giederungen bislang nur für die feinkörnigen Beckenablagerungen vor (Benda *et al.*, 1974; Zachariasse, 1975; Frydas *et al.*, 1999; Frydas & Keupp 1992, 1996; Santarelli *et al.*, 1998; Krijgsman *et al.*, 1999). Flachmarine Sedimentgesteine sind dagegen überwiegend lithostratigraphisch gegliedert und ihre exakte chronostratigraphische Parallelisierung scheint im Einzelnen recht problematisch (Meulemkamp *et al.*, 1979; ten Veen & Postma, 1999). Ursachen sind das Fehlen in, bzw. die schwierige Gewinnung von Leitfossilien aus den Gesteinen, sowie die starke tektonische Fragmentierung der Becken, bereits während des Ober-Miozäns, in zahlreiche Kippschollen, die je nach Physiographie und Position im Becken individuelle Faziesmuster aufweisen können. Nur für die flachmarinen, obermiozän-zeitlichen Sedimentgesteine

Südkretas existiert eine Chronostratigraphie, die auf Sr-Isotopenverhältnissen in Schalen von pectiniden Bivalven basiert (Kroeger, 2004). Für das Arbeitsgebiet (Westrand des Heraklion Beckens) ist darum eine coastal onlap Kurve als chronostratigraphisches Gerüst erstellt worden, die an der Sr-Kurve für Südkreta geeicht ist. Zusammen mit einer Analyse der paläogeographischen Muster in dem strukturell kontrollierten Becken über die Zeit erlaubt sie die Ausweisung und Korrelation chronostratigraphischer Einheiten und bildet die Grundlage für ein Faziesmodel der ober-miozänen Flachwasserkarbonate Zentralkretas.

Zooxanthellate Korallen sind häufige Bestandteile in den Flachwasserablagerungen heutiger und vergangener tropischer Meere und ihr Skelett stellt wegen seines jahreszeitlichen Zuwachsmusters und der relativ langen Lebensdauer einzelner Kolonien (einige 100 Jahre) ein zeitlich hochauflösendes und langfristiges Klimaarchiv dar (Grottoli, 2001). Während Biofazieswechsel nur die Über- oder Unterschreitung von Schwellenwerten der jeweiligen Organismenassoziation anzeigen und deshalb nur qualitative paläoklimatische Aussagen erlauben (Brachert *et al.*, 1996, 2001), geben die im Skelett von Flachwasserkorallen konservierten Verhältnisse von stabilen Isotopen quantitativ Auskunft über saisonale bis interannuelle Schwankungen von Wassertemperatur, Salinität und Photoautotrophie. Für die notwendigen geochemischen Analysen ist jedoch ein unverändertes, aragonitisch erhaltenes Korallenskelett erforderlich (McGregor & Gagan, 2003). Wegen der schnellen Diagenese von Korallen (Constantz, 1986; Dullo & Mehl, 1989) bleibt die Anwendung dieser Methodik deshalb hauptsächlich auf Material aus dem jüngeren Quartär beschränkt, gewinnt aber zunehmend an Bedeutung für das Holozän.

Demgegenüber beruhen paläoozeanographische Modelle für das Tertiär im Wesentlichen auf der Isotopen-Zusammensetzung von planktonischen Organismen in Tiefseesedimenten und erreichen nur eine geringe zeitliche Auflösung (Frakes *et al.*, 1993; Wefer & Berger, 1991).

Eine Besonderheit ist deshalb der Fund einer großen *Porites*-Kolonie in teilweise unveränderter, aragonitischer Erhaltung aus dem unteren Torton des NW-Messara Beckens (Zentralkreta). Ihre augenscheinlich gute Erhaltung kann mit verschiedenen analytischen Methoden bestätigt werden. Trotz der guten Erhaltung zeigt die Koralle eine schwache aber bereits mit bloßem Auge sichtbare Hell-/Dunkelbänderung, während „frische“ rezente Korallen im Auflicht keine Hell-/Dunkelbänder, dafür aber eine Dichtebänderung im Röntgenbild (Wachstumsbänderung) aufweisen. An fossilen, völlig rekristallisierten Korallen ist ebenfalls häufig eine Hell-/Dunkelbänderung zu beobachten, die analog zu heute lebenden Korallen als Wachstumsbänderung interpretiert wird und deshalb auch als paläoökologischer und -klimatischer Proxy Verwendung findet (Ali, 1984; Geister,

1989; Insalaco, 1996; Nose, 1999; Helmle & Stanley, 2003). Die Genese dieser Bänder ist aber nur teilweise geklärt und hängt außerdem von der Skelettarchitektur ab, die bei unterschiedlichen Taxa variieren kann. Röntgenographische Aufnahmen des aragonitisch erhaltenen Korallenskeletts aus dem Miozän zeigen, dass die im Auflicht schwach sichtbare Bänderung mit der Dichtebänderung korrespondiert und erlauben deshalb die sichere Identifizierung von Sommer- und Winterbändern. Da von Zentralkreta *Porites*-Kolonien in allen Stadien und Übergängen der Erhaltung von aragonitisch bis vollständig gelöst oder rekristallisiert vorliegen, kann ein Diagenese-Model der Wachstumsbänder für Korallen mit poritidem Skelettaufbau entwickelt werden.

Neben Informationen zum Alter und zur Wachstumsgeschwindigkeit der Koralle, gibt die Bänderung das chronologische Gerüst für eine hochauflösende Beprobung vor. Gemessen wurden $\delta^{18}O$ als Proxy für Oberflächenwassertemperatur und Salinität und $\delta^{13}C$ als Proxy für Photoautotrophie. Da Korallen der Gattung *Porites* überwiegend bei ähnlichen Rezentstudien verwendet werden (Pätzold, 1984; Felis *et al.*, 2000; Rimbu *et al.* 2001; Rosenfeld *et al.*, 2003), ergibt sich eine gute Vergleichbarkeit der Daten. Das ermöglicht die Rekonstruktion saisonaler und interannueller Schwankungen von Oberflächenwassertemperatur, Salinität und Photoautotrophie im unteren Torton für ein Zeitfenster von 69 Jahren.

Weil aragonitische Erhaltung die Ausnahme darstellt und geochemische Untersuchungen außerdem einen hohen analytischen und finanziellen Aufwand benötigen und daher nur in begrenztem Umfang möglich sind, stellt das Diagenese-Model der Wachstumsbänder die Grundlage für weiterführende sklerochronologische Untersuchungen an gebänderten aber vollständig rekristallisierten Korallen dar, die längere geologische Zeiträume (Unter-Torton - unterstes Messin) abdecken. *Porites* ist wegen ihrer Dominanz im mediterranen Miozän, sowie ihrer weiten ökologischen Bandbreite (Veron, 1995) hierfür hervorragend geeignet. Außerdem dürfte *Porites* die am besten untersuchte, rezente Korallengattung sein, da sie weltweit in den Tropen verbreitet ist und ihr massives Skelett ein ausgezeichnetes Datenarchiv für Paläoumweltanalysen darstellt. Dieser Umstand gewährt eine gute Vergleichbarkeit mit Rezentstudien. Deshalb wurden Bänderdicken in vollständig rekristallisierten, massiven *Porites*-Kolonien von verschiedenen Lokalitäten, Paläomilieus und stratigraphischen Niveaus vermessen und mit dem jährlichen Kalzifikationsraten von rezenten, massiv wachsenden *Porites* des tropischen Indopazifiks verglichen, für die eine klare Beziehung zur umgebenden Wassertemperatur vorliegt (Lough & Barnes, 2000). Dieser Ansatz erlaubt es Variationen der Oberflächenwassertemperaturen in einem größeren Zeitrahmen zu quantifizieren und soll helfen eventuelle Temperaturänderungen des Oberflächenwassers zu erkennen, bei denen der Schwellenwert für *Porites* nicht unterschritten wurde.

Die Arbeit ist in 5 Teile gegliedert. Kapitel 1, 3, 4 und 5 sind in der vorliegenden Form als Beiträge in englischsprachigen, geowissenschaftlichen Schriftenreihen eingereicht und deshalb auf Englisch abgefasst:

(1) **Reuter, M., Brachert, T.C.** and **Kroeger, K.F.** (2006) Shallow-marine carbonates of the tropical-temperate transition zone: effects of hinterland climate and basin physiography (Late Miocene, Crete/Greece). In: *Cool-water Carbonates: Depositional systems and environmental controls* (Eds. H.M. Pedley, S. Carannante), *Geological Society Special Publication*, **255**, 159-180. Geological Society Publishing House, London.

(3) **Reuter, M., Brachert, T.C.** and **Kroeger, K.F.** (2005) Diagenesis of growth bands in fossil scleractinian corals: identification and modes of preservation. *Facies*, **51**, 146-159.

(4) **Brachert, T.C., Reuter, M., Felis, T., Kroeger, K.F., Lohmann, G. Micheels, A.** and **Fassoulas, C.** (submitted) Late Miocene corals (10Ma) from Crete (Greece) document interannual climate variability controlled by the Icelandic Low. *Earth and Planetary Science Letters*.

(5) **Brachert, T.C., Reuter, M., Kroeger, K.F.** and **Lough, J.** (submitted) Coral growth bands: an efficient and easy to use paleothermometer in paleoenvironment analysis and paleoclimatology, *Paleooceanography*.

Die einzelnen Kapitel sind darum in sich geschlossen und enden jeweils mit Ergebnissen auf die nachfolgend verwiesen wird. Sie sind zu der vorliegenden Studie zusammengefasst worden, um deutlich machen, welchen Beitrag die Analyse von flachmarinen Karbonatsystemen und Biota für das Verständnis von Paläoozeanographie und Paläoklima im Neogen leisten kann. Die Arbeit ist um ausführliche Beschreibungen wichtiger Korallenfundstellen (Apomarma, Psalidha) aus dem Unter-Torton des NW-Messara Beckens erweitert worden (Kapitel 2), auf die in den Kapiteln 3-5 Bezug genommen wird.

Contents

1 Shallow-marine carbonates of the tropical-temperate transition zone: effects of hinterland climate and basin physiography (Late Miocene, Crete/ Greece)

Non-reefal, carbonate producing marine communities living on a flat sea floor (horizontal, parallel bedding, production *in situ*, zoned according to depth) and covering large areas termed “level-bottom carbonate communities” (Brenchley & Harper, 1998). They represent the common type of carbonate factories in shallow water areas and shelves of the temperate realm and the temperate-tropical transition zone. Extensive work has been carried out in modern oceans in order to understand processes that determine the distribution of sites of carbonate production and accumulation in such environments (James, 1997; Lees & Buller, 1972; Nelson, 1988). In open shelves exposed to oceanic swell, the level-bottom factory is located mostly above a deep storm wave abrasion depth (WAD) and correspondingly has a low net sediment preservation potential. Sediment grains are continuously redistributed into locations outboard below WAD or to some degree inboard, to accumulate as coastal carbonate sand prisms (Betzler *et al.*, 1997; Brachert *et al.*, 2003; James 1997; James *et al.*, 2001; James *et al.*, 1994; James & von der Borch, 1991). In marginal seas and embayments, sites of carbonate production and accumulation may coincide because the WAD is only a minor factor in controlling the sediment accommodation potential, or because carbonate production extends below the reaches of the shallow WAD (Betzler *et al.*, 1997b; Carannante *et al.*, 1988; Kroeger, 2004; Lukasik *et al.*, 2000; Pomar, 2001). At the interface of the tropical and temperate carbonate provinces, level-bottom and framework forming coral communities coexist on a very local scale as the maximum depth of active reef growth becomes increasingly shallow with latitude or decreasing water temperature (Perry, 2003; Rosen, 1977). A classic example is the western Australia continental shelf, where framework forming communities occur as “islands” within vast areas dominated by level-bottom carbonate communities (Collins *et al.*, 1991; Hatcher, 1991). Towards the south, in the more transitional temperate zone, coral growth represents isolated incrustations without any significant sea floor relief (Betzler *et al.*, 1997b; Playford, 1988).

With regard to the geological record, previous analyses of the sedimentary facies focussed on either the warm-water or cool-water end-members of the continuous climatic spectrum (Brachert *et al.*, 1998; Franseen *et al.*, 1996; James, 1997; Martín *et al.*, 1996), whereas so far studies on transitional systems are lacking. In this chapter, Late Miocene shallow marine carbonates are described, composed of level-bottom communities with occurrences of isolated colonial corals (*Porites*, *Tarbellastrea*) in the intramontane Iraklei-on Basin, central Crete (Greece). The laterally extensive, horizontally bedded coralline algal-bryozoan carbonates merge punctually into coral reefs composed of low-diversity framework forming coral associations (*Porites*, *Tarbellastrea*, *Acanthastrea*) without any ecological zonation. These reefs are interpreted to represent “tropical islands” in the level-bottom sediments of the tropical-temperate climate transition zone. The omnipresence of a temperate-type level-bottom carbonate skeletal association and the rare occurrence of isolated coral growths or frameworks may mislead interpretations of the sedimentary system. This case study thus aims at separating the effects of surface water temperature (SST) and hydrological balance, sea floor physiography and relative sea level as factors controlling the distribution of biotic associations and limestone facies at the scale of a multi-kilometre-sized intramontane basin, and at giving clues for identifying carbonates formed in the temperate-tropical transition zone. Shallow-water carbonates of Late Miocene age exist also in many other intramontane basins of the alpine chain (Franseen *et al.*, 1996). The model suggests, that they were formed preferentially in response to continuing aridification in oligotrophic, cool- and warm-water environments.

1.1 Miocene carbonate sediments of the Mediterranean area

The Late Miocene paleogeography of the Mediterranean was similar to the present-day configuration. It represented a marginal sea of the Atlantic Ocean without any connection to the Indopacific. An ephemeral sea strait linked the eastern Mediterranean via the Aegean and Black Sea with the Paratethys to the north of the alpine orogen system (Meulenkamp & Sissingh, 2003; Rögl & Steininger, 1984). During the Late Miocene, coral reefs were widespread over the Mediterranean area except for its northern segments (Gulf of Lyons, Adriatic Sea, northern Aegaen), were no reefs are documented. Reef growth appears to have been episodical and ephemeral, and constructional coral communites were intermittently replaced by level-bottom benthic communities of temperate carbonate systems in some areas (Brachert *et al.*, 1996; Martín & Braga, 1994). This spatio-temporal pattern and a low reefal coral diversity has been used to infer a position at the northern limit of the global coral reef belt (Esteban, 1996), because even subtle climate changes (Zachos *et al.*, 2001) have had a high potentiality to fluctuate across

critical threshold temperatures for colonial coral growth and coral reef systems (Brachert *et al.*, 1996).

Late Miocene tropical carbonate environments (in terms of sea surface temperature) from the Mediterranean area have been described with regard to sequence architecture and stacking patterns, facies distributions, and paleoceology (Franseen *et al.*, 1996) and references therein), (Brachert *et al.*, 2001, 2002; Pomar, 2001). Sediment dynamics, paleoecology and taphonomy of Mediterranean temperate carbonate systems have been documented by Martín *et al.* (1996), Betzler *et al.* (1997a, 2000), Brachert *et al.* (1996, 1998), and Franseen et al. (1997).

1.2 The Neogene basins of Crete

In the eastern Mediterranean, subduction of the African plate beneath the Euroasian plate has been active since the pre-Neogene. During the late Oligocene and early Miocene, subduction zone roll-back towards the south caused rapid extension and subsidence of the Aegean landmass (Rahl, 2004). Neogene basins related to this process are scattered all over the island of Crete and show a high degree of similarity with regard to sedimentary architectures and lithofacies (Meulenkamp *et al.*, 1979; Keupp *et al.*, 1994; Frydas *et al.*, 1999; ten Veen & Postma, 1999; Pomoni-Papaioannou et al. 2002). In a first step, systems of east-west trending graben subsided from the Early or Middle Miocene onward (Fassoulas, 2001). Maximum extensional stress leds to a rotation in an east-west direction during the Late Miocene (Messinian; Fassoulas, 2001). On from the middle Pliocene until the present, a multidirectional extension system has been established (Fassoulas, 2001).

Framed by the Ida Mountains in the west, the Dicti Mountains in the east (2500 m elevation above sea level), and the Messara Plain in the south, the intramontane Irakleion Basin in central Crete dips into the Cretan Sea to the north. The pre-Neogene substrate of the basin is formed by Mesozoic limestone (Tripolitza Unit, Plattenkalk Unit) and Paleogene sandstone and mudstone with large incorporated blocks of Mesozoic limestone (flysch sediments of the Tripolitza Unit). Situated at the western margin the Irakleion Basin, the area studied herein bis located between the cities of Kroussonas to the north and Agia Varvara to the south (Fig. 1.1).

The Neogene sediments of the western Irakleion Basin formed during the late Middle Miocene through early Pliocene (Meulenkamp *et al.*, 1979). The Upper Miocene section has been assigned to two lithostratigraphic groups, the Tefeli Group and the Vrysses

Group (Meulenkamp *et al.*, 1979). The Tortonian segment of the Tefeli Group comprises siliciclastics deposited in various marginal marine environments (Ambelousos Formation (Meulenkamp *et al.*, 1979; ten Veen & Postma, 1999). Shallow-marine carbonates (Pirgos Member), calcareous mudstone and evaporites of Messinian age (Varvara Formation) have been included in the Vrysses Group (Meulenkamp *et al.*, 1979; ten Veen & Postma, 1999). A general overview of the tectono-sedimentary evolution of Irakleion Basin is given by ten Veen & Postma (1999) and ten Veen & Kleinspehn (2000). High-resolution stratigraphic analyses of deep-water sediments have provided a robust stratigraphic framework and revealed a record of high-frequency climate fluctuations (Krijgsman *et al.*, 1999; Santarelli *et al.*, 1998; ten Veen & Postma, 1996). Using a detailed biofacies approach, climate oscillations have been documented also in shallow water sediments (Kroeger, 2004).

In this chapter, a stratigraphic model is presented that is based on the stratal geometries of the shallow water sediments (Fig. 1.2). The stacking pattern of seven discrete strati-

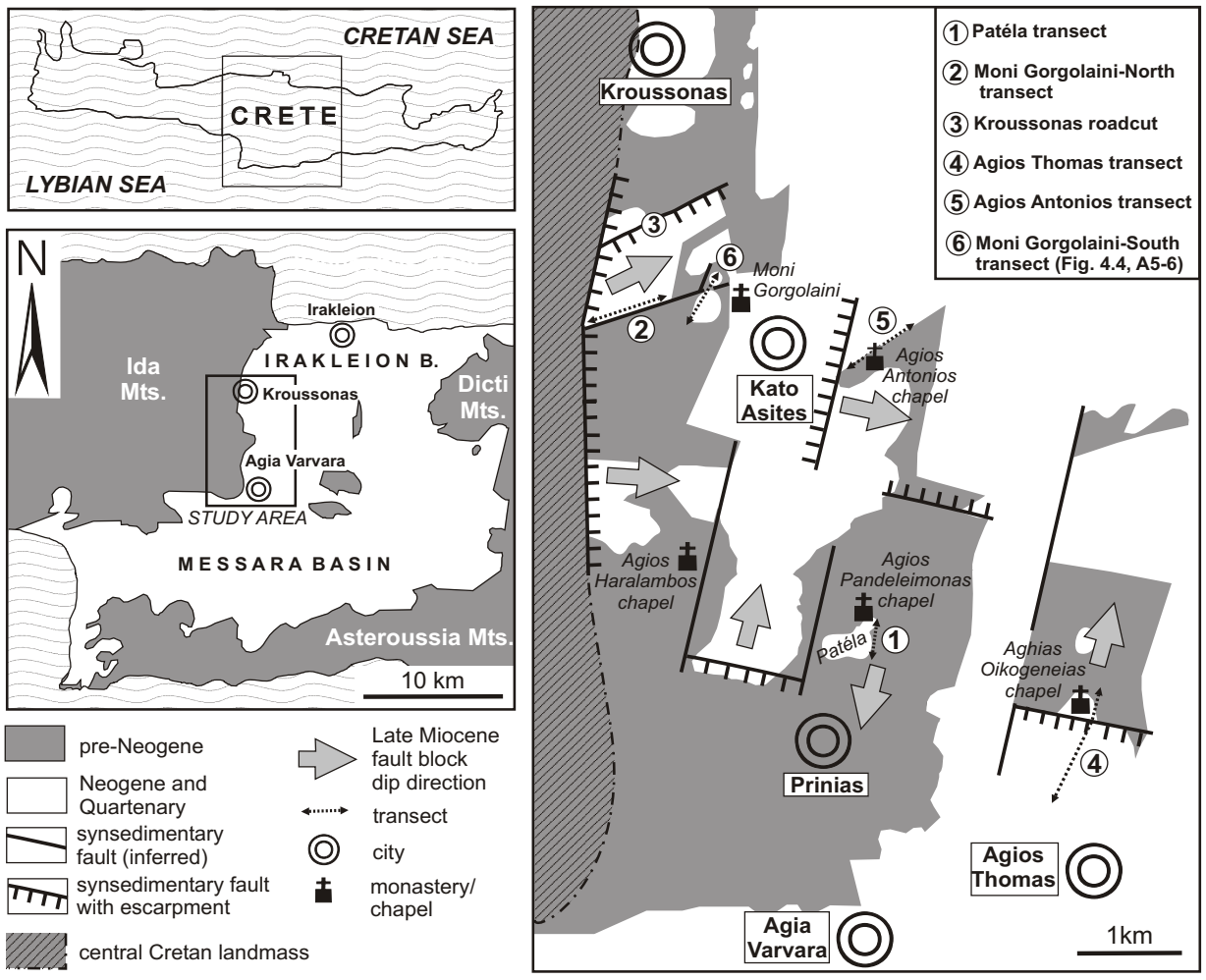

Fig. 1.1. Simplified geological map and location of the outcrops studied in central Crete (simplified from geological map of Crete, IGME). Light grey arrows show inclinations of dip-slope ramps as inferred from stratigraphic geometries.

graphic units defines three stratigraphic sequences. Two anchor points have been used to tie in the stratigraphic framework into the global chronostratigraphy: coral reefs equivalent to Unit 1 were dated as 10 Ma old (Kroeger, 2004), and base-of-slope deposits at the contact of the Ambelousos and Varvara Formations (Unit 7) were found to mark the Tortonian/Messinian boundary (ten Veen & Postma, 1999). Consequently, major events of a basinward displacement of coastal onlap that occur at the transition from Units 3 and 4 and Units 6 and 7 have been interpreted to represent global 3rd order sequence boundaries (Haq *et al.*, 1988; Hardenbol *et al.*, 1998) during the Tortonian and Tortonian/Messinian transition (Fig. 1.2).

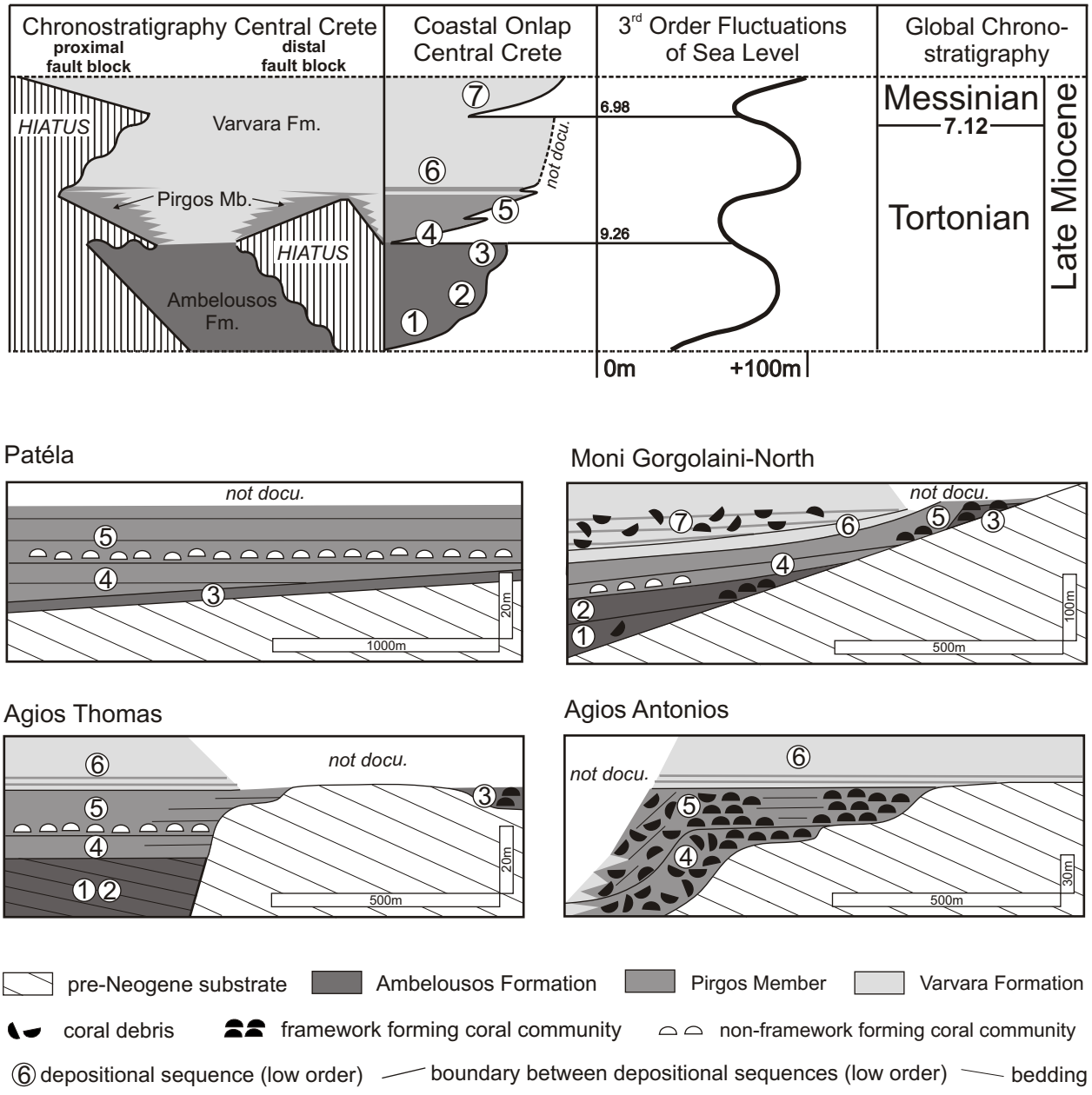

Fig. 1.2. Chronostratigraphy of shallow-water sediments in central Crete based on stratal geometries. Numbers in schematic transects refer to depositional units described in the text. 3rd order sea level curve from Hardenbol *et al.* (1998) as a reference frame.

1.3 Facies, submarine topography and depositional environments in the western Irakleion Basin

The paleogeography and distribution of sedimentary facies of the Late Miocene Irakleion Basin was controlled by movements of tilted fault blocks. The physiography of the fault blocks represents a gently inclined ramp formed by the tilted surface of the block and dips away from a steep scarp formed by normal faulting. This steep footwall scarp continues into the adjacent hangingwall basin (terminology *sensu* Leeder & Gawthorpe, 1987; Gawthorpe & Leeder, 2000). Additionally, steep slopes may exist associated with transfer faults orientated orthogonally to the master faults and compensating for individual tilt rates and orientations of the blocks.

In the western Irakleion Basin, an array of kilometre-sized tilted blocks bounded by an orthogonal system of ESE-WNW and NNE-SSW striking faults is mapped out (Fig.1.1). ESE-WNW trending normal faults reflect north-south extension due to roll-back of the Hellenic subduction zone during the late Serravallian through early Messinian (Meulenkamp et al. 1994, Fassoulas, 2001). The system of NNE-SSW striking faults forming transfer faults in between blocks, became rejuvenated and preferentially active as normal faults during the Messinian through early Pliocene in a context of east-west extension related to activation of the North Anatolian fault (Fassoulas, 2001).

Stratigraphic geometries of shallow water sediments covering the fault blocks permit to reconstruct the geometry and history of movement of the blocks within the basin and relative sea level changes. Four transects have been selected to document the submarine physiography of the basin, the facies distribution in relationship with relative sea level changes, and the position of the blocks relative to a central Cretan landmass (new term) to the west located in the present-day Ida Mountain area (Tab. 1.1). The location of the transects is shown in fig. 1.1. Units in transects are numbered according to the chronostratigraphic framework presented in fig. 1.2. A detailed account of the geometries, facies, stratigraphic thicknesses and environmental interpretations is summarised in tables 1.2-

Name of transect	Position on block	Position within basin	Description
Patéla	dip-slope ramp	distal	Table 1.2
Moni Gorgolaini-North and South	dip-slope ramp	proximal, attached to coast	Table 1.3, A5-6
Road from Asites to Kroussonas	hangingwall basin	proximal	Table 1.4
Agios Thomas	dip-slope ramp, footwall scarp, hangingwall basin	distal	Table 1.5
Agios Antonios	footwall scarp	distal	Table 1.6

Tab. 1.1. Stratigraphic transects, western Irakleion Basin, central Crete

1.6. This account of the sedimentary evolution of western Irakleion Basin starts with the documentation of Patéla transect, because it is an characteristic representation of the Late Miocene level-bottom communities.

1.3.1 Patéla transect

Fig. 1.3. Field photograph of Patéla transect. Beds of skeletal limestone wedge out in a northward direction, documenting a gently inclined dip-slope ramp.

The eastern escarpment of Patéla mountain is formed by a 13 m thick sequence of parallel bedded, skeletal floatstone and rudstone (Unit 4 and 5; fig. 1.3). The contact surface to the pre-Neogene is not fully parallel to the internal stratification of the limestone unit, because the lowermost limestone beds wedge out at a very low angle in a northerly direction against a marine conglomerate that covers the pre-Neogene substrate (Unit 3). Within the limestone, skeletal grains are embedded in a micritic matrix and mostly intact and do not exhibit any preferences according size, shape or orientation.

The conglomerate in Patéla transect reflects rapid transgression. The limestone sequence on top of the conglomerate was formed in shallow water, as indicated by the presence of a level-bottom coral-coralline algal community. Because lithoclasts are absent and effects of waves or storms are not documented by discrete sedimentary structures (cross bedding) or fabrics (graded beds), this community lived in a calm water environment, either too deep for effective wave influence or protected from the open ocean.

The near horizontal dip of the limestone section and the small angles of onlap reflect a very gentle dip of a dip-slope ramp (Fig. 1.3). Although the climbing pinch-out relationship of the limestone units on the top of the conglomerate may not represent a true coastal onlap geometry, we infer a relative rise of sea level subsequent to a relative fall for the onset of limestone deposition (Units 3-5).

Unit (Fig. 2)	Geometry of sediment body	Lithofacies, depositional textures and bedding	Max. thickness (m)	Fossil content	Interpretation
3	sheet-like; covers Tripolitza flysch (tilted sandstone-mudstone couplets)	grain-supported, poorly-sorted (pebbles to boulder size), conglomerate with well-rounded lithoclasts (Paleogene sandstone); rudstone matrix	0.5	coralline red algae, *Clypeaster*, pectinid bivalves	shallow marine; turbulent water
4	low-angle wedge; onlaps Unit 3	skeletal limestone (floatstone); skeletals are mostly intact and embedded in a micritic matrix with no preference regarding to shape, size and orientation; massive beds; large-scale concordant parallel stratification	3.0	coralline red algae, celleporiform bryozoans, *Heterostegina*, pectinid bivalves, *Clypeaster*, decapods (e.g. *Petrochirus*)	calm, moderately shallow marine; no sediment import from the shallow high-energy zone
5	sheet-like; covers Unit 4	skeletal limestone (floatstone); skeletals are mostly intact and embedded in a micritic matrix with no preference regarding to shape, size and orientation; massive beds; large-scale concordant parallel stratification	9.5	coralline red algae, celleporiform bryozoans, *Heterostegina*, bivalves (*Spondylus*, pectinids), isolated *in situ* colonial corals (massive *Porites* and *Tarbellastrea* colonies with ragged margins (Fig. 5.6d), *Clypeaster*	calm, moderately shallow marine, warm; no sediment import from the shallow high-energy zone

Tab. 1.2. Patéla transect (Fig. 1.3). Stratal geometries, facies, stratigraphic thickness and fossil content. N 35.17075° E 025.00845°.

1.3.2 Moni Gorgolaini-North transect

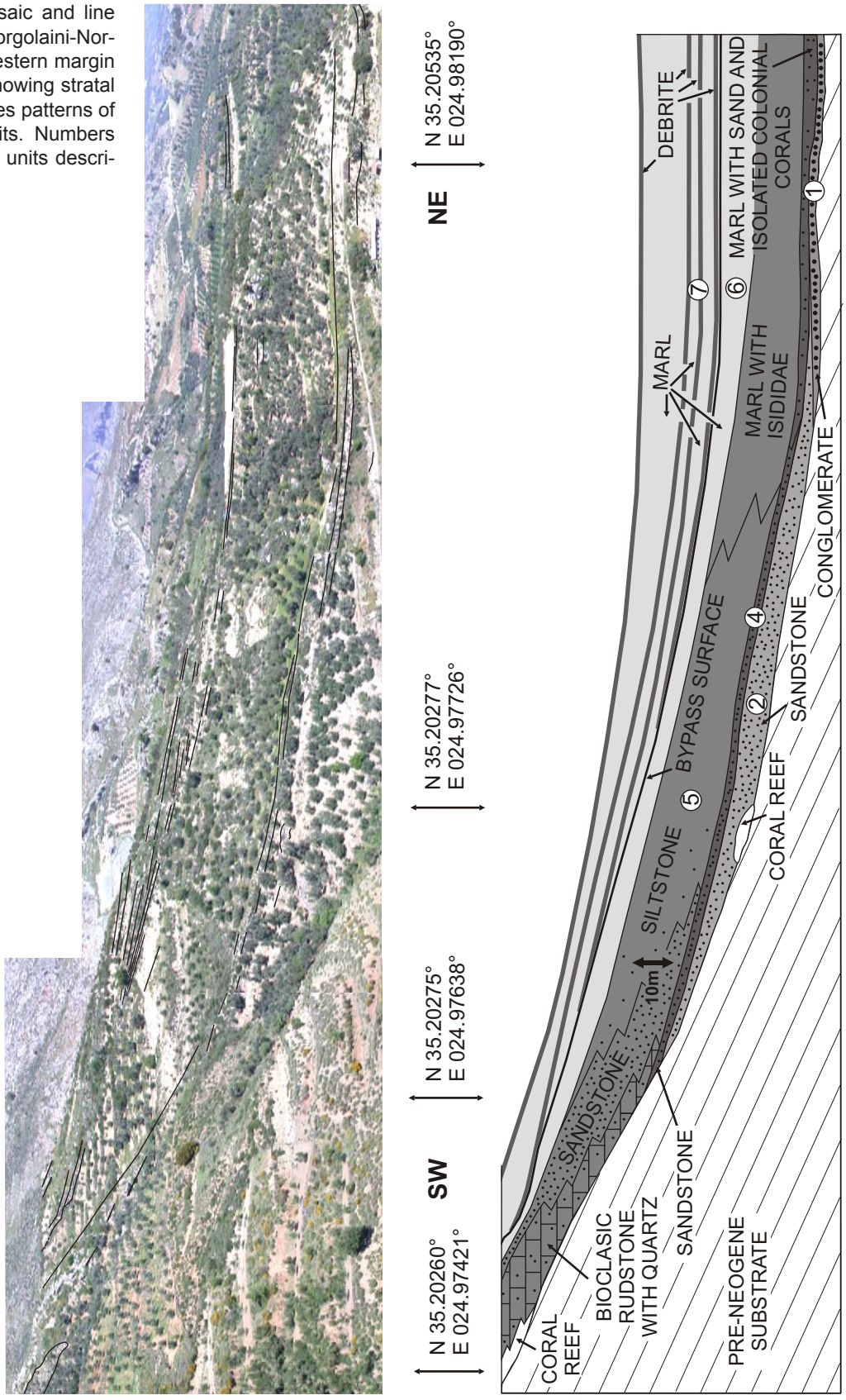

Fig. 1.4. Photo mosaic and line diagrame of Moni Gorgolaini-North transect at the western margin of Irakleion Basin showing stratal geometries and facies patterns of the depositional units. Numbers refer to depositional units described in the text.

The Moni Gorgolaini-North transect (Fig. 1.4) is orientated in NE-SW direction, which resembles the dip direction of the original Late Miocene paleogeography (Fig. 1.1). Using stratigraphic architecture and sedimentary facies, the transect is divided into two segments separated by a distinct sedimentary surface. The lower segment is composed of a stack of six wedges all pointing towards the southwest, i.e. in a landward direction (Units 1-6). The six units represent depositional systems including coastal clastics, coral reefs (Figs. 1.5, 5.6a-c) and offshore calcareous mudstone deposits. Stratigraphic patterns reflect two episodes of rapid landward shift of coastal onlap (Units 1-3, 4-6), separated by a basinward displacement of onlap. The backstepping (drowning) of the coastal sand facies and reefs was accompanied by an overall fining upward trend and reflects a rapid long-term relative sea level rise and deepening of a ramp-type basin margin in northeastward direction. Upward, the coastal facies change from conglomerate to sandstone with coral constructions (patch reefs) and finally merges into carbonate rocks (skeletal rudstone with quartz sand and coral constructions), suggesting a decrease of continental sediment discharge.

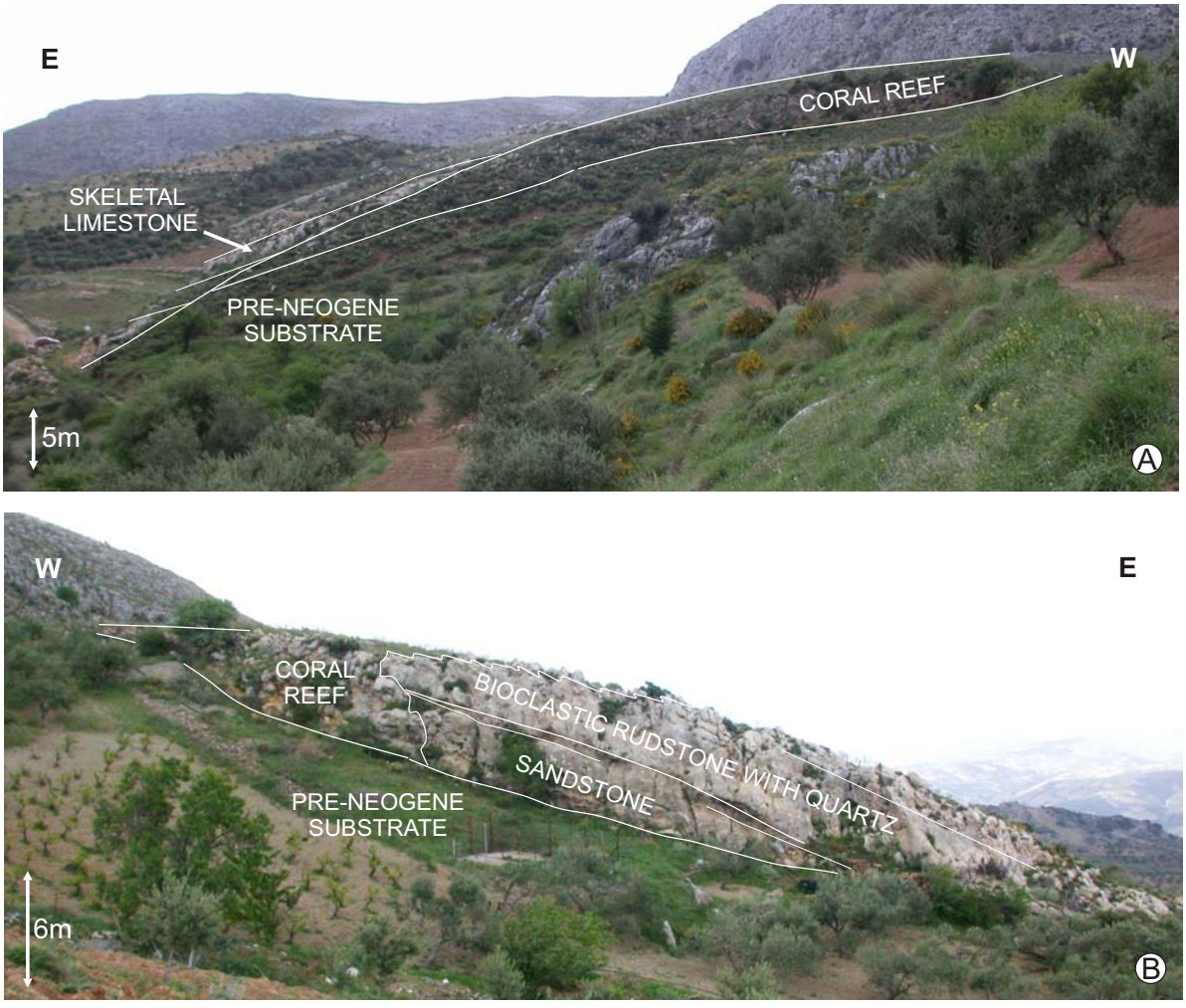

Fig. 1.5. Field photographs of a mound-shaped coral buildup showing facies distributions and geometric relationships highlighted by white lines. Unit 3, Moni Gorgolaini-North **(A)** View from the north, **(B)** view from the south.

The upper segment of the transect documents a change of the depositional environment of the basin. A wedge of rhythmically bedded deep water marl and calcareous mudstone with intervening beds of debrites (Fig. 3.3c) and calciturbidites were formed in a toe-of-slope setting, affected by episodical sediment import from a shallow water source area. Intervening beds of debrites and calciturbidites show a successively more landward encroachment along a discrete stratigraphic interval (Fig. 1.6a). It is interpreted as a surface of sediment bypass in a slope setting oriented in a 065°E direction. Large reworked shallow water biota, such as coralline red algae, zooxanthellate corals (*Porites*, *Tarbellastrea*) (Fig. 3.3c) and fragments of vermetid trottoirs (Fig.1.6c) document extensive carbonate production with little clastic dilution in the neritic zone. Benthic carbonate production, however, also took place in the slope environment as indicated by small *in situ* bioherms formed by the green algae *Halimeda* (Fig. 1.6b).

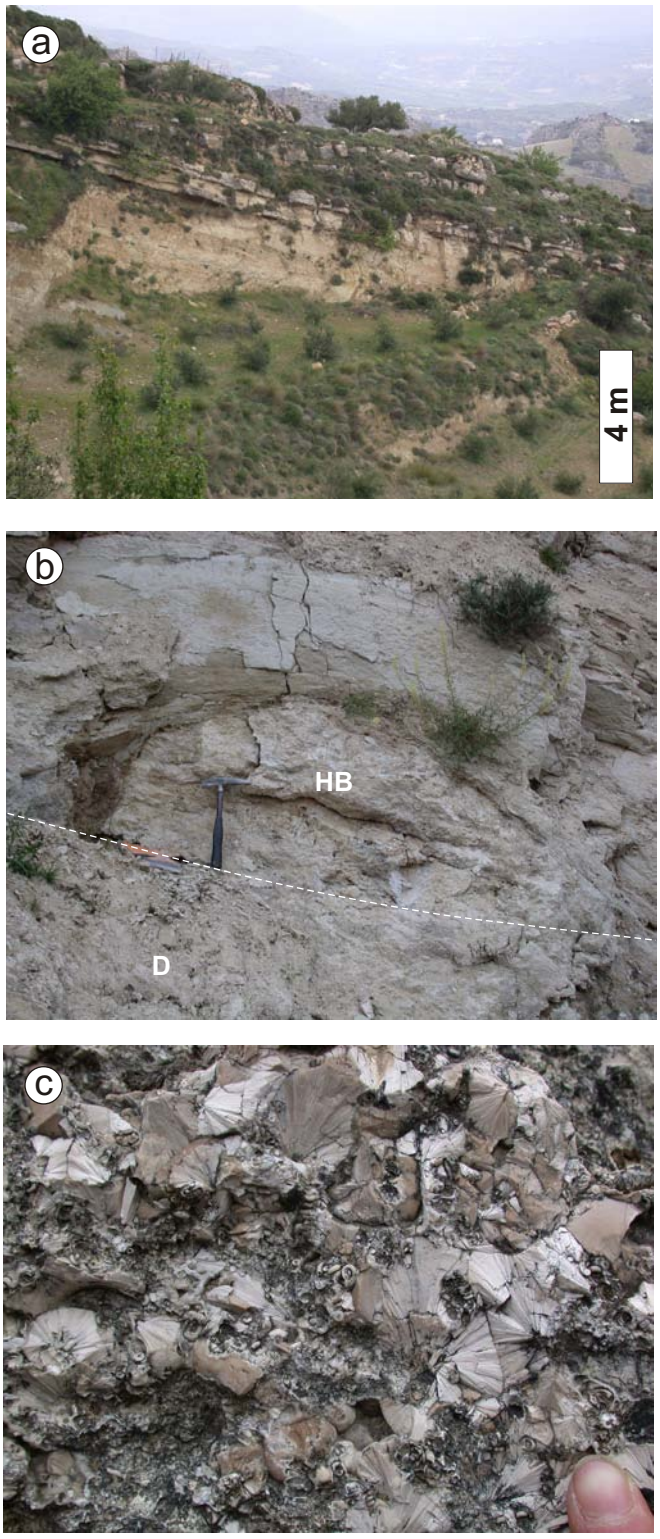

Fig. 1.6. Lithologies in a proximal fault block setting, Moni Gorgolaini-North transect. **(a)** Debrite beds and calciturbidites of Unit 7 wedge out upslope along a bypass surface. **(b)** Lense-shaped *Halimeda* buildup (HB) colonizing a debris flow deposit (D) of Unit 7. The buildup is intercalated with light grey marl. Hammer for scale. **(c)** Allochthon block of vermetid framestone intercalated with light grey marl of Unit 7. Large botryoidal cements cover the walls of caverns and vermetid tubes. Such blocks are very common in slope deposits of Unit 7. They could reach a length of several metres and are interpreted to be derived from vermetid trottoirs that encrusted the rocky shoreline. A comparable facies is described from the Messinian of Salento Peninsula in Italy (Bosellini *et al.*, 2002). Fingertip for scale.

Unit (Fig. 2)	Geometry of sediment body	Lithofacies, depositional textures and bedding	Max. thickness (m)	Fossil content	Interpretation
1	wedge pointing to the SW; covers pre-Neogene substratum (Tripolitza flysch)	grain supported conglomerate with well-rounded lithoclasts (gravel to cobbles) of pre-Neogene rocks (Mesozoic limestone; Paleogene sandstone); beds with poor and good sorting; fining basinward and upward into an alternation of well-sorted conglomerate and sandstone	12	**conglomerate**: bivalve and sponge borings in limestone lithoclasts, oysters, rare coral fragments (*Porites*) **sandstone**: pectinids (e.g. *Amussium*), oysters, *Conus*, biotubation	coastal sediments
2	wedge pointing to the SW; covers Tripolitza flysch (SW) and Unit 1 (NE)	brown, poorly-sorted sandstone, composed of coarse grained angular lithoclasts and quartz (pre-Neogene rocks). Small coral buildup (1.4 m thick); framestone composed of large (up to 1 m) massive corals; matrix: marl with bioclasts and quartz	6	**sandstone**: *Clypeaster*, pectinids **coral buildup**: *Porites*, *Tarbellastrea*	coral patch reef and coastal sands
3 (Fig.4)	isolated lense (reefs and flanking beds); situated on pre-Neogene substratum (Tripolitza flysch). Reef showing progradational geometry. Unit 5 onlaps lense	coral framestone composed of large (up to 1 m) massive corals; matrix: marl with bioclasts and quartz. Interfingers with poorly-sorted sandstone, composed of coarse grained angular lithoclasts (pre-Neogene rocks) and quartz in lower part; upper part interfingers with bioclastic rudstone and quartz sand.	8	**coral buildup**: *Porites*, *Tarbellastrea*, *Acanthastrea* (rare) sandstone: isolated *in situ* colonial corals with massive growth form (*Porites*, *Tarbellastrea*), coralline red algae **rudstone**: cidarid echinoids, oysters, *Clypeaster*, coral clasts (*Porites*, *Tarbellastrea*)	coral patch reef and coastal sands
4	wedge pointing to the SW; covers Units 1, 2 (SW) and Tripolitza flysch (NE). More basinward position as compared to Unit 3	brown sandstone, composed of coarse grained angular lithoclasts (pre-Neogene rocks), quartz and large fossils; grades distally into grey, fossiliferous marl with a abundant dark angular lithoclasts (sand-size, pre-Neogene)	4.5	**sandstone**: *Clypeaster*, celleporiform bryozoans, bivalves (e.g. pectinids), *Heterostegina*, rhodoliths **marl**: bivalves (e.g. pectinids, cardiids, veneroids, *Spondylus*, small ostreids), gastropods (e.g. *Astraea*, *Cyprea*, *Cerithium*, *Turritella*, *Natica*, vermetids), scaphopods, coralline red algae, celleporiform bryozoans, isolated *Porites* and *Tarbellastrea* colonies (nodules up to 40 cm consisting of cm thick concentric coral layers and coralline algae around a sediment nucleus), *Clypeaster*, cidarid echinoids, terebratulid brachiopods, solitary corals (*Flabellum*), fish teeth (*Sparus*, sharks)	coastal clastics grading into offshore silt

5	wedge pointing to the SW; covers Unit 4 (NE) and Tripolitza flysch (SW); onlaps Unit 3.	bioclastic rudstone with quartz sand and retrogradational reef (coral framestone composed of large (up to 1 m) massive and subordinate branching corals (Figs. 5.6b, c); matrix: marl with bioclasts and quartz sand); interfingers distally with sandstone, siltstone and marl; quartz decreases up-section.	Units 5+6 110	**rudstone**: rhodoliths, celleporiform bryozoans, molluscs (e.g. pectinids, *Glycimeris*, oysters), *Clypeaster*, coral fragments (*Porites*, *Tarbellastrea*) coral buildup: *Porites*, *Tarbellastrea*, *Borelis* **sand- and siltstone**: pectinids, *Glycimeris*, *Glossus*, *Natica*, archaeogastropods **marl**: octocorallia (Isididae)	coastal sands and patch reef grading into offshore silt
6	wedge pointing to the SW	Alternating beds of laminated and homogeneous light grey marl		**laminated marl**: terrestrial plants, fish remains **homogeneous marl**: bivalves, gastropods, echinoids, bioturbation	distal offshore environment with recurrent bottom water stagnation
7	wedge pointing to the SW; intercalated mass flow deposits wedge out up-dip along a discrete common surface (Fig. 1.6a) on top of Unit 6	Alternating beds of laminated and homogeneous bedded light grey marl and calcareous mudstone; intervening beds of debrites and calcitubidites **debrites** (Fig. 3.3c): dm to m thick mud supported breccias composed, poorly-sorted (size of particles: mm-dm) bioclasts and lithoclasts (Mesozoic limestone, Paleogene sandstone, single vermetid-framestone clasts up to 4 m); large particles protrude from the base and deform the underlying beds; erosive base, flute marks **calciturbidites**: mm to cm thick elongated lenses or discrete beds of bioclastic packstone; normal grading	>42	**laminated deposits**: sponge spicules, terrestrial plant remains, fish remains **homogeneous deposits**: sponge spicules, bivalves, gastropods (e.g. *Aphorrais*), echinoids, small brachiopods (*Mergelia*, *Terebratulina*), *Discospirina italica*, bioturbation **mass flow deposits**: *Halimeda*, vermetids, sponge spicules, coralline red algae (rhodolithes, protuberances), coral fragments (*Porites*, *Tarbellastrea*), bryozoans; sometimes aragonitic preservation of *Halimeda* and corals (Fig. 3.3c)	bypass slope and toe-of slope environment; recurrent bottom water stagnation

Tab. 1.3. Moni Gorgolaini-North transect (Fig. 1.4). Stratal geometries, facies, stratigraphic thickness and fossil content. N 35.20277°, E 024.9807°.

1.3.3 Road from Kato Asites to Kroussonas

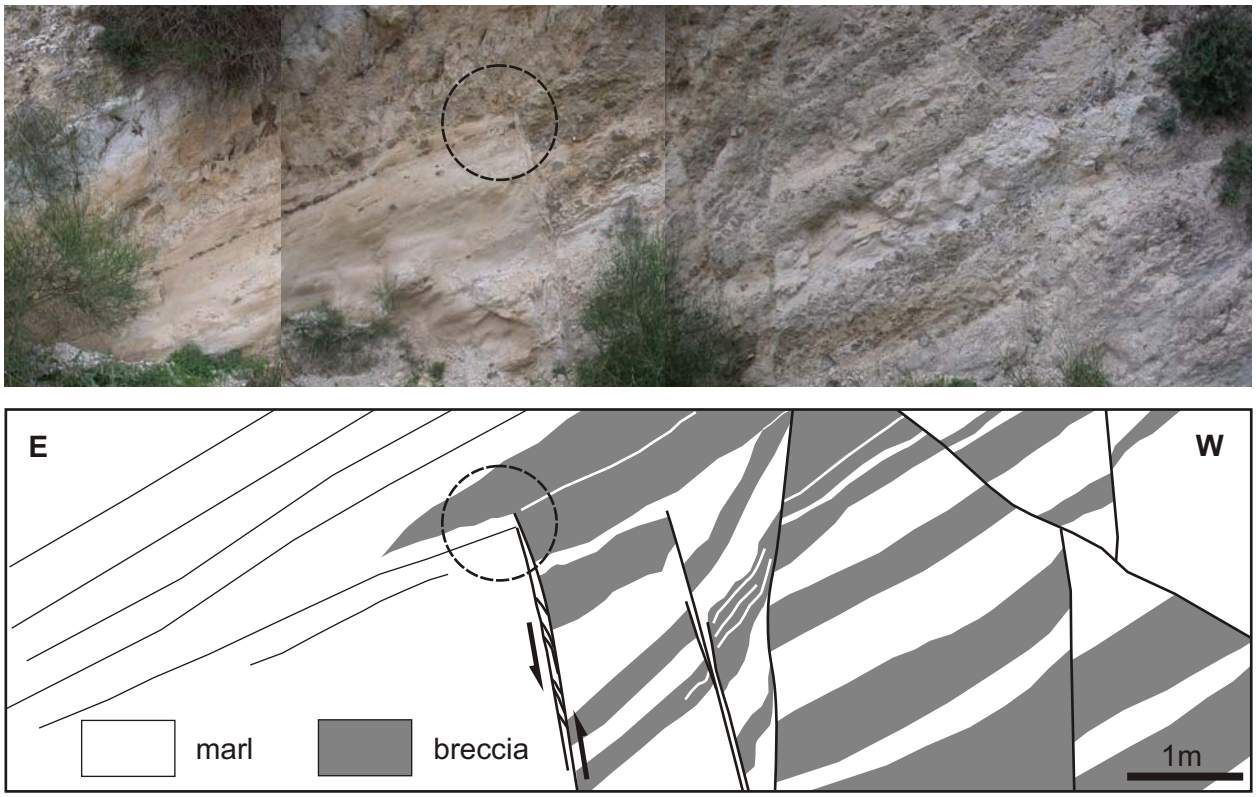

Fig. 1.7. Photomosaic and line diagrame showing tilted section of marl and breccia (Unit 7). Circle marks synsedimentary fault (E060°-E070° strike). Road from Kato Asites to Kroussonas.

The public road from Kato Asites to Krousonas cuts through a tilted section of yellowish-brown homogeneous marl and laminated calcareous mudstone, that is assigned to Unit 7. A series of breccias is intercalated in the fine-grained sediment. Some of the breccias wedge out rapidly in an eastward direction, or have been affected by faults orientated at N060°E- N070°E. The youngest bed of breccia in outcrop seals a synsedimentary fault (Fig. 1.7).

Laminated calcareous mudstone and laminated marl were formed in a deep environment. The angularity of the lithoclasts in the breccias implies little reworking in a high-energy environment, either alluvial or coastal, before redistribution into the basin. The breccias are interpreted to represent submarine rockfall deposits in a submarine debris cone environment sourced from a steep escarpment. The presence of synsedimentary faults in Unit 7 suggests that the escarpment was formed by faulting during the earliest Messinian.

Unit (Fig. 2)	Geometry of sediment body	Lithofacies, depositional textures and bedding	Max. thickness (m)	Fossil content	Interpretation
7	?	faulted section of rhythmically bedded homogeneous and laminated marls and intercalated breccias (Fig. 1.12d); gentle dip of beds towards NE; some breccia-beds wedge out within outcrop towards NE or are cut by faults orientated N060°E-N070°E; the youngest bed of breccia exhibits an erosional base and seals fault **marl**: light grey; contains single angular lithoclasts (<10 cm) of Mesozoic limestone breccia: grain-supported; poorly sorted, angular lithoclasts (Mesozoic limestone) up to 10 cm; matrix: light grey marl	>5	**homogeneous marl**: small brachiopods (*Terebratulina*, *Mergelia*), isolated, broken branches of coralline red algae, bryozoan-nodules (*Calpensia*), irregular echinoids **laminated marl**: terrestrial plant remains, fish scales	toe-of-slope environment; talus breccia sourced from a steep escarpment; faulting corresponds with accumulation of breccias, which suggests the escarpment formed by faulting; entry of bioclasts from a shallow water source area; recurrent stagnation of bottom water

Tab. 1.4. Road from Kato Asites to Kroussonas (Fig. 1.7). Facies, stratigraphic thickness and fossil content. N 35.21469° E 024.97892°.

1.3.4 Agios Thomas transect

Agios Thomas transect is divided into two segments according to the presence of an uplifted block in the north and stratigraphic geometries. The southern segment is formed by fossiliferous sandstone, skeletal limestone (Figs. 1.9a-c), and marl (Fig. 1.9d). The stratigraphic relationships of the sandstone and limestone at the base of the section are not clear because of a thick alluvial covering. However, the presence of *Crassostrea*-biostromes in the lower part of the sandstone section is characteristic for the Ambelousos Formation, whereas the presence of abundant coralline red algae, pectinids and *Clypeaster* echinoids in the upper part of the sandstone section tipify the Pirgos Member (ten Veen & Postma, 1999). In outcrops further to the east, both units are separated by an angular unconformity (Fig. 1.9e), and, according to IGME 1:50.000 “Archanes” geological map sheet, the distribution of the Ambelousos Formation is limited to the north by an east-west trending fault that can be considered the master fault forming the Miocene cliff observed in Agios Thomas transect (Fig. 1.1). Both units, sandstone (Units 1-2) and limestone/marl (Units 4-6), therefore, most probably show an angular contact in the southern segment of the transect. Stratifications in the limestone and marl, however, are concordant and parallel. Towards the northern segment of the transect and fault zone, stratifications within these units terminate or drape over a terraced surface formed on top of Mesozoic limestone. This extensively perforated (bivalves, sponges) transgressive surface (Fig. 1.9f) is interpreted as a sea cliff, shaped by coastal erosion. It was originally formed through tectonic uplift. An isolated conglomerate and a coral reef on the northern flank of the transect may represent erosional remnants of originally more widespread highstand deposits (Unit 3). These highstand deposits were destroyed by erosion prior to the accumulation of the skeletal limestone. The stepwise retreat of the cliff and deepening

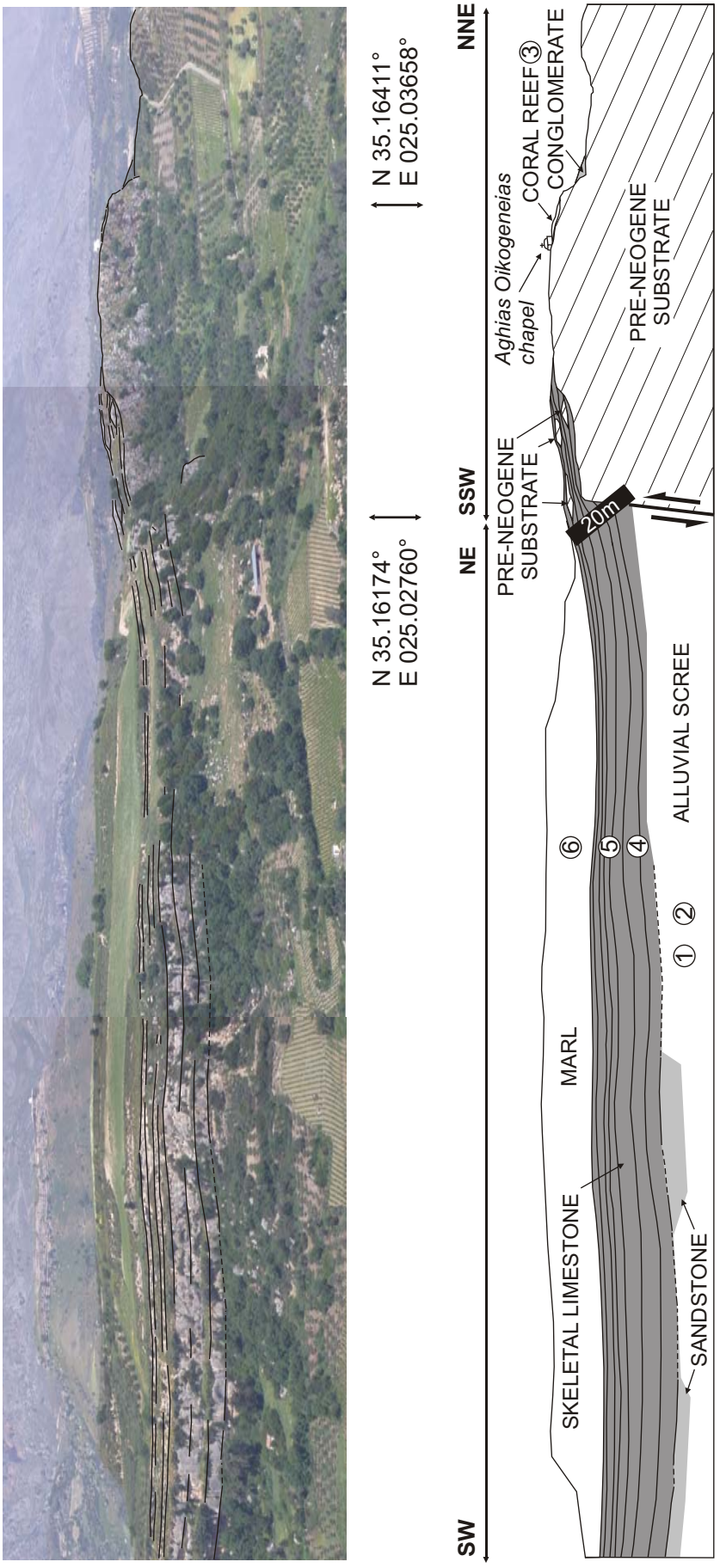

Fig. 1.8. Photo mosaic and line diagrame of Agios Thomas transect showing strata geometries and facies distributions in a distal fault block setting. Numbers refer to depositional units described in the text. Black bar shows location of measured section shown in fig. 1.13.

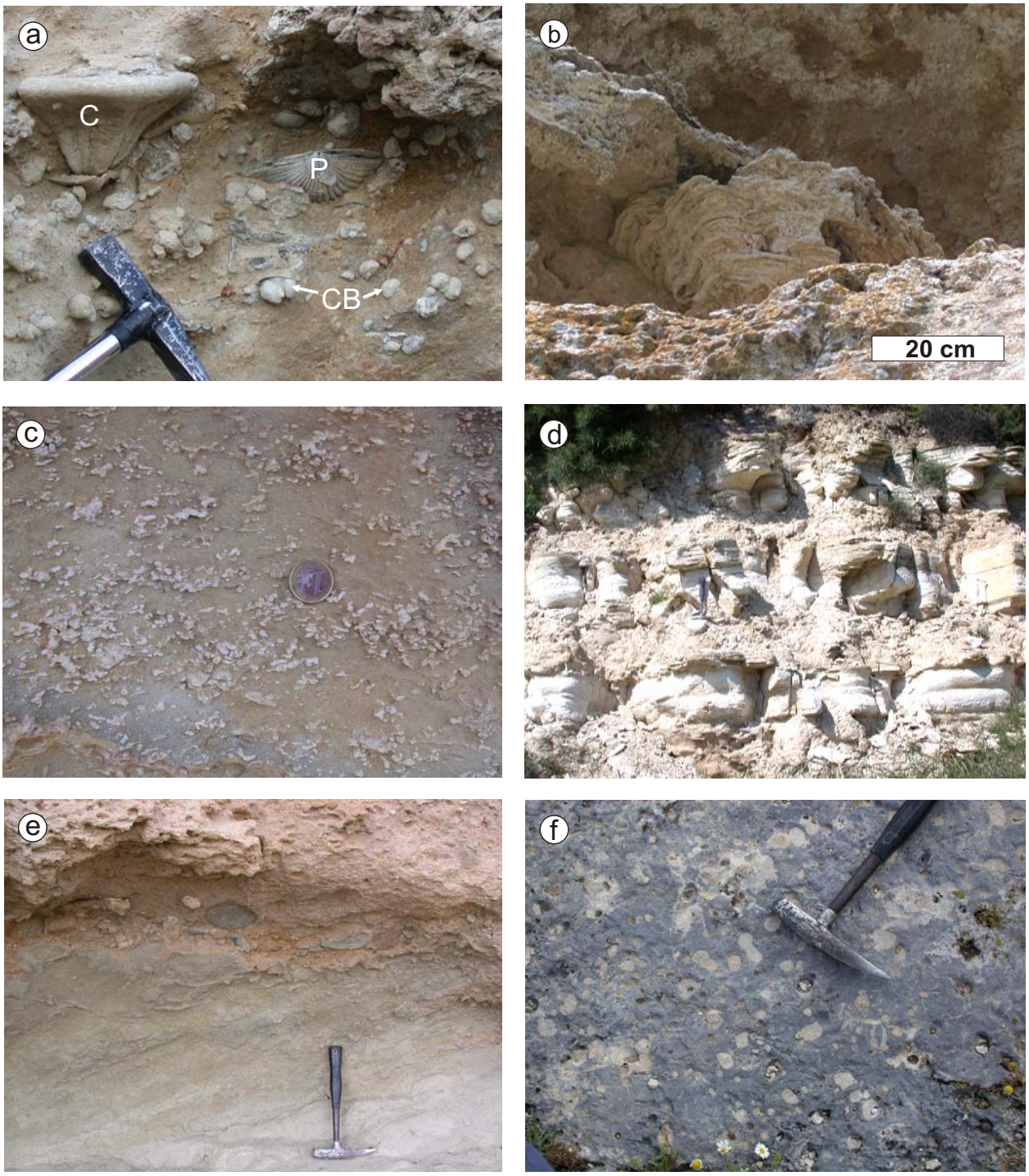

Fig. 1.9. Lithofacies of a distal fault block setting, Agios Thomas area. **(a)** Skeletal rudstone with *Clypeaster* echinoids (C), large pectinids (P) and celleporiform bryozoan nodules (CB). Unit 4, hammer for scale. **(b)** Isolated massive *Porites* coral in a level-bottom carbonate. Ragged margin of colony documents growth keeping up with sediment accumulation. Unit 5. **(c)** Coralline red algal floatstone. Unit 6, coin for scale. **(d)** Rhythmic alternation of homogeneous and laminated marl from the southern segment of Agios Thomas transect. Unit 6, hammer for scale. **(e)** Angular unconformity separating tilted sandstone (Units 1-2) and horizontal skeletal limestone (Unit 4). Hammer for scale. **(f)** Close-up of abrasion surface perforated by bivalves and sponges, and filled with bioclastic limestone. Hammer for scale.

upward trend suggests that these limestones are equivalent with Units 4 and 5. The fact that the skeletal limestone drapes over the cliff without facies change, and the absence of any distinct lithoclast accumulations or physical sedimentary structures implies, that it was formed at some distance from the coast in moderately deep water not affected by any significant wave reworking when the cliff was drowned. Agios Thomas transect thus is interpreted to document movements of an east-west extensional fault between Units 3 and 4, and a drowning of the cliff due to rapid relative sea level rise taking place during deposition of Units 4-6.

Unit (Fig. 2)	Geometry of sediment body	Lithofacies, depositional textures and bedding	Max. thickness (m)	Fossil content	Interpretation
1 2	section partially covered by scree (invisible geometry); tectonic contact with Mesozoic limestone to the NE	sandstone; coarse-medium grained; brown; well-sorted	>10	*Crassostrea*-biostromes	marginal marine
3	wedge on footwall scarp and/or dip-slope ramp; onlaps substrate formed of Mesozoic limestone and folded pre-Neogene mudstone-sandstone couplets	grain supported, conglomerate with bioclasts and well-rounded lithoclasts (gravel to cobble size; single blocks up to 3 m; Mesozoic limestone and pre-Neogene sandstone); matrix: rudstone with quartz sand. Coral buildup on top of conglomerate and Mesozoic limestone: framestone constructed by massive (<1 m) and branching (40 cm high) colonies; matrix: bioclastic marl	10	**limestone block**: surface densely bored by sponges and bivalves **conglomerate**: coral clasts (*Porites*, *Tarbellastrea*), pectinid bivalves, *Borelis* coral buildup: *Porites* (massive), *Tarbellastrea* (massive, branching), rare *Acanthastrea* (massive), coralline red algae, cidarid echinoids, *Borelis*	coastal conglomerate and fringing reef attached to sea cliff
4	sheet-like; covers Units 1 and 2 (angular unconformity?); blunt vertical contact with protruding block of Mesozoic limestone in the NE	basal sandstone, well-sorted (1.5 m). Covered by skeletal rudstone or floatstone (Fig. 1.9a); large-scale parallel horizontal stratification; skeletals are mostly intact and embedded in a micritic matrix with no preference regarding to shape, size and orientation	10	coralline red algae, cellepori-form bryozoans, *Heterostegina*, pectinids, *Clypeaster*	calm, moderately shallow water; drowned cliff; no sediment import from the shallow high-energy zone
5	low-angle wedge; drapes over Unit 4 and terraced surface on protruding block of Mesozoic limestone in the NE	skeletal or floatstone; large-scale parallel horizontal stratification; skeletals are mostly intact and embedded in a mikritic matrix with no preference regarding to shape, size and orientation	9	coralline red algae, cellepo-riform bryozoans, *Heterostegina*, bivalves (*Spondylus*, pectinids), isolated *in situ* colonial corals (massive *Porites* and *Tarbellastrea* colonies with ragged margins, fig. 1.9b, 3.3e), *Clypeaster*	calm, moderately shallow and warm water; drowned cliff; no sediment import from the shallow high-energy zone
6	sheet-like; drapes over Unit 5	alternating beds of laminated and homogeneous light grey marl (Fig. 1.9d); intercalations of two massive beds of corallinacean floatstone (Fig. 1.9c) at the base; skeletals of floatstone are mostly intact and embedded in a micritic matrix with no preference regarding to shape, size and orientation	>15	**marl (laminated beds)**: terrestrial plant remains, fish remains **marl (homogeneous beds)**: bivalves, gastropods (e.g. *Aphorrais*), *Discospirina italica*, bioturbation floatstone: coralline red algae	moderately shallow water environment, deepening upward into distal offshore environment with recurrent stagnation

T**ab. 1.5.** Agios Thomas transect (Fig. 1.8). Stratal geometries, facies, stratigraphic thickness and fossil content. N 35.16174° E 025.02760°.

1.3.5 Agios Antonios transect

A steep, NE-SW oriented gorge at Agios Antonios chapel near the town of Kato Asites cuts trough a section of pre-Neogene sandstone and limestone forming a Miocene coastal cliff covered by three sedimentary sequences of Late Miocene reefal limestone (Units 4-5) and level-bottom carbonates (Unit 6).

The surface forming the coastal cliff is perforated by various borings and displays the original late Miocene submarine topography. In Unit 4, conglomerates cover the cliff where it was vertical. Seaward, but at the same water depth, the conglomerate grades into reef limestone formed by massive *Porites* and *Tarbellastrea*, interfingering basinward with coral breccia and marl of a forereef environment. Unit 5 has a more landward distribution due to backstepping of the cliff as a consequence of relative sea level rise. Two thick bioherms (30 m) present in Unit 5 do not exhibit any significant synoptic relief as compared to the interreef areas, that housed extensive carbonate producing level-bottom communities, and that received only minor amounts of reef debris. Basinward from the reefs, a steep progradational slope was present, that downlaps onto Unit 4 and grades into calcareous mudstone and marl. Synchronous, with a third pulse of coastal backstepping through relative sea level rise, coral reef growth stopped by the

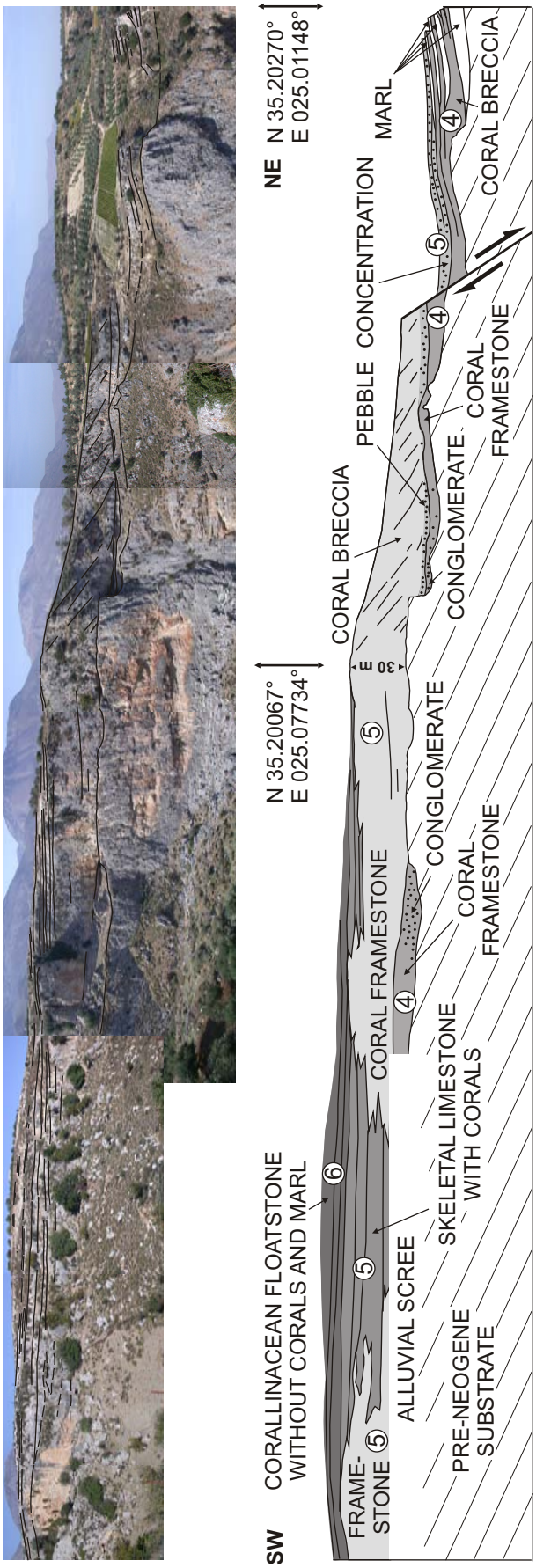

Fig. 1.10. Photo mosaic and line diagrame of Agios Antonios transect showing stratal geometries and facies distributions in a fault scarp setting. Numbers refer to depositional units described in the text.

end of Unit 5, and was replaced by level-bottom communities forming pure carbonate sediments without any contribution by zooxanthellate corals (Unit 6). These relationships imply that Units 4, 5 and 6 can be assigned to individual high-order depositional sequences formed in a context of long-term relative sea level rise. Further, from the stratal geometries a steep depositional gradient is infered in northern directions related to a fault scarp setting. In this reconstruction, Agios Antonios transect was located on the uplifted footwall block. However, uplift rates were slow as compared to eustatic sea level rise.

Unit (Fig. 2)	Geometry of sediment body	Lithofacies, depositional textures and bedding	Max. thickness (m)	Fossil content	Interpretation
4	low-angle wedge, terminates with vertical blunt contact against pre-Neogene substratum (Mesozoic limestone)	coral buildup; framestone with *in situ* corals (massive growth form), grades to NE into grain-supported coarse coral breccia with chaotically arranged coral clasts and toppled colonies. Breccia interfingers with light grey marl. Coarse, grain-supported, poorly-sorted conglomerate with well-rounded lithoclasts (pebble to boulder size) along vertical contact with pre-Neogen substrate; gradational into coral framestone	10	*Porites* and *Tarbellastrea* with massive growth forms, coralline red algae, echinoids; horizontal and vertical surfaces of Mesozoic limestone densely perforated by sponges and bivalves	sea cliff, covered with marine conglomerate and fringing reef complex
5	thick sheet; covers Unit 4 and pre-Neogene substrate; progrades to the NE. Unit wedges out to the E	two coral buildups interfinger with horizontally, parallel bedded interreef sediments; north-eastern buildup exhibits clinostratification **coral buildups**: coral framestone composed of massive and branching (rare) corals; matrix is a bioclastic marl or floatstone. Subdued submarine topography. Prograding clinobeds consits of a coarse, grain-supported coral breccia with chaotically arranged coral fragments and toppled colonies (matrix: marl) interfingering with light grey marl; downlap surface at the base of the clinobeds with concentration of pebbles (Mesozoic limestone; Paleogene sandstone) interreef sediments: skeletal floatstone or rudstone with broken and intact skeletal grains embedded in a micritic matrix	30	**coral buildup**: *Porites*, (massive, branching), *Tarbellastrea* (massive); coralline red algae, cidarid echinioids **interreef sediments**: coralline red algae, celleporiform bryozoans, isolated colonial corals (massive, *in situ*) and coral clasts (*Porites*, *Tarbellastrea*), bivalves (e.g. *Spondylus*, pectinids), gastropods (e.g. *Strombus*, *Conus*), echinoids (*Clypeaster*, cidarids), decapods (e.g. *Petrochirus*), shark teeth (Odontaspidae), bioturbation	sea cliff, covered with marine conglomerate and fringing reef complex
6	sheet-like; drapes over Unit 5	marly corallinacean floatstone grades vertically into bright marl; skeletal grains in the floatstone are mostly intact and embedded in a micritic matrix; concordant parallel stratification	>10	**corallinacean floatstone**: coralline red algae, pectinids **marl**: *Neopycnodonte*	drowned cliff; depth: moderate (limestone) - deep (marl); no sediment import from shoals

Tab. 1.6. Agios Antonios transect (Fig. 1.10). Stratal geometries, facies, stratigraphic thickness and fossil content. N 35.20067° E 025.07734°.

1.4 A mosaic of fault blocks: key to the facies model for the transitional carbonates (Fig. 1.11)

Western Irakleion Basin was formed by an array of fault blocks during the Late Miocene, bounded by the central Cretan landmass in the west (Fig.1.1). Such a tectonic setting is comparable with other examples of shallow-water carbonates of Late Miocene age described from the western and eastern Mediterranean (Brachert *et al.*, 2001, 2002; Karabiyikoglu *et al.*, 2005). Tortonian stratigraphic geometries and sedimentary facies at Moni Gorgolaini reveal a narrow coastal system characterized by clastic beaches and coral reefs, and a steep ramp-type slope into the basin to the east (Units 1-6). In the more distal positions, documented at Agios Antonios, Patéla, and Agios Thomas, carbonate sediments predominate, whereas clastic sediments are minor and present only in Units 1 and 2 of early Tortonian age. In this area, carbonate production and accumulation (Units 3-6) was controlled by fault blocks dipping to NNE or SSW that corresponded with normal faults and steep escarpments orientated ESE-WNW (Fig. 1.1). From alternating orientations of dip-slope ramps observed in the transects the movements of transfer faults orientated NNE-SSW are inferred (Fig. 1.1). The complex topography of the sea floor, therefore was an efficient barrier for the dispersal of continent-derived clastics during the Tortonian. Correspondingly, coarse shallow-water carbonates formed *in situ* are widely distributed over the distal fault blocks. However, although isolated colonial corals (*Porites*, *Tarbellastrea*) may occur from place to place in the skeletal carbonates, coral reefs are uncommon in this setting and were encountered at one steep footwall scarp position only (Agios Antonios).

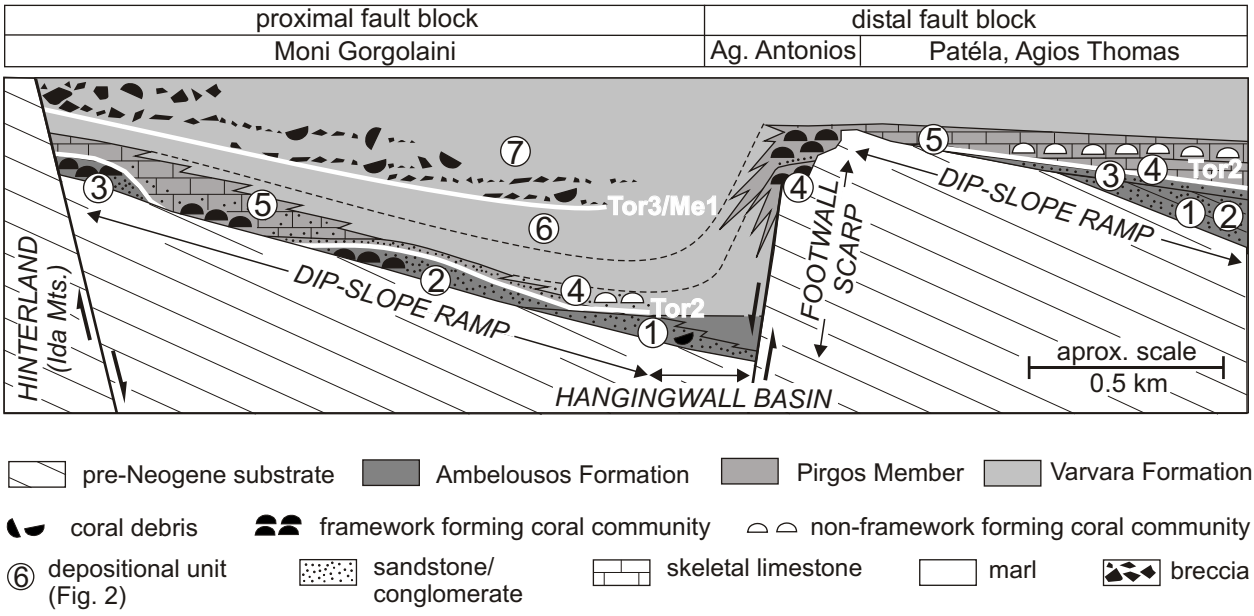

Fig. 1.11. Stratigraphic and sedimentary model of the Tortonian - early Messinian western Irakleion Basin. During the Tortonian, a complex mosaic of fault blocks controlled the distribution of shallow water facies. Proximal ramps were covered by coastal clastics and coral reefs. In settings protected from clastic input, pure carbonates spread over the ramps of tilted blocks. Level-bottom communities occurred on laterally extensive dip-slope ramps, whereas coral reefs were confined to fault scarps of shallow blocks. Later, in the Messinian the shallow ramp systems drowned, but coral reef growth persisted along a newly emerged steep escarpment slope of the western margin of Irakleion Basin. Numbers refer to depositional units described in the text.

Moni Gorgolaini-North transect documents a marked change in the depositional style from the Tortonian coastal system (Units 1-6) into a submarine debris cone environment (Unit 7) of Messinian age. Shallow-water biota of Messinian age are present only as clasts in gravity flow deposits along the present-day margin of the basin (Figs. 1.12a-b, 3.3c). These deposits may co-occur with chaotic slump masses and breccias formed through slope collapse (Fig. 1.12c). The section at the road Asites - Kroussonas documents isochronous (Unit 7) marine rockfall sediments associated with synsedimentary faulting (Figs. 1.7, 1.12d). This provides evidence for reorganisation of the Tortonian marginal ramp system into a deep hangingwall basin bounded by fault scarps orientated N-S and an uplifted hinterland during the early Messinian. An analogous scenario of tectonic reorganisation has been presented by Fassoulas (2001).

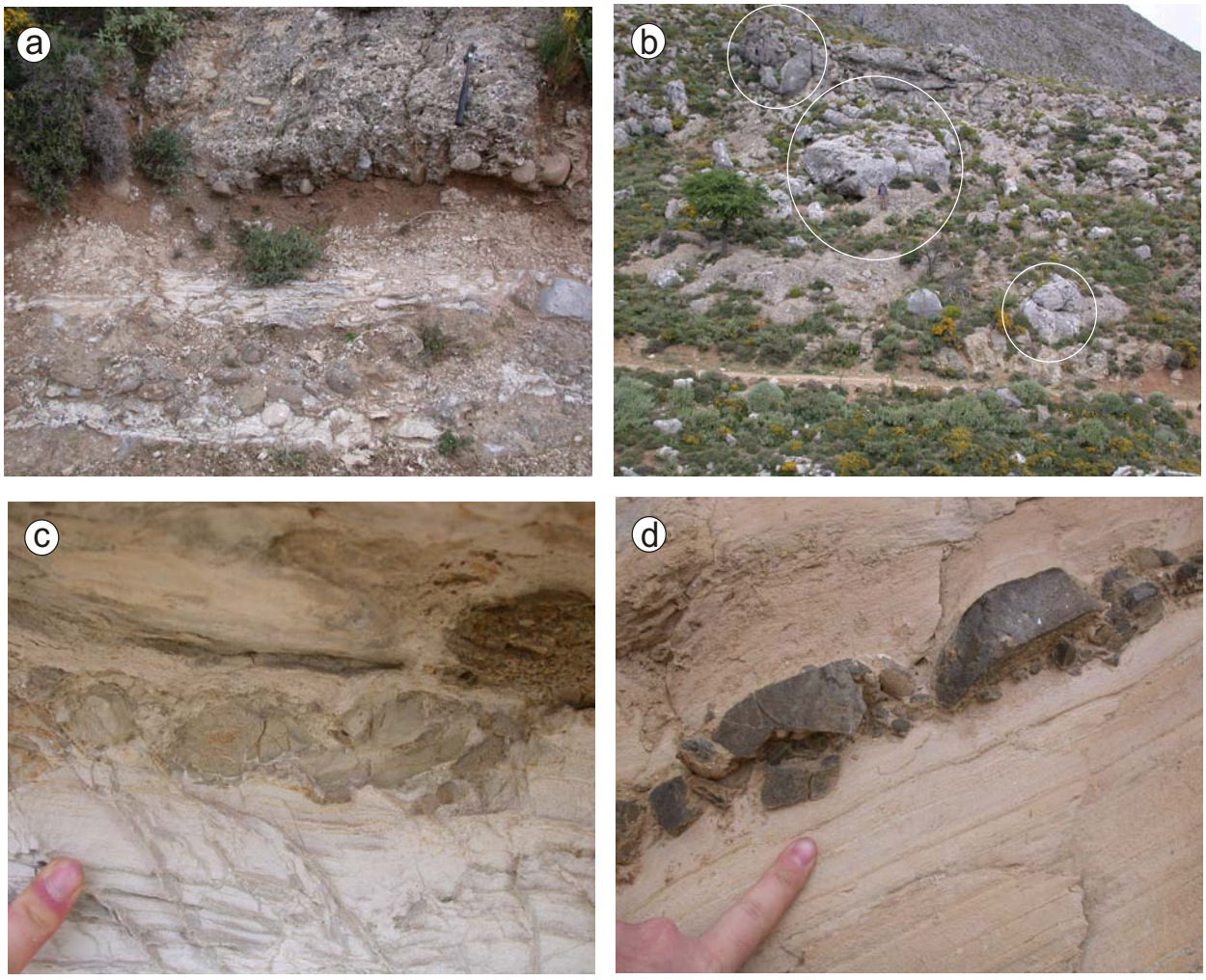

Fig. 1.12. Sediments of a deep submarine debris cone environment, proximal hangingwall basin adjacent to a steep escarpment; Unit 7. **(a)** Bright laminated marl and coarse, poorly classified conglomerates with single displaced corals (*Tarbellastrea*). Corals and rounded lithoclasts within the conglomerates indicate a shallow and high-energy source area. (a-b) NW of Agios Haralambos chapel (N 35.18519°, E 024.97892°). Hammer for scale. **(b)** Proximal facies: conglomerate with single boulders of extreme size (highlighted by white circles) that could reach a length of nearly 10 m. This facies is interpreted to represent a submarine rockfall deposit sourced from a coastal cliff via steep escarpment slope. Person for scale. **(c)** Densely packed breccia. Lithoclasts derive from Neogene marl. NW of Agios Haralambos chapel (N 35.18530°, E 024.98165°). **(d)** Thin bed of poorly classified breccia in laminated marl. Road from Asites to Kroussonas.

1.4.1 Nutrient budget: clues from continental climate

In addition to a topographical control of the dispersal patterns for clastic sediments within the basin, coastal sediments on the proximal ramps of the basin exhibit a gradual change from clastics to carbonates over the course of the Late Miocene (Fig. 1.4). Although such a pattern suggests hinterland subsidence, stratal geometries document subsidence of the basin and relative uplift of the hinterland. The change in sediment character, therefore, reflects a continuous climatic aridification (Postma *et al.*, 1993) as documented in various Tortonian and Messinian paleobotanical records from Crete (Benda *et al.*, 1974; Sachse, 1997; Sachse & Mohr, 1996; Zidianakis *et al.*, 2004). In addition to the paleobotanical data, a thick unit of laminated gypsum present in Irakleion Basin may be considered the acme of climatic aridity and clastic sediment starvation of the basin during the Messinian. A minimum of continental weathering and sediment flux, on the other hand, is suggested to reflect a declining input of dissolved and particulate organic nutrients from the hinterland into the basin. Coral reef growth in the most turbid clastic marginal environments therefore is a clear indication of low nutrient concentrations or light levels in shallow water were at no stage critical as to shut down growth of colonial corals or other mixotrophs (larger foraminifers) and to favour the thriving of heterotrophic biota and algae in carbonate communities adapted to high trophic resources in warm-water environments (Hallock & Schlager, 1986). The pure carbonate environments, therefore have been interpreted to reflect a highly oligotrophic system. It is suggested, that the Late Miocene trend of climatic aridification observed elsewhere along the alpine chain (Quade *et al.*, 1995; Krijgsman *et al.*, 2000) may have advanced the occurrence of oligotrophic shallow-water carbonate systems, both, warm-water and cool-water, in otherwise clastic intramontane basins of the Mediterranean area (Brachert *et al.*, 2001, 2002; Franseen *et al.*, 1996) and the existence of a modern-type ocean surface circulation (Meijer *et al.*, 2004).

1.4.2 Facies distributions in the transitional carbonate system

Fault scarps: The steep fault scarps of tectonic blocks reaching the shallow water zone show narrow rims of coral bioherms (Fig. 1.10) formed by massive *Porites* and *Tarbellastrea* with minor contributions of binding biota. Bioherms do not exhibit any visible stratification or zonation although clinoforms document the forereef prograding over talus deposits and older reef terraces. This indicates a steep topographical gradient along the fault scarp. The horizontal bedding of the interreef sediments continues into the bioherms without any significant slope, thus implying a subdued submarine topography of the bioherms (stratigraphic reef *sensu* Dunham, 1970). Correspondingly, interreef sediments received little reef debris and formed in a slightly deeper water than the reef crest, were carbonate production by a coralline red algal-bivalve-bryozoan community was roughly equal to that within the reef.

Dip-slope ramp and hangingwall basin: Horizontally bedded limestone formed by coralline red algal-bivalve-bryozoan-foraminiferan communities are widely distributed on ramps (Figs. 1.3, 1.5), fault scarps of drowned tilt blocks (Fig. 1.10) and hangingwall basins (Fig. 1.8). Skeletal grains are mostly intact and embedded in a micritic matrix with no preference according to shape, size and orientation (Figs. 1.9a, c). These depositional textures do not exhibit signs of physical disturbance by waves and storms, reflecting accumulation in a protected sedimentary environment below WAD and beyond the reaches of any carbonate sediment input from the shallow high-energy zone. Individual beds of skeletal limestone may contain isolated, massive corals in life position (*Porites*, *Tarbellastrea*; figs. 1.9b, 5.6d). Ragged margins of the colonies indicate that sedimentation rates were lower than, or equal to coral growth. Toppled colonies and coral fragments were not observed, thus excluding a potential shallow, high-energy environment or import from a shoal area. The coral facies is taken to infer calm, moderately shallow and warm water in a soft substrate environment. A protected shoal area with a low wave energy level is discarded because of the open and unsheltered setting of the dip-slope ramps.

1.4.3 Depth zonations and production rates: evidence from sea level changes

Stratal patterns of landward and basinward shift in coastal onlap are consistent in all transects and thus document sea level changes. These geometrically defined units comprise three phases of long-term relative sea level rise that are considered equivalent to 3rd order eustatic sea level changes (Haq *et al.*, 1988; Hardenbol *et al.*, 1998; fig. 1.2). Coral bioherms present in ramps (proximal transects) or fault scarps (distal transects) do not exhibit any vertical or lateral ecological zonations within a given unit. Thus, they kept up with sea level rise but did not develop significant sea floor relief and ecological zonations. Within the same units, in a more distal position, skeletal carbonates formed by level-bottom communities, however, exhibit vertical (and horizontal) drop-out sequences of photoautotrophic biota related to water depth changes (Fig. 1.13). In such a drop-out sequence, lower units exhibit a corallinacean-*Porites*-*Heterostegina* association that lived in shallow water which passes upwards (and outwards) into a corallinacean-*Heterostegina* association from intermediate depths, and finally into an association consisting entirely of corallinacean algae in the deepest water setting of the *in situ* formed skeletal carbonates. The alveolinid *Borelis* occurs in coral reef environments. The zonation and distributions patterns of both foraminiferan taxa (*Borelis*, *Heterostegina*) fits their modern depth and substrate relationships (Langer & Hottinger, 2000). The deepening upward sequences formed by the level-bottom carbonate systems imply, that net sediment accretion (production and accumulation) in this setting did not keep up with relative sea level rise (4th order) and was, therefore, not as efficient as in the shallow reef systems.

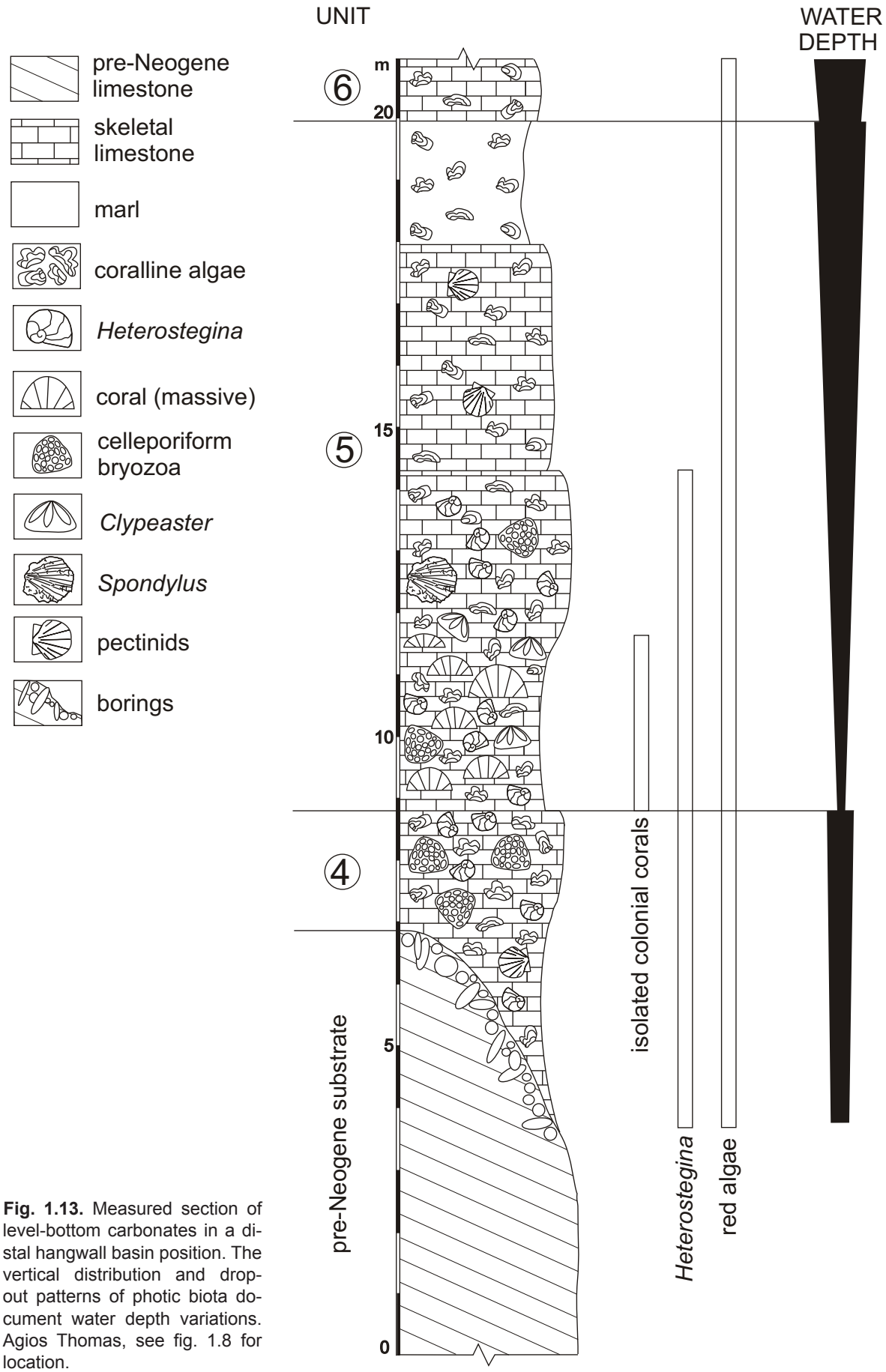

Fig. 1.13. Measured section of level-bottom carbonates in a distal hangwall basin position. The vertical distribution and drop-out patterns of photic biota document water depth variations. Agios Thomas, see fig. 1.8 for location.

1.4.4 Temperature: a true tropical-temperate transitional system

The existence of true coral reefs over the Tortonian and Messinian in the western Irakleion Basin documents “tropical” sea surface temperatures (SST) above 18°C in winter (Abram *et al.*, 2001). Correspondingly, associated skeletal carbonates formed by level-bottom communites do not likely reflect cool water conditions or high trophic resources (Hallock, 1987; Hallock & Schlager, 1986; Carannante *et al.*, 1988). However, extensive carbonate production takes place in modern reef systems below the zone of active reef growth by level-bottom coralline algal-bryozoan and foraminiferan communities (Dullo *et al.*, 1990). In the Late Miocene carbonates of the western Irakleion Basin, the restricted geographical distribution of reef frameworks do not exhibit any ecological zonation, and the coexistence of the reef and level-bottom systems on very small spatial scales (i.e. stratigraphic reefs and level-bottom systems of Agios Antonios transect) suggests a shallow transition depth for the reef and level-bottom carbonate systems. Because a turbid muddy water loaded with nutrients can be discarded from the low clastic content of the carbonates, the shallow transitional depth of the two carbonate systems found for the Late Miocene carbonates is not an effect of low light penetration or high nutrient concentrations (Hallock & Schlager, 1986). It is concluded to be an effect of SST near the lower threshold temperature of reef systems were the base of the reefs emerges into very shallow water (Betzler *et al.*, 1997b). Such an interpretation supports SST reconstructions based on coralline red algal communities that document moderate SST variation around the reef threshold level for the Late Miocene of southern Crete (Kroeger, 2004).

1.5 Conclusions of chapter 1

(1) Laterally extensive level-bottom carbonate production and accumulation took place in the Tortonian and early Messinian Irakleion Basin, Crete (Greece). These coralline algal -mollusc-bryozoan carbonate sediments may be easily confused with cool-water carbonates, because coral reef growth was sporadic and confined to the marginal zone of the basin and of uplifted blocks.

(2) Analysis of stratal geometries along continuous outcrops provides the basis for the chronostratigraphy of the shallow water sediments. Although the geometries of the sediment bodies were controlled by active fault blocks, consistent patterns of shifting coastal onlap reveal a dominant control by 4^{th} and 3^{rd} order eustatic sea level changes.

(3) Late Miocene sea floor topography of the basin created by active fault blocks prevented the dispersal of clastics imported from the central Cretan landmass. Increasing aridity and decreasing continental weathering, sediment discharge and continental nutrient flux (dissolved and particulate organic matter) led to an oligotrophic and clear water column forming an ideal environment for carbonate production. Also, the Late Miocene trend of aridification may have effected the widespread occurrence of shallow-water carbonate systems over the whole Mediterranean province.

(4) Drop-out sequences of phototrophic biota in vertical section define three relative water depth zones for the shallow water carbonates. Massive colonial corals (*Porites*, *Tarbellastrea*) and the foraminifer *Borelis* occured in the shallow zone, the foraminifer *Heterostegina* persisted into the intermediate zone, whereas coralline red algae were still present in the deepest zone.

(5) Small coral reefs formed principally by massive *Porites* and *Tarbellastrea* did not develop any vertical nor lateral zonations and significant submarine topography. On a short distance/shallow water depth, the reefs were replaced by level-bottom carbonate systems (horizontal and parallel stratification, *in situ* production) dominated by coralline red algae, molluscs and bryozoans present in dip-slope ramps and hangingwall basins. The low diversity of reef corals and the shallow transitional depth from the reefs into the level-bottom systems reflects surface water temperatures that were close to the lower threshold level of the tropical carbonate systems.

2 Early Tortonian coral growth patterns in central Crete (NW Messara)

The patterns of early Tortonian coral growth have been studied in the northwestern Messara Basin near the towns of Ambelousos and Gergeri, Rouvas municipality (Fig. 2.1). Here, laterally extensive beds formed by branching (Fig. 2.8b) or massive (Figs. 2.8c, 3.3a, d) corals (*Porites* and *Tarbellastrea*) intercalate and interfinger with conglomerate and sand- or siltstone of the Ambelousos Formation deposited in coastal environments (Meulenkamp *et al.*, 1979). The coral beds overlie dark grey lagoonal shales. Changing compositions of mollusc faunas in the shales indicate repeated salinity shifts from brackish to marine. The coastal clastics border the margins of the Ida Mountains and a fault-block north of Agia Deka. Both coastal sediment bodies are separated by an area with a thick succession of offshore deposits.

Although, this region exhibits extensive outcrops of coral biostromes, outcrop conditions are not good enough to document stratal geometries for the specification of depositional units and detailed correlation with the western Irakleion Basin.

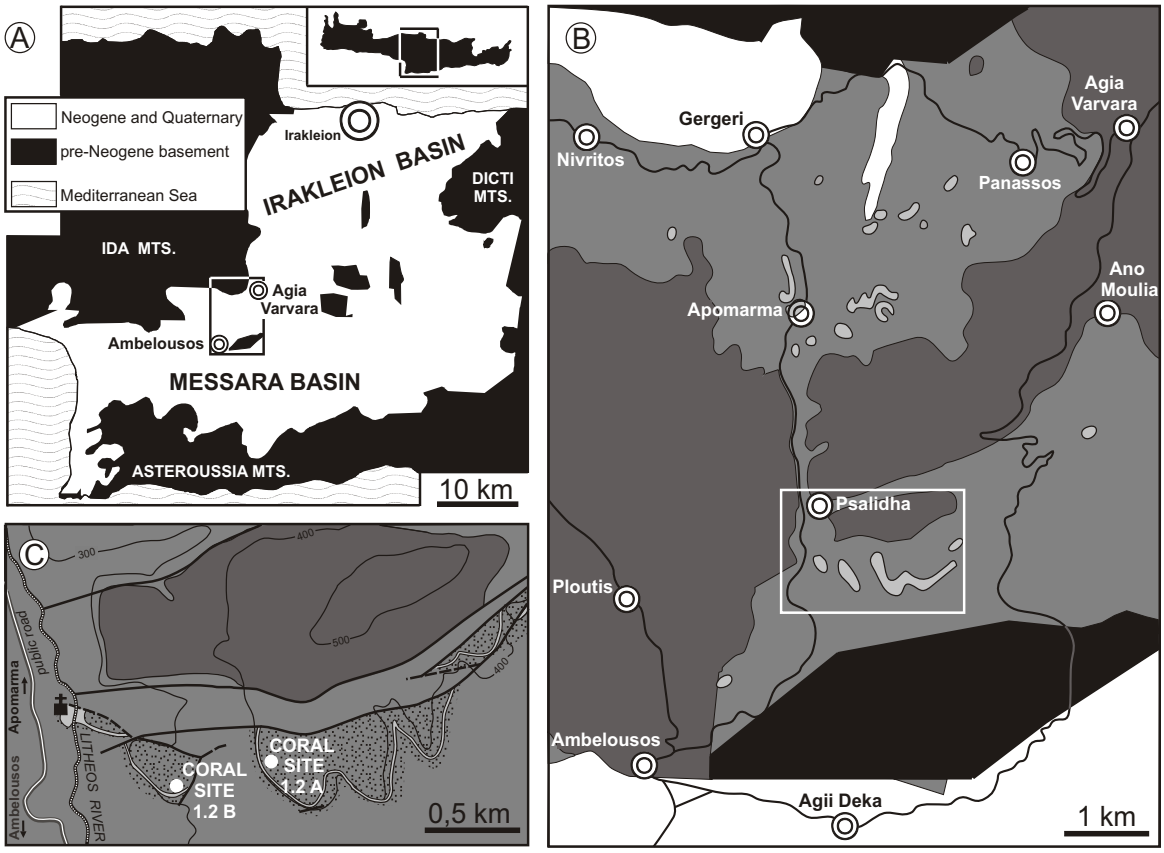

Fig. 2.1. Location of Apomarma and Psalidha fossil reef sites, Rouvas Municipality, Central Crete (Greece). **(A)** Geological overview map; inset shows location of geological map shown in fig. 2.6. Modified from Meulenkamp *et al.* (1979).

2.1 Apomarma locality

In the surrounding of Apomarma, *Porites*-biostromes consits of sheet-like, metre-thick piles composed of poorly classified, randomly arranged branch fragments of *Porites* and toppled *Porites*-bushes (Fig. 2.3c; allobiostromes *sensu* Kershaw, 1994). They are intercalated with coastal sandstones and conglomerates (Figs. 2.3a, 3.2B) and show no internal lateral facies zonation, even in outcrops with 100 m lateral exposure (Fig. 2.3a). Interstital sediment is sandy silt and marl that contain spins of cidarid echinoids (abundant), small gastropods (rare), small bivalves (rare), decapods (abundant) and bryozoans (common).

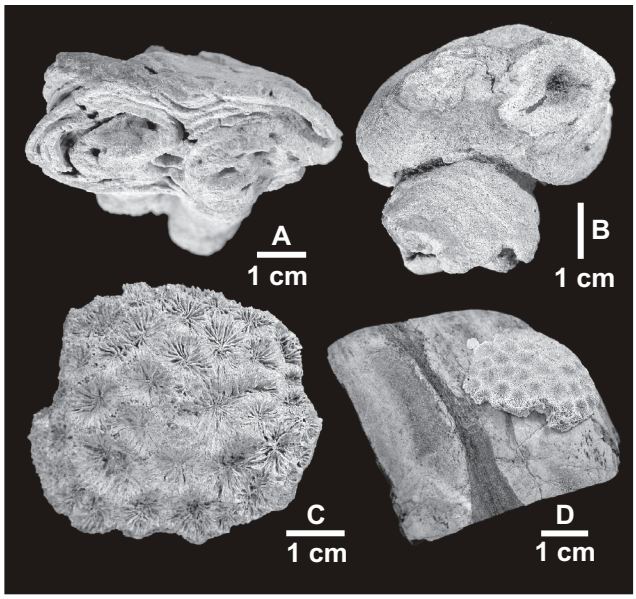

Fig. 2.2. Corals from the pioneer coral community of the Apomarma coral rubble fields (Ambelouzos Fm, NW Messara). **(A)** A *Porites* with flat platy growth form encrust two *Porites* branch pieces. By doing so, the coral bound loose coral debris and stabilized the substratum. **(B)** Mushroom-shaped *Porites*. This growth form developed from a branched coral fragment that proceeded its growth after deposition as a flat overlying colony and points to the high regeneration potential of *Porites* (van Woesik, 1998; Henry & Hart, 1999). **(C)** Flat *Acanthastrea* colony. The small size of the colony reflects the unfavourable living conditions for this taxa. In other Late Miocene coral locations in central Crete that are associated with a more pure carbonate facies, this coral is more common and build up massive colonies up to 0.5 m in diametre. **(D)** Pebble from a coastal conglomerate colonized by *Siderastrea*.

Rarely, ramose branching *Porites* in live position occur. They are found preferentially at the roof of a coral rubble pile (Fig. 2.3b), or occasionally also as layers or patches encased in coral rubble. Some outcrops show areas with diagonal growing *Porites*, that all point to the same direction similar to a cornfield, allocated by storm. Characteristic for this corals are rootlike, platy extensions at their base that interfinger with the surrounding sediment.

The broken coral pieces are encrusted with flat *Porites* plates that overlay the sediment surface (Fig. 2.2A). Some of them developed at the end of a branch fragment with still living tissue that continued its growth with platy morphology after breakage (Fig. 2.2B). *Siderastrea* (Fig. 2.2D; small nodules, <10 cm) is also very common in this facies. Small (15 cm diametre), *in situ Tarbellastrea* and *Acanthastrea* appear sporadically with thin platy growth forms (Fig. 2.2C). Encrusters (vermetids, bryozoans, serpulids, small oysters) and borers (bivalves, polychaets) in/on corals are very rare, while prasitic, coral inhabiting barnacles (Pyrogomatinae) are abundant.

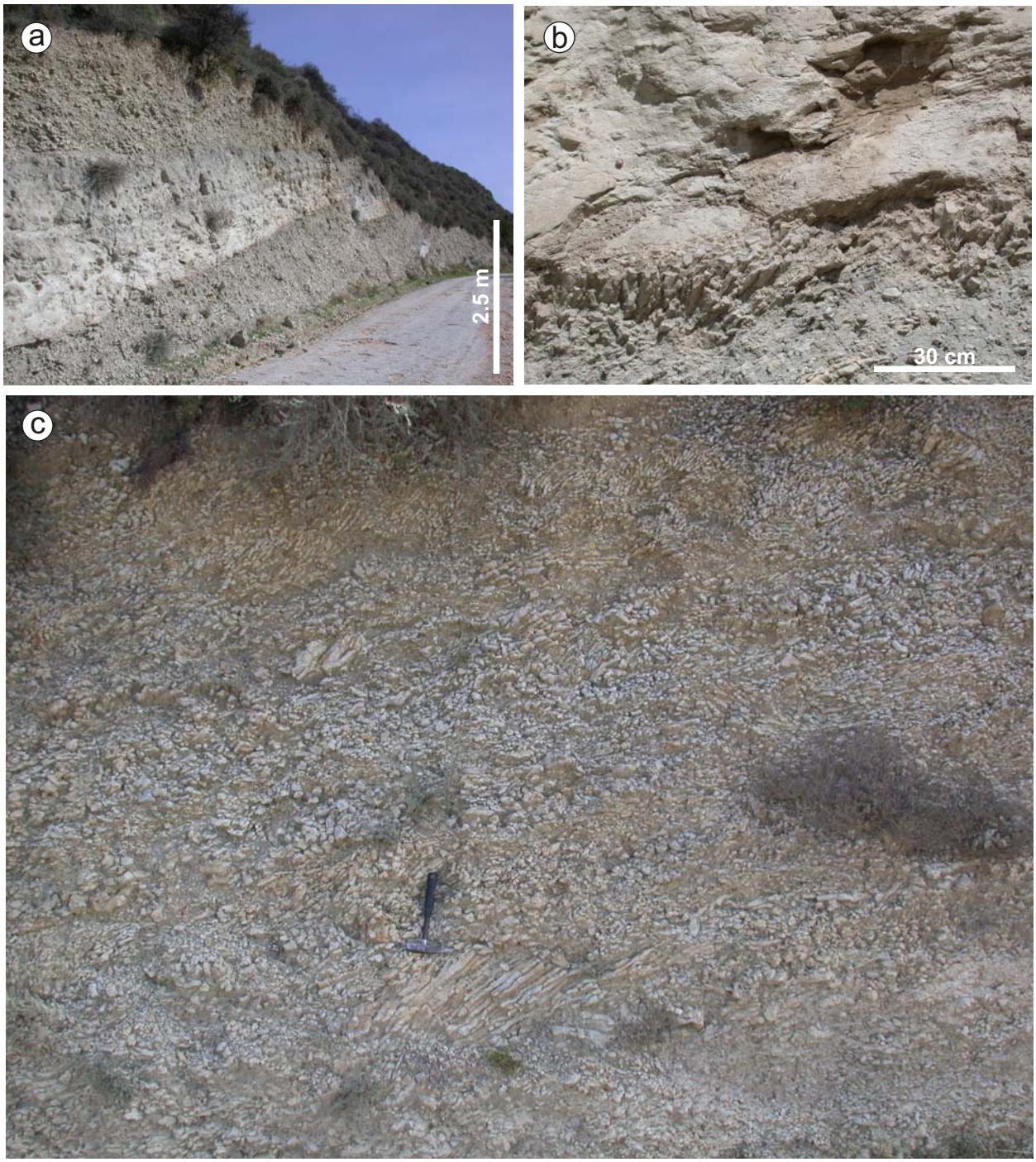

Fig. 2.3. Coral rubble accumulations from the Apomarma area (Amblousos Fm., NW Messara Basin; N 35.11420°, E 024.96412°). **(a)** Sheet-like accumulations of coral debris (allobiostrome) with intercalated coastal sandstone. Field aspect of geological section B (Fig. 3.2). **(b)** Relict of *in situ* thicket-framework on top of the lower coral rubble pile in fig. 2.3a. Vertical, dense standing *Porites* branches are capped by the overlying sandstone. At its base, the sandstone abundantly contain coral fragments. **(c)** Inner texture of a coral rubble pile showing chaotically distributed, elongated coral pieces and toppled coral bushes in a muddy matrix. Hammer for scale.

Because of their uniform branch-form and poorly classification, the coral pieces are interpreted to be derived from *Porites*-biostromes with thicket-like framework that regularly had become destroyed and has been deposited on site. The vast stratiform and uniform extension of the coral debris deposits (Fig. 2.3a) points to a flat, gentle sloping sea floor relief.

A pioneer coral community with platy *Porites* and *Siderastrea* stabilized the loose coral rubble and provided the base for restarted thicket growth (Fig. 2.2; Rasser & Riegl, 2002). Other binding agents are absent (e.g. coralline red algae) or not preserved (e.g. seagrass). The rarity of borings and biogene encrustations in/on coral clasts indicates that the majority of coral debris was not exposed for long time and therefore must have been formed by rapid catastrophic events that were intermitted by episodes with framework regeneration. The climax situation is represented by vertically orientated, dense *Porites*-thickets on top of the rubble piles. Weakening of the framework is displayed in areas with dense stands of diagonal growing *Porites.* Here, the framework was allocated by strong currents as shown by the adjusted alignment of colonies. But because of their dense stand, corals are interlocking and base upon each other. Additionally, platy outgrowths at their base anchored the corals after tilting. Both stabilized the framework and hampered its total destruction. Because of the minor affection by boring and encrusting biota, but high abundance of coral inhibiting barnacles, free standing parts of the corals must have been completely covered by tissue. In deeper regions of the thicket, trapped sediment covered dead colony parts instead of living tissue. Bioerosion was therefore only a neglecting factor for framework destruction.

Each rubble pile represents several of the ecological successions described above as indicated by intercalated relicts of *in situ* thicket framework and the presence of platy corals in growth position over the full section. The composition of coral fauna demonstrates, that the setting was unconfortable for *Acanthastrea* and *Tarbellastrea*, prefering a calcareous environment with low terrigenous supply. In contrast, *Siderastrea* is very common. Modern *Siderastrea* species are charactristic inhabitants of mobile substrates and tolerate even complete spillage for some time (Lirman *et al.*, 2002).

Towards offshore, coastal sandstones and conglomerates pass into marl with abundant molluscs (e.g. *Ancilla*, *Aphorrais*, *Cerithium*, *Clavilithes*, *Conus*, *Cyprea*, *Lemintina*, *Turritella*, *Turris*, *Vittularia vindobonula*, *Xenophora*, cassoidea, naticidae, muricidae, *Glycimeris*, *Crepidula*, *Chama*, cardidae, veneridae, scaphopods). At the distal edge of the coastal sediment body (sandstone/conglomerate), *in situ* thicket framework composed of vertical standing *Porites*-branches (Fig. 2.4a) is preserved that is situated directly on coarse coastal clastics. Interstitial sediment is sandy marl. It grades on a short distance

(10 m) in a talus, build up by elongated *Porites*-fragments, that is attached on foot of the thicket-facies and interfingers with the offshore marl. This thicket-type is interpreted to represent an equivalent of the rubble fields in a deeper, more calm environment, where *Porites*-thickets are better protected against wave destruction. The rapid facies change from *in situ* thicket to talus and offshore deposits indicate a highly inclined slope.

Besides, coral biostromes occur on top of coastal clastics or older *Porites*-thickets. They are mainly composed of massive corals in life position (Figs. 2.5A, 3.3d). The corals form lateral extensive, sheet-like biostromes without any facies zonation, indicating a flat topography of the seaground. *Porites* and *Tarbellastrea* are dominating. Ancillary, *Acanthastrea* occurs. Some colonies reach a length of 1.5 m. Interstitial sediment is bioclastic rudstone with coral fragments, bryozoans, corallinaceans, molluscs, cidarid spines, which implies a high water turbulence.

Branching corals in life position dominate distally in more calm environment at the edge of the coastal sandbody (*Porites*; fig. 2.5B). The corals are situated on reef derived rubble (rudstone), that interfingers with the offshore marl (Fig. 2.4b). Massive corals occur only subordinatley ingrown between the *Porites*-branches. More abundant are reworked, massive corals that are imported from a shallower source area.

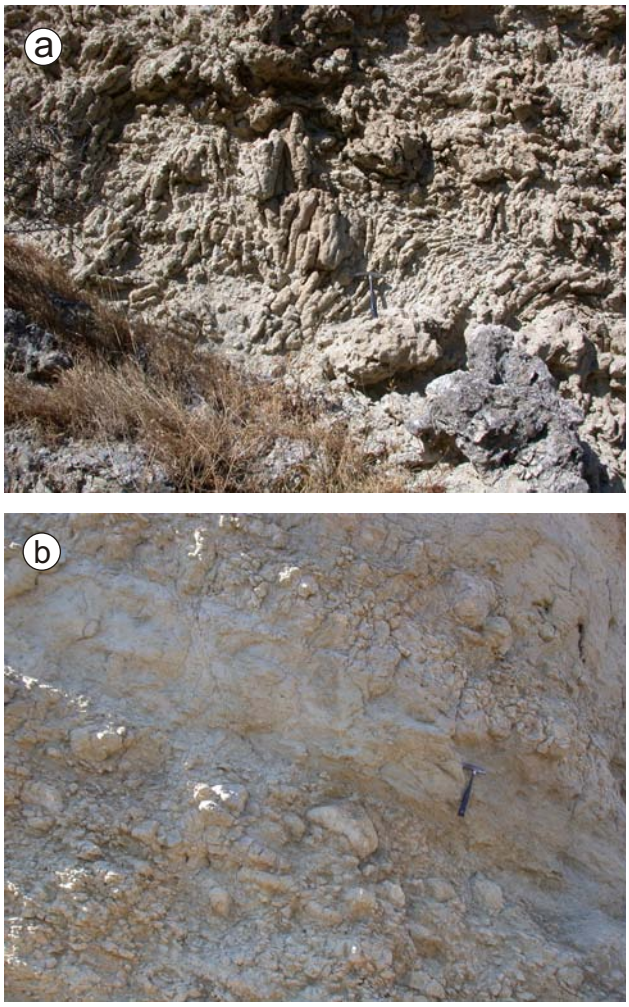

Fig. 2.4. (a) Branching *Porites* in life position at the distal edge of the coastal sedimentbody in the Apomarma area. N 35.12436°, E 024.96802°. **(b)** Coral breccia in front of the coastal sediment wedge interfingering with offshore marl. Older breccia beds contain only *Porites*-branches (not in the picture), younger beds includes additionally massive corals. This reflects a transition from siliciclastic evironment with *Porites*-thickets to a more carbonate-dominated environment with higher diverse coral constructions composed of predominantly massive growth forms. Apomarma area, early Tortonian. The distance between locations of outcrops of figs. 2.4a and 2.4b is 40 m. Hammer for scale.

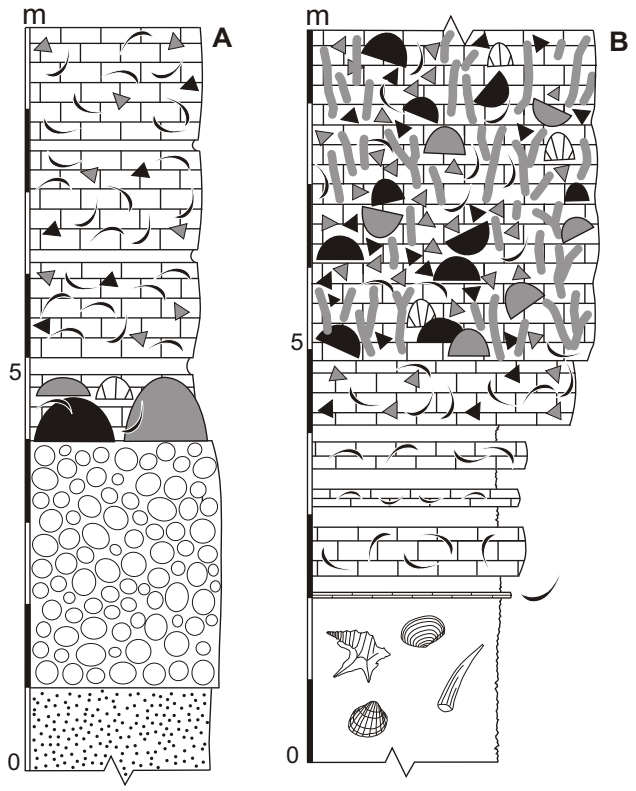

Fig. 2.5. Measured sections of biostromes in carbonate facies. from the Apomarma area. **(A)** Proximal setting (N 35.12128°, E 024.96757°): The biostrome is situated on a nearshore conglomerate. Drowning of the biostrom is indicated by reef derived bioclastic detritus that covers the corals and interfingers with offshore marl. Coral Site 1.1 of chapter 5 **(B)** Distal setting (SE Nivritos): A prograding talus of reef rubble is colonized by deeper water coral association, dominated by branching *Porites* in life position. See fig. 2.9 for key of signatures.

2.2 Psalidha locality

Near Psalidha (Figs. 2.1, 2.6), corals form sheet-like bodies of metre thickness (biostromes). Thicket-like biostromes, constructed by branching *Porites* with a muddy siliciclastic matrix (sandy marl or silt) alternate with biostromes composed of massive corals (*Porites*, *Tarbellastrea*, minor *Acanthastrea*) and carbonate interstitial sediment (poorly classified rudstone). The biostromes are stacked vertically, forming a carbonate buildup with a layer-cake stratigraphy (Figs. 2.8a, 2.9). At the base (Fig. 2.8b) and at the top (Fig. 3.3a) of the buildup, biostromes with preserved framework exist (autobiostromes *sensu* Kershaw, 1994). Otherwise, toppled and *in situ* corals coexist (Fig. 2.8c; parabiostromes *sensu* Kershaw, 1994).

Offshore, in deeper water a talus with bioclastic debris (packstone and rudstone) is attached at the bioherms (Fig. 2.9).

The buildup developed on a gentle inclined dip-slope ramp, that dips to NW and is bordered by NE-SW trending normal faults that divided the buildup in 4 tectonic blocks (Fig. 2.6).

At the base of the structure, an erosional surface exists that documents emersion (Fig.

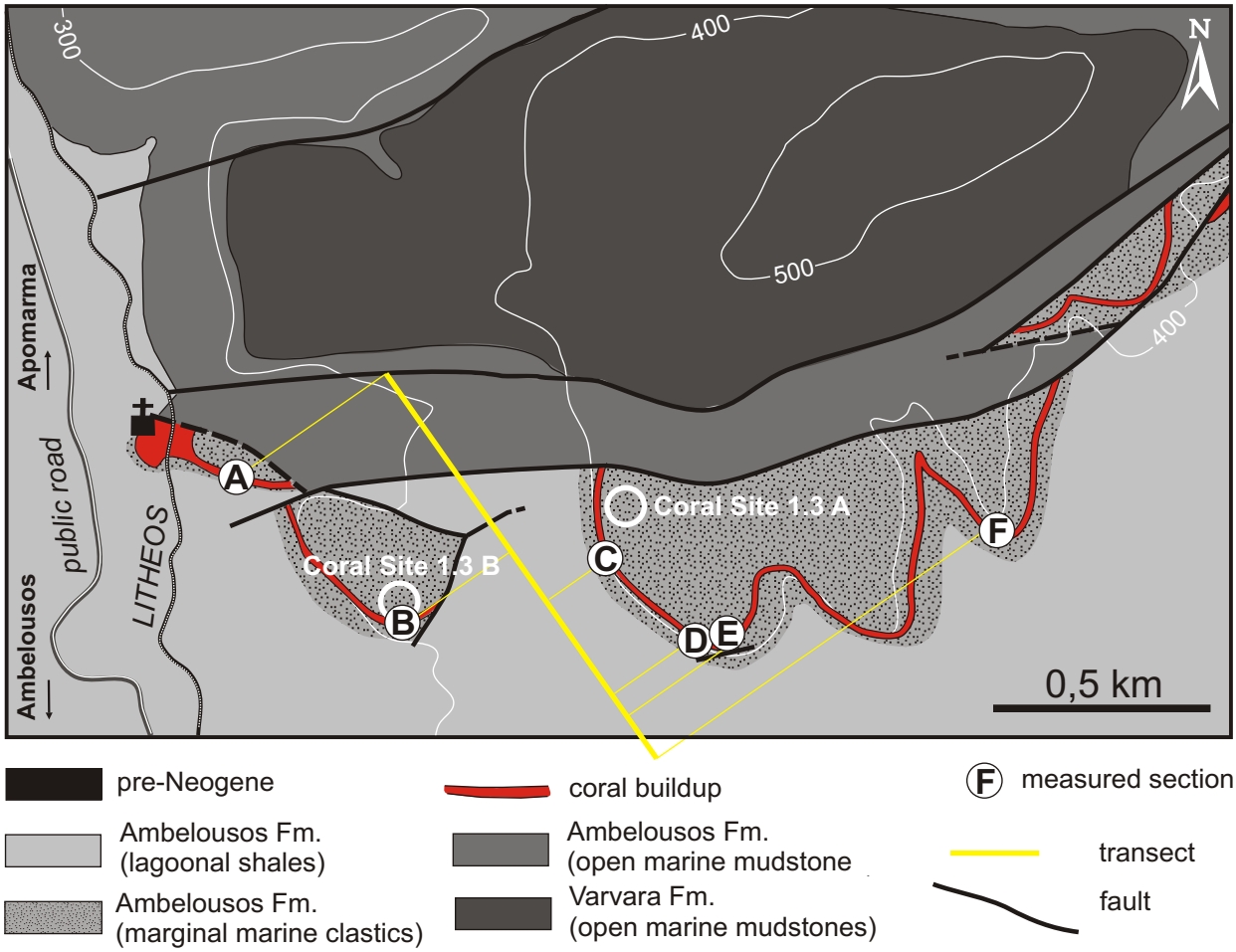

Fig. 2.6. Detailed geological map of Psalidha coral buildup with locations of Coral Sites 1.3A & B of chapter 4, measured sections and course of the schematic transect in fig. 2.9.

2.9). It is cut in coastal sands that contain a coral community with predominantly platy encrusting *Porites* (Fig. 2.8d) and subsidiary ramose branching *Porites* that are mostly toppled and broken. This facies indicate a turbulent, very shallow environment by intensely interlocking of corals with coarse coastal clastics (conglomerates and sandstones) and the streamline shape of the dominant sheet-like encrusting growth form, resulting in a high resistance against wave agitation.

Some channels that protuding from the erosional surface are populated by massive *Tarbellastrea* and branching *Porites* in live position (Fig. 2.7). Others are completly filled with coral rubble, sandstone and conglomerate. Mostly, corals populated only the channel margins. Here it is conspicious that massive and branching colonies show flattened top sides at the time when they reach the upper edge of the channel. Instead, corals that grew in deeper parts of the central channel have convex top sides (Fig. 2.7).

It is suggested, that in active channels coral growth did not take place or was restricted to the channel margins and inactive channels were colonized by corals in total. This pattern is well-known from other fossil (Santisteban & Tarberner 1988; Hayward 1982) and

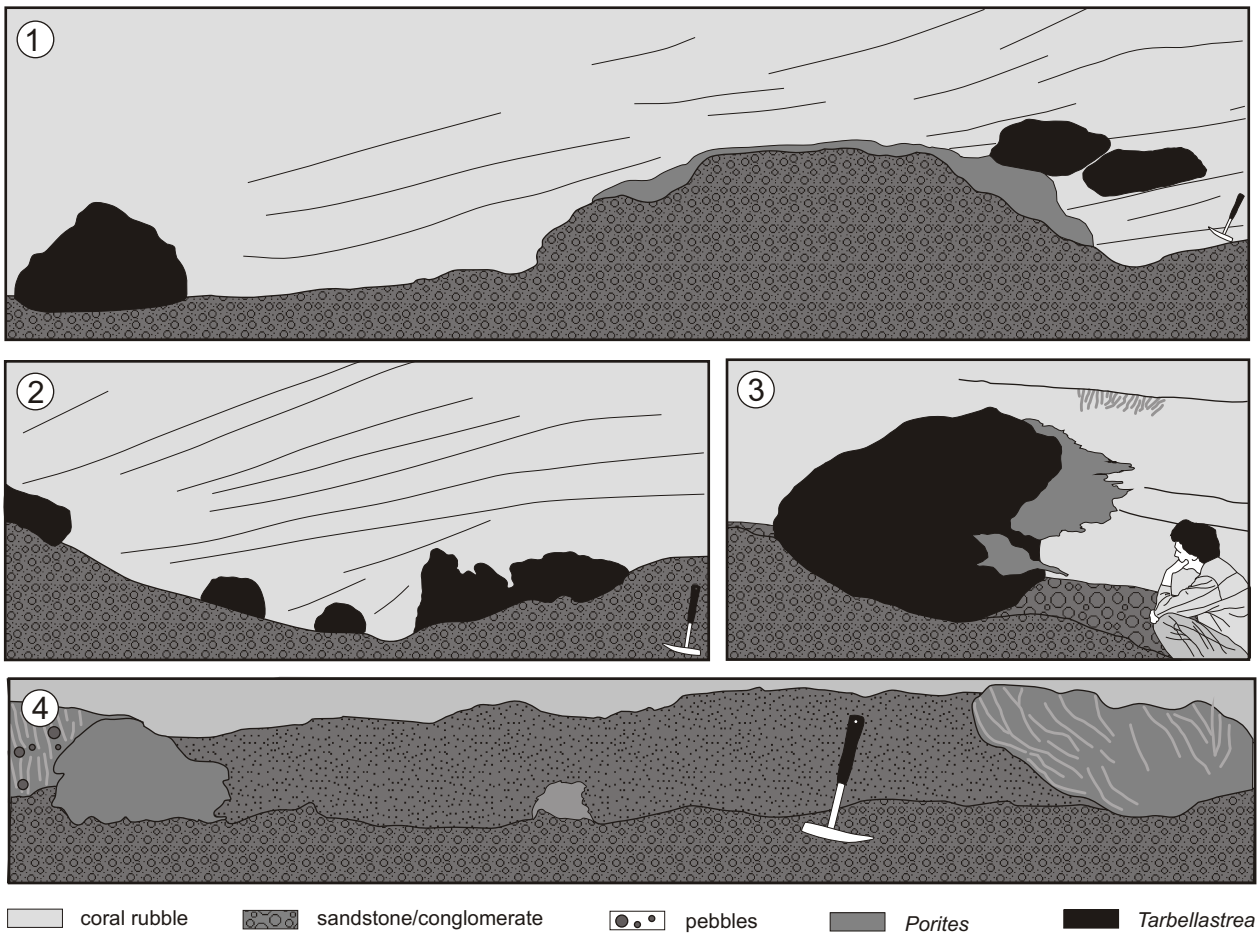

Fig. 2.7. Schematic line drawings showing zonation of coral morphologies in channels at the base of Psalidha buildup (sections 1-3 are slightly tilted). **(1-3)** In deeper position of the channel center, higher convex colonies developed. Vertical growth at the channel margins was limited by the sea level as indicated by planar top sides of corals. In the shallowest areas between the channels, thin, platy colonies developed, which gave wave action little working surface. The presence of corals at the channel margins as well as in the channel center shows, that no deposition took place during coral growth. **(3)** A massive *Tarbellastrea* is encrusted by thin platy *Porites* colonies. In protected settings, e.g. in lee of the large coral, the encrusting *Porites* produced fan-shaped outgrowths, which loomed in the open water. **(4)** Branching *Porites*, situated at the channel margins and trapped coarse gravel that was transported in the middle of the channel during growth. Because current velocity and abrasion was highest in the channel center, fragile branching *Porites* favored higher areas at the channel margins that are less affected by transport processes, whereas platy encrusting *Porites* populated also the center of the channel. They build up massive coral heads, that consists of adnate *Porites*-plates with ingrown pebbles. Finally, the channel were filled with sandy mudstone and covered with coral debris that drowned the corals.

recent reefs (Perry 2003, Riegl 2001) and is interpreted as an adaption to avoid sedimentation rates and abrasion that are highest in the center of the channels (Riegl 2001).

The shallowest areas between the channels were populated by platy encrusting *Porites* only (Fig. 2.7/1). From the observation that higher colonies are restricted to depressions while shoals are occupied by lower, platy corals that gave wave action little working surface, it is inferred that the distribution of coral growth forms are related to water depth. This is further indicated by planar coral surfaces from neighboured colonies (branching, massive) that always correlate to a distinct level that is equivalent to the channel surface and therefore must tag a former sea level pointing to a water depth shallower than 5 m.

The backstepping geometries of the biostrome units above the erosional surface document a relative sea level rise and the layercake-like growth pattern of the biostrome stack demonstrate, that coral growth was inline with newley created accomodation space (Fig. 2.9). From the large size (1x1x2 m) and massive growth forms of *Porites* and *Tarbellastrea,* a maximum water-depth of 10 m is inferred for massive corals (Pomar *et al.*, 1996; Perrin *et al.*, 1995). Analogue, this is also assumed for massive corals in the Apomarma area. The development of a *Porites*-thicket directly on the erosional surface (oldest biostrome unit) and the backstepping of the younger biostrome units implies that such thickets established themselves in even shallower water. Generally, branching *Porites* are thought to occur in deeper water than their massive counterparts, due to their higher susceptibility against breakage in turbulent water. The apparently invers zonation pattern that branching *Porites* occur in shallower water than the massive growing *Porites* is also documented in many Late Miocene examples of the Mediterranean realm (Spain, Almeria Province: Dabrio *et al.*, 1981; Riding *et al.*, 1991; Braga & Martín, 1996); Spain, Fortuna Basin: Santisteban, 1981; Algeria: Saint Martin, 1990; Sicily and Pelagian Islands: Grasso & Pedley, 1989; Pedley, 1996; Italy, Salento Peninsula: Bosselni *et al.*, 2002) and has been explained as a fast growth response to relatively rapid sea level changes or to increasing cooler and high-nutrient level, or as a morphological adaption to withstand high levels of fine-grained clastic sedimentation (Bosselini *et al.*, 2002). The latter is suggested for the Apomarma area, where coral biostromes constructed by massive and branching corals developed in the same setting, as shown in the geographically congruent facies-belts (biostrome-facies, slope-facies, talus-facies) of biostromes with muddy (branching corals) and carbonatic matrix (massive corals). Discrepancy between both biostrome-types consists only in the predominantly coral growth form and the amount of terrigeneous supply from the hinterland.

Synsedimentary block movement produced a backreef lagoon on the subsided block south to Psalidha buildup (Fig. 2.9). It is filled with light grey marl that contains abundant molluscs (burrowing bivalves, *Pinna*, *Spondylus*, *Conus*, *Turritella*, archaeogastropods), rare isolated manatee bones and *Siderastrea* corals (nodules, < 10 cm). Other *in situ* corals are oberserved only exceptionally and occur on secondary hardgrounds (e.g. a

Fig. 2.8. *(next page)* Field aspects of Psalidha locality, NW Messara Basin, Unit 1. **(a)** A layercake-like stack of horizontally lying biostromes is continuous over hundreds of metres. The coral buildup is dissected by normal faults and distributed over different tectonic blocks (see fig. 2.6). Double arrow marks position of measured section B. Boxes b, c and d refer to locations of figs. 2.8b, c, d. Circles mark Coral Sites 1.3 A, B of chapter 4. **(b)** Biostrom with dense thicket-like framework, constructed by ramose branching *Porites* in live position. Interstitial sediment is sandy mudstone. **(c)** Parabiostrome composed of massive corals (predominantly *Porites* and *Tarbellastrea*, minor *Acanthastrea*). Growth-framework pores are filled with bioclastic rudstone. Coral Site 1.2 of chapter 4. **(d)** Sheet-like encrusting *Porites* in coastal conglomerate. Earliest growth stage of Psalidha buildup (below the erosion surface). Hammer for scale **(e)** Reef wall facies: branching *Porites* in live position. Hammer for scale.

Fig. 2.8. Field aspects of Psalidha locality

thin *Tarbellastrea* colony on a *Spondylus* shell). During the stage before the last bioherm developed, synsedimentary faulting formed a steep escarpment slope at the northern margin of the builup that was populated by a coral association of branching (dominant; *Porites*) and massive (minor; *Porites*, *Tarbellastrea*, *Acanthastrea*) corals *in situ* (reef wall facies; figs. 2.8e, 2.9). Coral fragments and intact toppled colonies deposited between them. This facies is assigned to a deeper, more calm environment with import of coral debris from the shallow zone (Pomar *et al.*, 1996; Perrin *et al.*, 1995). The high amount of coral debris give evidence that the coral framework became periodically destroyed in the shallow water. But the large size of some massive corals (*in situ* and toppled) points to relative long time intervalls (some hundreds of years) with constructive coral growth between the destruction phases. Before the last growth stage of the buildup, faulting stopped, as indicated by the vast expansion of the youngerst biostrom (Fig. 2.9). Its fabric and topography is well preserved by a drape of poorly classified sandstone and conglomerate with a high amount of silt (Fig. 3.3a). The sandstone contains a bed with allocated and often broken *Crassostrea* shells.

Whereas most of the corals have been transformed into calcite, some corals of the uppermost biostrome, situated along the contact with the hangingwall sandstone/conglomerate, have fully retained their original aragonite mineralogy, microstructure and skeletal porosity (see chapters 3-4). Here, a Sr-isotope age of 10 Ma has been assigned (Kroeger, 2004). Contrary, in the interstitial bioclastic rudstone in carpets with predominantly massive corals, aragonitic constituents are selective solved, so that the limestone has a characteristic high moldic porosity.

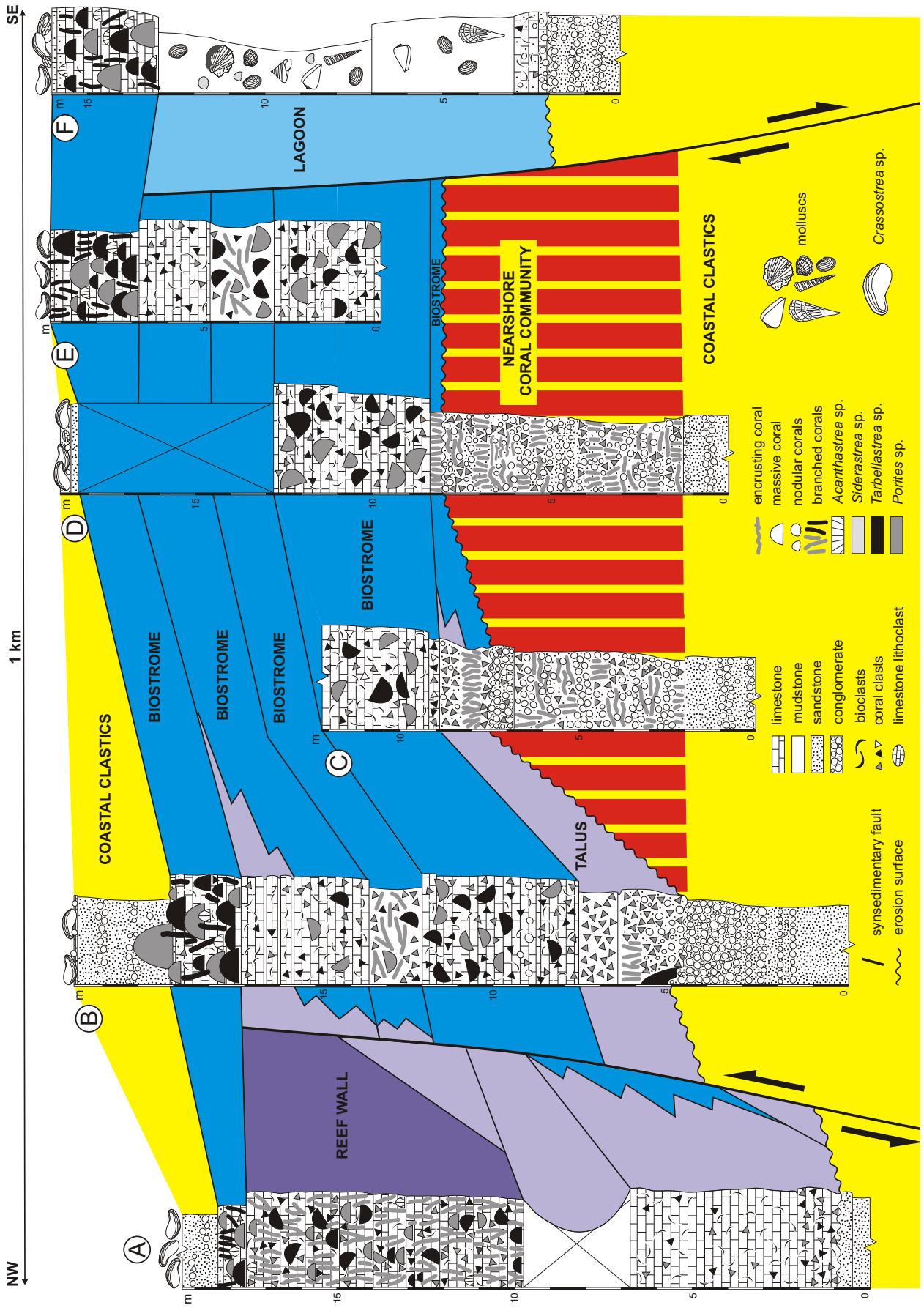

Fig. 2.9. Diagram showing stratigraphic relationships and facies architecture of Psalidha buildup. Measured sections are correlated along a schematic proximal (SE) - distal (NW) transect, orientated perpendicular to the infered paleoshoreline. Blue: biostrome facies; purple: slope facies; light blue: back-reef facies; red: coral community intercalated with coarse grained coastal clastics; yellow: coastal clastics.

2.3 Influence of climate and synsedimentary block movement on sediment entry and biostrome composition

The apperance of biostromes shows a strong dependence to the surrounding sediment type. In a siliciclastic environment, coral buildups are composed of branching *Porites*, while in a carbonatic environment massive *Porites* and *Tarbellastrea* prevailed. Potential mechanisms that managed sediment supply are block uplift and precipitation rates.

Similar to in the western Irakleion Basin, coastal clasics border the margin of the Ida Mountains, which corresponds to a Late Miocene central Cretan landmass (see chapter 1) that prevailed the siliciclastics. Uplift and subaerial exposure of an isolated distal fault block north of Agia Deka providing siliciclastics is documented in its border by shallow marine siliciclastics. The activity of NE-SW trending normal faults is linked to the block uplift and displayed in the sedimentary development of Psalidha buildup. Both coastal sedimentbodies are separated by an area with thick filling of offshore deposits. They interfinger with the nearshore shallow water sediments and indicate continuous drawdown by their enormous thickness and deep water facies.

At the Psalidha and Apomarma localities, the facies of all biostromes point to a persistent shallow water depth below 10 m for the biostrome facies. Measured sections and mapping of coral facies show that facies-belts (talus-facies, slope-facies, biostrome-facies) of biostromes build-up by massive and branching corals remained at geographically nearly fixed positions over the time of coral growth in the nortwestern Messara Basin. Independently from the predominantly growth form of corals, the biostromes at the bottom (branching *Porites*, high amount of clastics) and at the top (massive corals, low amount of clastics) of Psalidha buildup were not affectetd by synsedimentary block movements.

Consequently, quantitative changes in the siliciclastic fraction are neither a proximal-distal effect nor triggered by synsedimentary tectonic that may have been isolated the more calcareous biostromes from siliciclastic supply by uplift. Despite of regional differences in sea-floor relief and uplift history (Apomarma: vast steep sided coastal platform; Psalidha: gentle inclined ramp, stepped by synsedimentary tectonic) that had affected the biostrome facies, both biostrome-types are recognized in the Apomarma and Psalidha area. Therefore, a superior, probably climatic controlled mechanism must have been assigned responsible for quantitative transitions in terrigenous input and the two different biostrome-types reflect changes in precipitation (*Porites*-thickets = wet; biostromes composed of massive corals = dry).

2.4 Conclusions of chapter 2

(1) The distribution of coastal clastics with intercalated coral constructions reflects the early Tortonian paleogeography in the northwestern Messara Basin. Shallow marine clastics with intercalated coral buildups follow the coastline of the central Cretan landmass (Apomarma locality) and a preliminary isolated fault-block (Psalidha locality).

(2) At both localities, two types of coral buildups developed:

(a) thicket-like *Porites*-biostromes dominated by branching corals in siliciclastic environment (Figs. 2.3, 2.8b, 3.3b)
(b) sheet-like *Porites*-*Tarbellastrea* biostromes constructed by massive corals in carbonatic environment (Figs. 2.8c, 3.3d)

Porites-thickets are interpreted to have been developed during wet stages with high terrigenous input from the mainlands. In contrast, the more calcareous biostromes with predominantly massive growth forms are supposed to represent more dry episodes with clastic sediment starvation of the basin.

(3) Differences in facies and composition of type (a) and (b) coral buildups from proximal (Apomarma locality) and distal (Psalidha locality) fault blocks are triggered by regional variations of the sea floor topography, created by synsedimentary block movement due to north-south extension of the basin.

3 Diagenesis of growth bands in fossil scleractinian corals: identification and modes of preservation

The massive skeletons of colonial corals represent high-resolution archives of past sea surface temperatures, salinity and productivity (Grottoli, 2001). The coral record has therefore proven to be an important source of information for studying seasonality and climatic oscillations on inter-annual to inter-decadal timescales in historic and prehistoric time (Druffel, 1997). However, coral skeletons are susceptible to mineralogical and geochemical alteration, and corals older than Pleistocene are frequently recrystallized and transformed from original aragonite into secondary calcite (Constantz, 1986; Dullo, 1986; Dullo & Mehl, 1989; McGregor & Gagan, 2003). Nonetheless, conspicuous light-dark banding couplets are commonly present in many Cenozoic and Mesozoic hermatypic corals such as *Porites* and *Thamnasteria*, *Isastrea*, *Fungiastrea* or *Microsolena*. Although fully recrystallized and cemented, general agreement exists that the banding visible in these corals reflects annual growth cyclicity. These banding patterns have been in wide use for estimates of carbonate production and reconstructions of climatic gradients during the Jurassic (Geister, 1989; Insalaco, 1996; Nose, 1999). The presence of growth bands interpreted as annual density bands has been taken to suggest that the Triassic constructional coral *Ceriostella variabilis* was already a photosymbiotic zooxanthellate coral (Helmle & Stanley, 2003).

Paradoxically, couplets of light and dark bands interpreted to reflect annual growth increments are conspicuous in recrystallized skeletons, both visible on weathered surfaces and polished slabs, whereas in fresh materials from modern reefs, the growth bands remain mostly invisible and require radiographs for proper documentation. This circumstance raises the question of the origin and significance of the distinct bandings in fossil corals. In this chapter, banding patterns in colonial *Porites* from the Late Miocene of the island of Crete (eastern Mediterranean Sea) are described. Some of the skeletons have fully retained their original aragonite mineralogy and microstructures, whereas others are transformed into secondary calcite and are fully cemented. Documentation of transitions from unchanged to altered *Porites* allows to identify annual growth bands and the mechanism of how they have been produced in recrystallized skeletons. The style of the banding, however, is not restricted to the poritid skeletal architecture (Miocene), and exists also in microsolenid corals (Jurassic). Further, the pathway of diagenetic alteration and two principal mechanisms of how growth bands get recorded in recrystallized skele-

tons are demonstrated here. Preservation of annual growth bands strongly depends on the preferential dissolution of the high-density band during freshwater or shallow burial diagenesis. A second type of growth rhythm originates from concentrations of marine micropelletoidal cements along tabulate dissepiments. The latter potentially formed on a lunar basis, both in Cenozoic and Mesozoic hermatypic corals, and therefore gives an example of the potential pitfalls when interpreting growth rates of corals for the purpose of paleoclimatology and paleoecology.

3.1 Material and Methods

Porites corals with massive and branching growth morphologies in different stages of alteration were sampled from upper Miocene sections in central Crete (Figs. 3.1, 3.2). Corals with the original aragonite skeleton preserved derive from the top of the Psalidha coral buildup (Ambelousos Formtion, northwestern Messara basin; fig. 3.2A; see chapter 2.2 for details of location), whereas partially recrystallized massive *Porites* skeletons (coral fragments) were taken from a debris flow deposit (Varvara Formation, western Irakleion Basin, Moni Gorgolaini-North locality; fig. 3.2C; see chapter 1.3.2 for details of locality), and totally recrystallized massive *Porites* colonies were sampled from lower segments of Psalidha buildup and patch reef localities in the area of Kroussonas (Pirgos Member, Western Irakleion Basin; see chapter 5 for details of locations). Recrystallized *Porites*-branches originate from a *Porites*-debris biostrome (Ambelousos Formation, northwestern Messara Basin, Apomarma locality; see chapter 2.1 for details of location; fig. 3.2B).

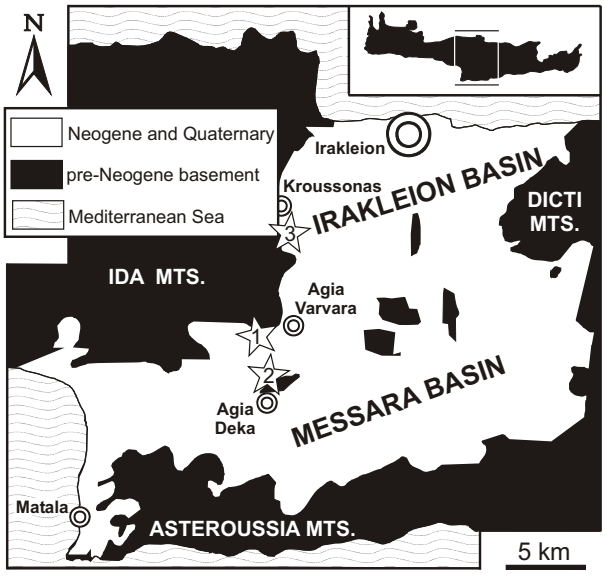

Fig. 3.1. Location of Coral Sites (asterisks) in central Crete. **(1)** Apomarma (N 35.11252°, E 024.96398°), **(2)** Psalidha (N 35.08424°, E 024.96094°), **(3)** Moni Gorgolaini (N 35.20535°, E 024.98190°)

Samples of microsolenid corals were taken from the Korallenoolith (Oxfordian, Hainholz-Member), NW-Germany (Hainholz quarry; see Reuter *et al.*, 2001 and Helm *et al.*, 2003 for details of location).

Fragile aragonite coral skeletons were embedded in polyurethane foam in the field to prevent disintegration during transport. Slabs and thin-sections were stained with Feigl´s solution to reveal the distribution of aragonite and calcite. Radiographs from selected coral slabs (thickness 6 mm) were prepared at the Research Center for Ocean Margins, University of Bremen (T. Felis). Growth increments were measured parallel to the axis of maximum growth. In SEM view, broken and polished surfaces of the corals were analysed for ultrastructures. X-ray diffraction for the determination of aragonite and calcite was carried out at the Institut für Geowissenschaften, Mainz (H.-D. Werner) using a Seifert XRD 3000 diffractometer. Samples were scanned from 2Φ of 20° to 60°. In all samples from aragonite corals, calcite concentrations remained below the detection limits of the method (1-2%).

One aragonite coral specimen was selected according to visibility and thickness of the growth bands for stable isotope analysis (sample P1). Sampling was performed along a continuous transect following the growth axes of the colony. Stable isotope analysis was performed by M.M. Joachimski (Erlangen University, Germany). Carbonate powders were reacted with 100% phosphoric acid at 75°C using a Kiel III online carbonate preparation

line connected to a ThermoFinnigan 252 mass spectrometer. All values are reported in per mil relative to V-PDB by assigning a $\delta^{13}C$ value of +1.95‰ and a $\delta^{18}O$ value of -2.20‰ to NBS19. Reproducibility was checked by replicate analysis of laboratory standards and is better than ±0.03‰ (1σ). Determined isotope values are documented in A1.

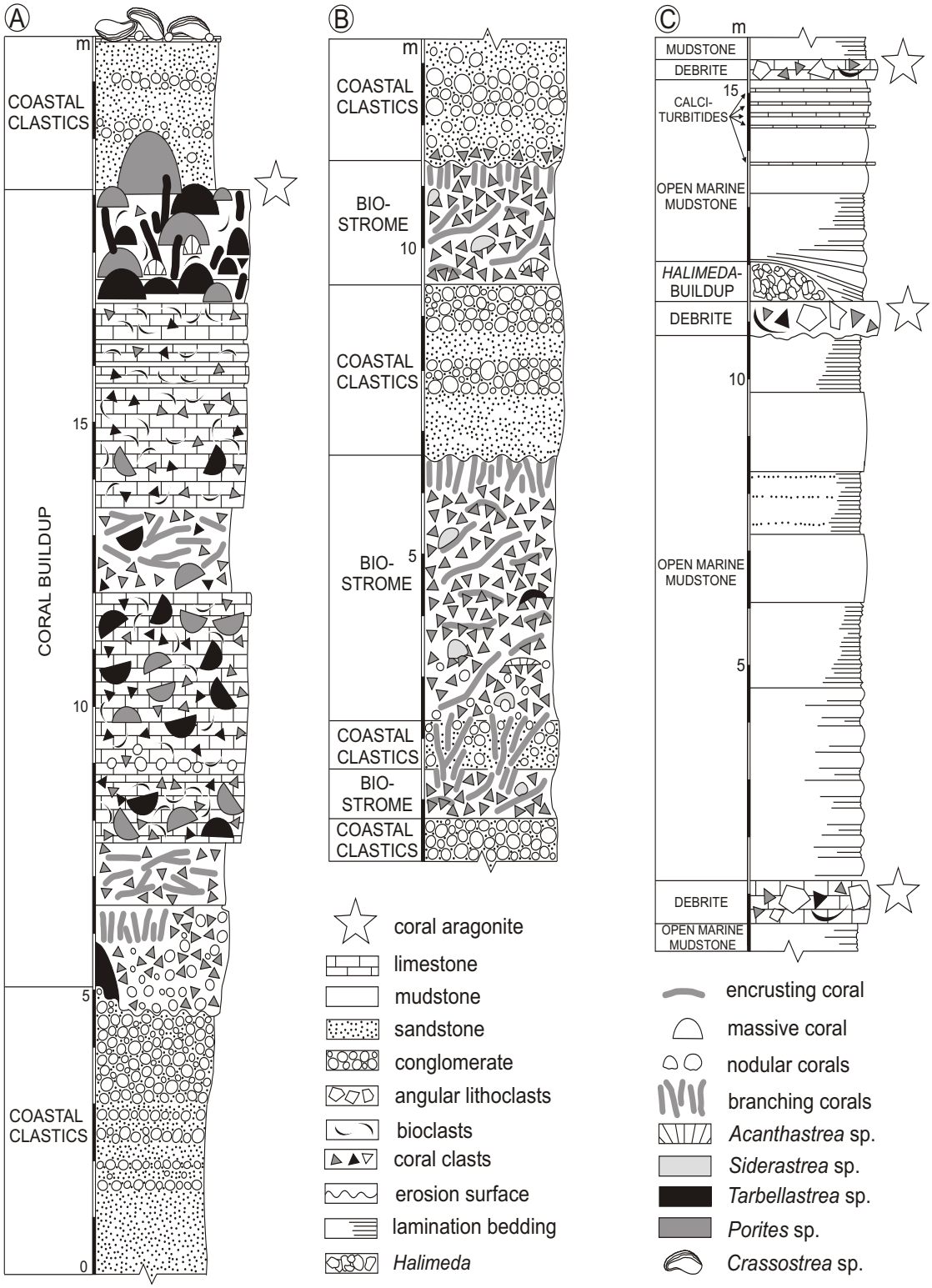

Fig. 3.2. Geological sections of **(A)** Psalidha, **(B)** Apomarma and **(C)** Moni Gorgolaini, Central Crete. (A-B) Early Tortonian, (C) Early Messinian.

3.2 Paleogeographical setting of the island of Crete

The Late Miocene paleogeography of the Mediterranean Sea was similar to the present situation: it formed a marginal sea of the Atlantic ocean, not connected with the Indopacific. A sea strait temporally linked the eastern Mediterranean via the Aegean with the Paratethys epicontinental sea to the north of the alpine orogen system (Rögl & Steininger, 1984). In contrast to the present situation, extensive coral reef growth occurred almost everywhere in the Mediterranean area. This biogeographic pattern and the remarkably low diversity of reef corals is generally believed to reflect a warmer-than-present climate and a position of the Mediterranean area at the northern margin of the global coral reef belt (Brachert *et al.*, 1996; Esteban, 1996).

3.3 The Late Miocene section of central Crete: distribution and preservation of corals

The Late Miocene section of central Crete starts with clastics of the Ambelousos Fm. of Tortonian age (Meulenkamp *et al.*, 1979). Depositional environments range from brackish lagoons to marginal marine environments. Coarse clastics formed along the coastline and were intermittently colonized by laterally extensive coral biostromes and patch reefs. Coral biostromes composed of large massive colonies of *Porites* and *Tarbellastrea* with minor contributions of *Acanthastrea* (Figs. 3.3a, d) developed during episodes of low terrigenous input, whereas thicket-like coral biostromes constructed by ramose branching *Porites* formed during episodes of high siliciclastic influx (Fig. 3.3b). At a single locality in northwestern Messara Basin, a stack of biostroms (autobiostromes and parabiostromes, *sensu* Kershaw, 1994), constructed either by massive or by ramose branching corals form a coral buildup of 15 m thickness (Psalidha locality; see chapter 2.2 for detailed information).

The sediments of the Ambelousos Formation are covered by marl and finely bedded calcareous mudstone of the Varvara Formation of late Tortonian - early Messinian age (Fig. 1.9d; Meulenkamp *et al.*, 1979; Moisette *et al.*, 1993). At the basin margin and on uplifted fault blocks, the Varvara Formation sediments grade into coralline algal-bryozoan skeletal limestone of the Pirgos Member (Figs. 1.9a, c). Locally, the Pirgos Member is formed by small patch reefs build up by massive corals (*Porites*, *Tarbellastrea*) with minor contributions of branching *Porites* (Fig. 5.6a-c). In more distal settings, the reefs are replaced by non-framework coral communities formed by large (>1 m), massive *Porites* and *Tarbellastrea* colonies that are often preserved as empty molds (Fig. 3.3e; see chapter 1.4 and 4.4 for detailed information). The Pirgos Member is compositionally identical with calciturbidites and debrites with coral blocks intercalated with the laminated marl of

the lower Varvara Formation (Fig. 3.3c). Some down-slope carbonate buildups exist in the Varvara Formation, formed by the green alga *Halimeda* (Fig. 1.6b) and bryozoans. The Late Miocene sequence terminates with laminated gypsum that interfingers with the Varvara Formation mudstone and was deposited in distal parts of the basin.

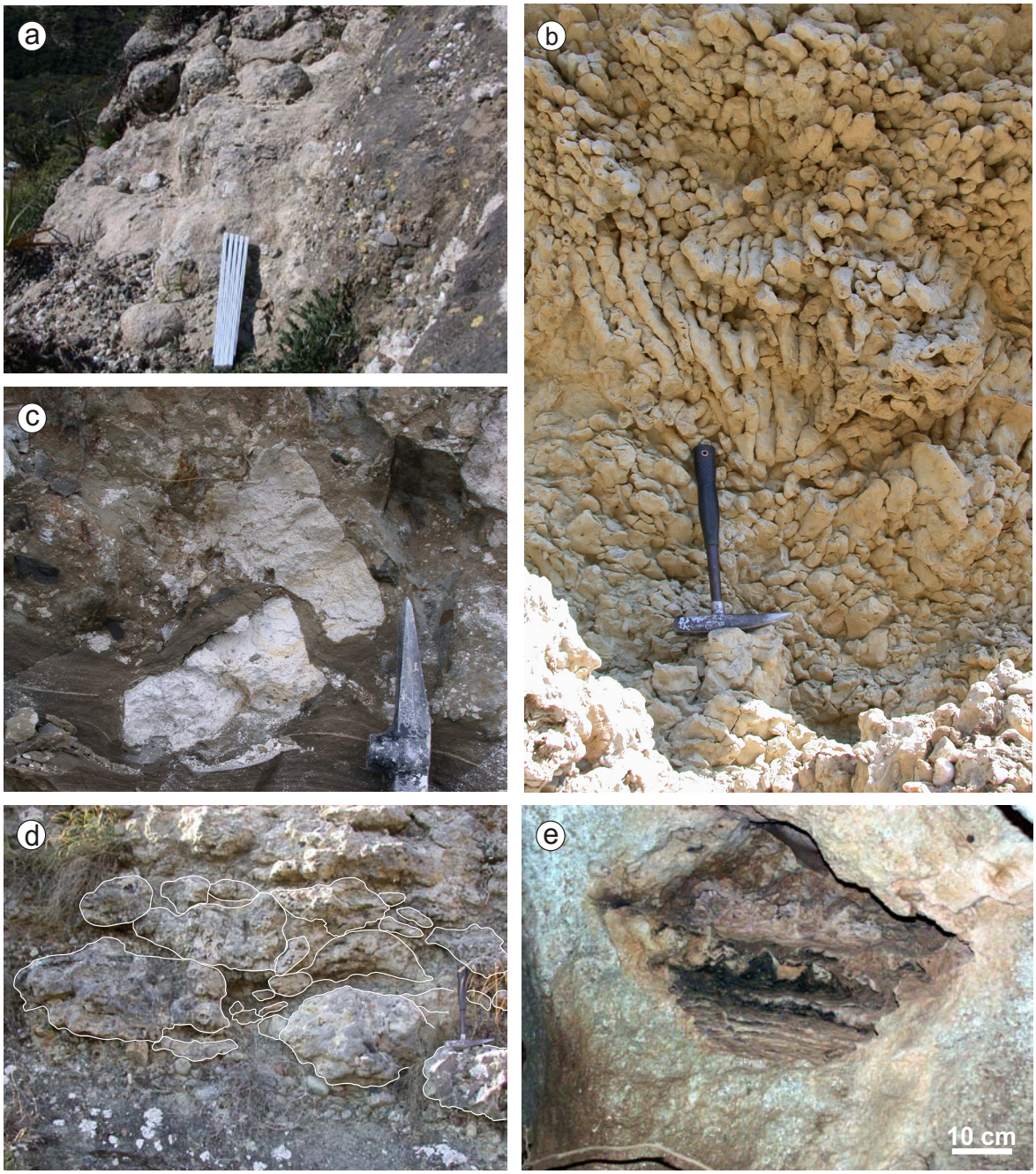

Fig. 3.3. Weathering aspects of massive and branching *Porites*, Late Miocene, central Crete. **(a)** The growth topography of the buildup is very well preserved by a drape of poorly classified sandstone and conglomerates. Psalidha, early Tortonian, Unit 1, Coral Site 1.3B of chapter 4. **(b)** Weathering aspect of a coral biostrome formed by interlocking branches of *Porites*. Psalidha, early Tortonian. Unit 1. **(c)** Mud supported breccia (debrite flow deposit) with angular coral fragments (*Porites*) and fine grained bioclastic debris. The base is erosional with protuding particles. Moni Gorgolaini, early Messinian. Unit 7. Coral Site 7.2 of chapter 5. **(d)** Coral biostrome composed of massive colonies (highlited by white lines) of *Porites* and *Tarbellastrea* with minor contribution of *Acanthastrea*; all fully recrystallized. Unit 1. Coral Site 1.1 of chapter 5. Apomarma, Tortonian. Unit 1. **(e)** Mold formed after massive *Porites* colony in skeletal limestone, Agios Thomas,late Tortonian. Unit 5.

3.4 Rhythmic banding in Late Miocene *Porites* corals

Although preserved at various stages of transformation from aragonite into calcite, cementation and recrystallization, all corals analysed show a rhythmic banding. In massive "aragonite corals" this banding is a representation of the annual growth bands, whereas in recrystallized corals the banding is either due to preferential dissolution of the high density band (annual rhythmicity) or is an effect of micropelletoidal marine carbonate cement concentrated along tabulate dissepiments (monthly rhythmicity).

3.4.1 Banding in "aragonite corals"

The aragonitic coral skeletons were easily identified in the field by their conspicuous white colour and very low weight due to retention of the original porosity. Slabs of the massive aragonite *Porites* exhibit a faint banding on a millimetre scale (~4.0 mm). It is formed by alternating "light" (1-2 mm thickness), and thick "dark" laminas (2-5 mm thickness) (Figs. 3.4a, d). The laminations reflect growth of the colony formed by laterally linked convex upward laminations. X-ray radiographs from coral slabs show a very prominent wavy banding, that is fully equivalent with density bands described from modern *Porites* (Knutson *et al.*, 1972; figs. 3.4b-c). Between individual areas of convex upward growth of the colony, a narrow zone of low X-ray density exists (Figs. 3.4b-c). Such a zone of low skeletonization also is present in modern corals (Grigg, 1982; Felis *et al.*, 2004), which can be taken as an indication of the pristine state of preservation of the skeleton, because no later dissolution has occurred. The zone of low density is where most late fractures have formed. Some of the fractures have been filled with cryptocrystalline carbonate, whereas a second generation has remained open (Fig. 3.4b). However, the X-ray radiographs show, that carbonate infills of fractures or weathering crusts do not extend into the skeleton.

In thin-section, the banding is hardly visible. However, as shown by Pätzold (1984), the coral skeleton of the coenosteum and calyces is more massive in the high density bands

Descriptive terminology	Aspect in reflected light	Aspect in transmitted light	Aspect on X-ray radiographs (positive)	Stable isotope composition	Interpretation
„light band"	high reflection (light)	dark	dark	positive $\delta^{18}O$ negative $\delta^{13}C$	„high density band" cool and/or dry season
„dark band"	low reflection (dark)	light	light (X-ray transparent)	negative $\delta^{18}O$ positive $\delta^{13}C$	„low density band" warm and/or wet season

Tab. 3.1. Terminology used in this study for growth bands in "aragonite corals"

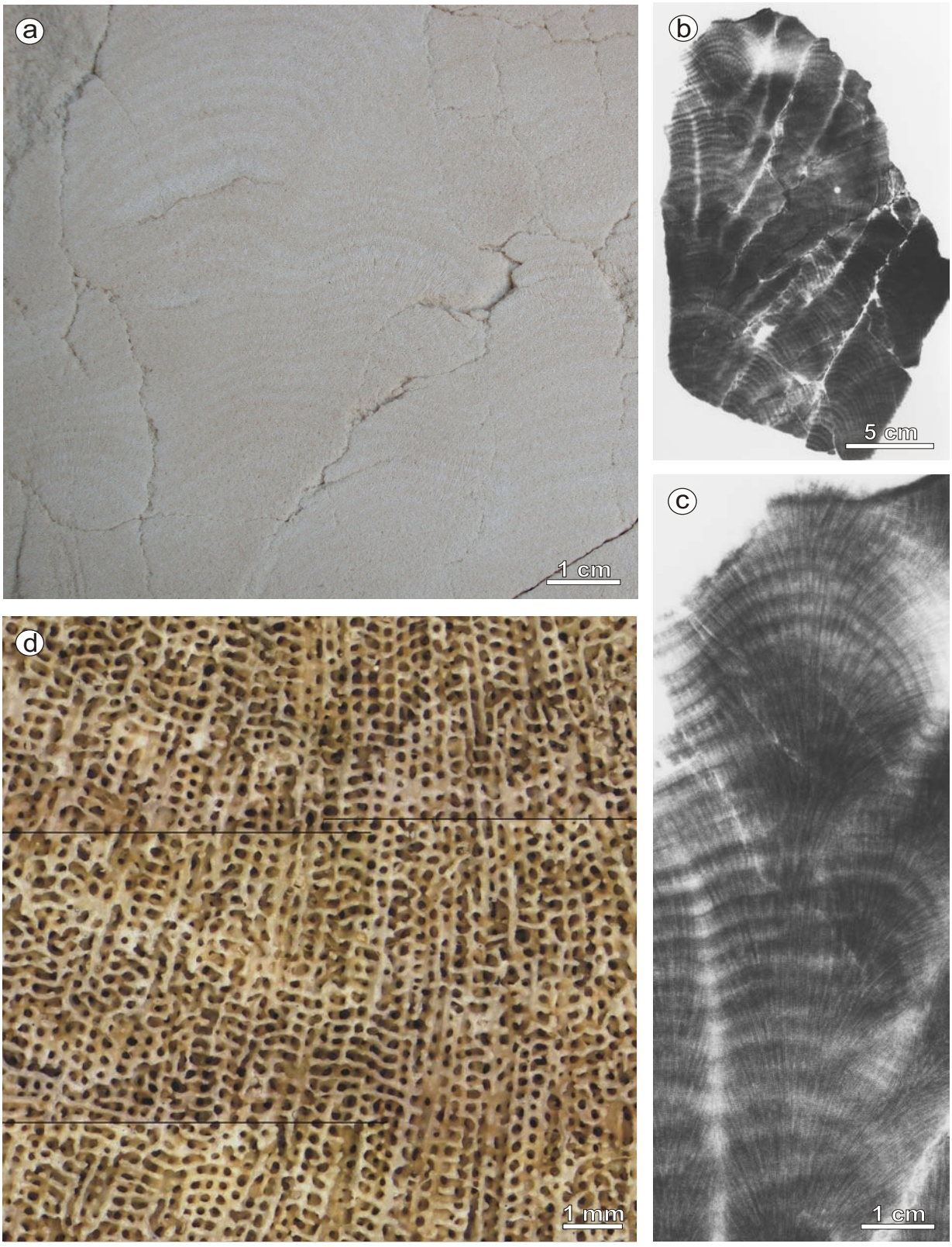

Fig. 3.4. Polished surfaces and X-ray radiographs from "aragonite *Porites*". Psalidha, early Tortonian. **(a)** Large fragment of a massive *Porites* showing couplets of "light" and "dark" bands. **(b)** X-ray radiograph (positive print) showing density bands and abundant fractures. Microcrystalline calcite in fractures appears dark in the radiograph. The skeleton immediately adjacent to the calcite veins remains unchanged. A second system of fractures is still open and unfilled (white). **(c)** Close-up from fig. 3.4b showing density banding. Contact zone of individual convex upward growth zones is X-ray transparent, which reflects reduced skeletonization. Positive print. **(d)** Detailed view of coral slab showing couplets of "light" and "dark" bands.

as compared to the low-density bands. In addition, the trabecular fans appear darker (i.e. more fine) in the “light” bands (“light” in reflected light) tend to have central micritic linings and clots composed of smaller crystallites than within the “dark” bands (in reflected light) (Figs. 3.5a-b). For the purpose of consistency, the terms “light” and “dark” bands always refers to the aspect of the corals in reflected light, although in thin-section the “light bands” appear dark, the “dark” bands light (Tab. 3.1). The micritic lining and clots represent the centres of calcification. However, according to their unusual large size in some bands, they must have been affected by recrystallization or dissolution (Figs. 3.5d, 4.4c; McGregor & Gagan, 2003). Thus, the conspicuous banding visible in slabs and some thin-sections reflects incipient diagenetic alteration, which preferentially affected the bands appearing “light” in reflected light.

In SEM view, the radial trabecular fibres do neither show significant signs of dissolution nor recrystallization (Figs. 3.5c-f). The surface of the skeleton is either smooth and formed by crystal aggregates with blunt crystal terminations (Figs. 3.5e, 4.4e), or ragged due to acute tips of trabecular fans and crystal aggregates (Fig. 3.5f). Both surface types have been found in a close spatial relationship and are normally separated by thin meniscate bridges within the skeleton (Figs. 3.5d, f). In growth direction, the meniscate bridges exhibit a smooth upper and ragged lower surface due to tiny crystals (Fig. 3.5f). In direct contact with the coenosteum and calyces, the crystals of the meniscate bridges are in a clear structural continuity with trabecular fans (Fig. 3.5d). The microstructure of the meniscate bridges therefore reflects an original growth fabric (the dissepiment) and is not a secondary cement. In living corals, the dissepiments form along the lower surface of the calcioblastic tissue. It is concluded that smooth surfaces of the skeleton formed in contact with the calcioblastic tissue of the coral, and were not overgrown later by cement (Figs. 3.5e-f, 4.4e). However, syntaxial early marine cement overgrowths formed deeper in the coral, after withdrawal of the calcioblastic tissue from the skeleton during growth, forming the ragged undersides of the dissepiments and syntaxial cements of the deeper skeleton (Fig. 3.5f). All in all, these observations rule out the possibility of significant structural modifications of these skeletons during diagenesis.

Stable isotopes of oxygen ($\delta^{18}O$ V-PDB) and carbon ($\delta^{13}C$ V-PDB) exhibit a mean composition of -2.76‰ and -1.54‰ respectively. Both isotope systems show a cyclic signal, which systematically reflects the growth bands. In $\delta^{18}O$, the high density bands are more positive, at -2.0 to -2.5‰, whereas the low density bands are at -3‰. The cyclic carbon isotope signatures ($\delta^{13}C$) are phase-shifted relative to $\delta^{18}O$: minima in (-2.0‰) coincide with the high-density bands, whereas the maxima (0 to -1.0‰) coincide with the low-density bands of the couplets. A sharp decrease in $\delta^{13}C$ occurs at ~13 years and synchronous with a distinct plateau in $\delta^{18}O$ (Fig. 3.6). From a compatible rhythmic $\delta^{18}O$ pattern in

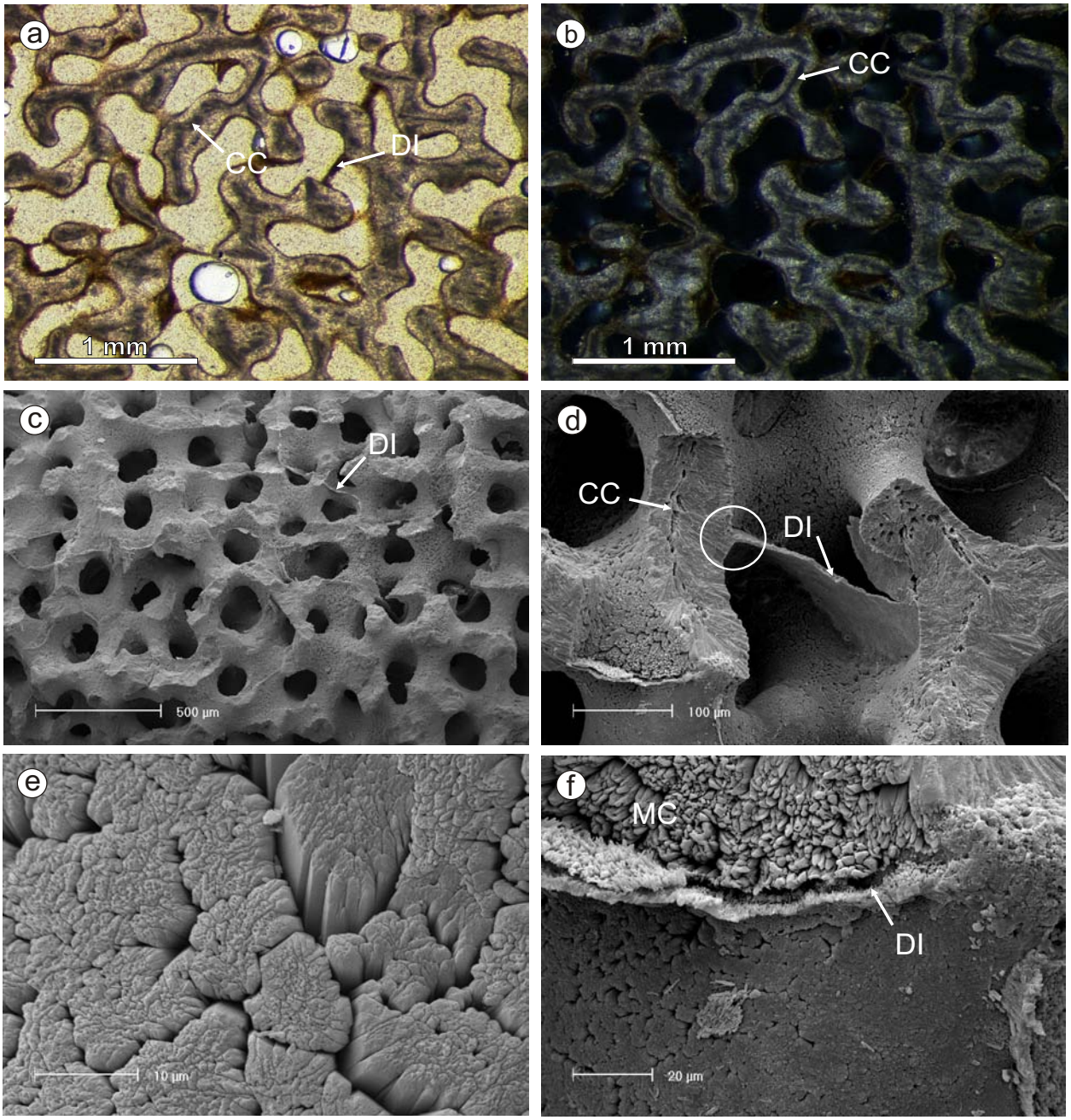

Fig. 3.5. Microscopic aspects of "aragonite corals". Psalidha, early Tortonian. **(a)** Thin-section view of the coral skeleton. Dissepiments (DI) forming meniscate bridges and the centres of calcification (CC) are clearly visible. Micrite envelopes cover most of the skeleton, but diagenetic overgrowths are volumetrically not significant. Bright circles represent air bubbles within epoxy resin. Plane light. **(b)** Same picture as in fig. 3.5a, crossed nicols. **(c)** Overview of the pristine aragonite texture with well preserved dissepiments (DI), SEM micrograph from fresh fracture. **(d)** The skeleton formed of trabecular fans is well preserved; the centres of calcification (CC) are affected by some dissolution. The dissepiments (DI) form diaphragms in continuity with trabecular fans *(circle)*. SEM micrograph. **(e)** Smooth surface of the skeleton formed by blunt crystal terminations. **(f)** Dissepiments (DI) mark the boundary of smooth skeletal surfaces and surfaces covered by early marine cement (MC).

modern corals it is inferred that the thin high-density bands formed during the suboptimal season (winter), whereas the thick high density bands during the optimal season (summer). Rosenfeld *et al.* (2003) also found that the phase-shift of the carbon and oxygen isotope cycles common in many modern corals can be referred to seasonal changes in photosynthesis, i.e. less photosynthesis in winter. The highly consistent relationship of growth banding and isotope variations documents seasonal growth and is evidence of a pristine state of preservation, because diagenesis tends to homogenize isotopic compositions (McGregor & Gagan, 2003). Consequently, the marked decrease in $\delta^{13}C$ at ~13 years (internal chronology) and the rather negative plateau in $\delta^{18}O$ can be considered the expression of diagenetic alteration of the skeleton related to a small fracture.

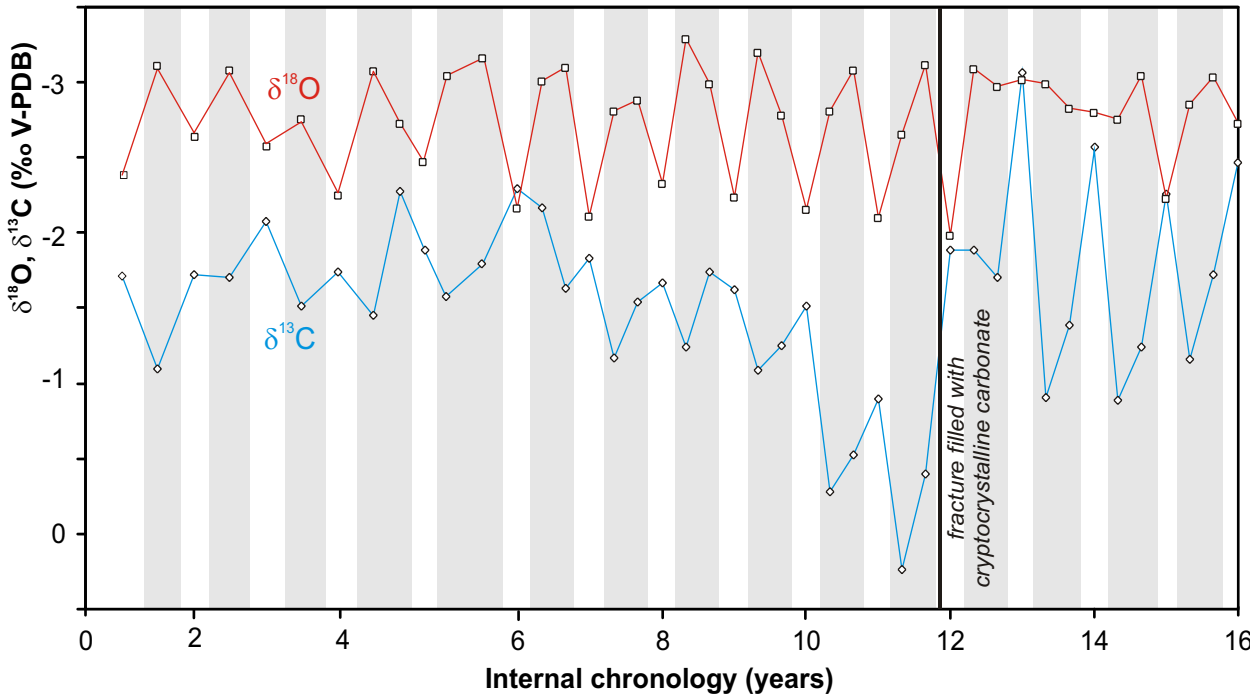

Fig. 3.6. Stable isotope record ($\delta^{18}O$ and $\delta^{13}C$, V-PDB) resolved for the density bands of a massive *Porites*. The oxygen isotope signal shows a pronounced plateau at 13-15 years related to diagenetic alteration of the skeleton extending from a small fracture. Gray bars mark the "dark" bands (= summer) of the annual couplets. Sample P1, Psalidha locality, early Tortonian.

3.4.2 Banding in recrystallized corals

The vast majority of corals from the Ambelousos and Varvara Formations are leached (Fig. 3.3e) or transformed into coarse blocky calcite (Figs. 3.3b, d). This is the typical state of preservation of zooxanthellate corals from Neogene sediments (Martín *et al.*, 1989; Brachert *et al.*, 2001). In the aragonite corals from Psalidha outcrop, skeletons with a perfectly preserved outer zone (50-100 cm) may coexist with a fully recrystallized nucleus along a narrow chalky zone (10 mm). Beyond this zone, the original aragonite textures of the coral skeleton have been entirely transformed into calcite spar and/or empty voids. Adjacent to the chalky zone, original intraskeletal void space of the coral skeleton is filled with coarse blocky calcite spar (size 100-150 μm). Thin-sections stained with Feigl´s solution reveal that fibre-shaped aragonite relicts of the skeleton (trabecular fibres) may be present preferentially along the periphery of the skeletal elements, whereas centres represent open voids formed by dissolution (Fig. 3.7a). Leaching, therefore, started along the centres of calcification and continued to form a hollow canal system within the skeleton (Figs. 3.7b-c). However, in a sub-millimetric spatial relationship, no

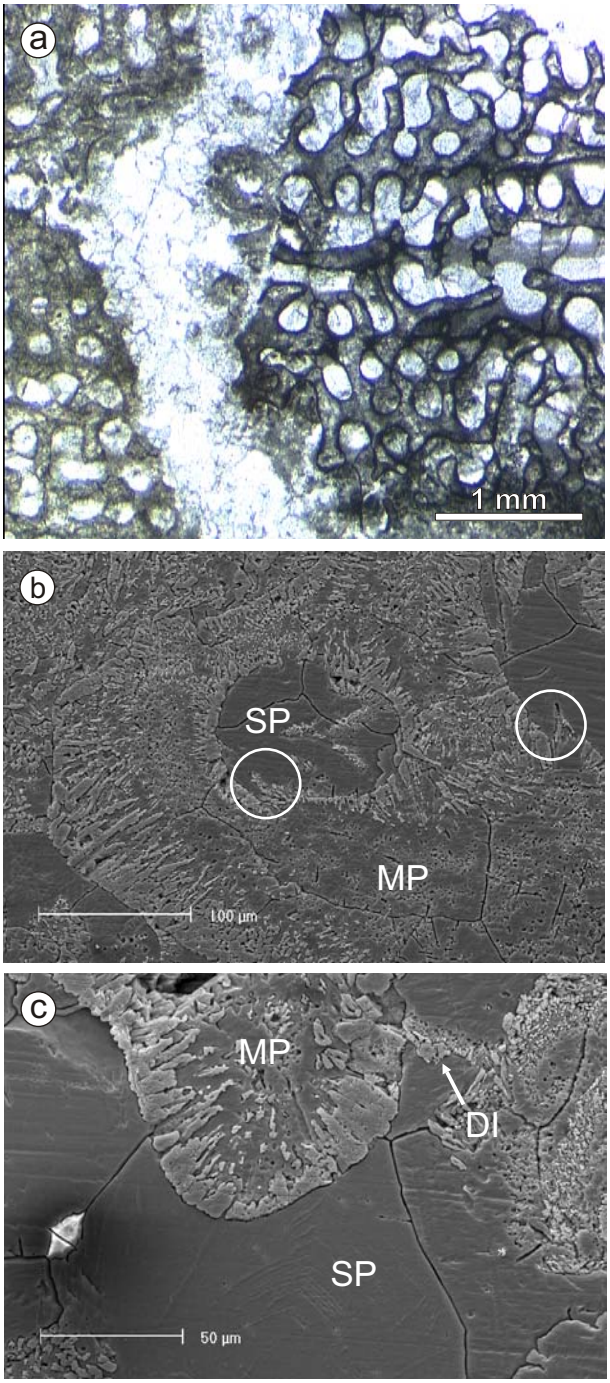

Fig. 3.7. Microscopic aspects of recrystallized massive *Porites*. Psalidha, early Tortonian. **(a)** Thin-section micrograph. To the left of a veinlet, the skeleton is fully transformed into blocky calcite spar. Intraskeletal porosity is sealed by blocky calcite cement, leaving ghost structures of the original skeleton. To the right of the veinlet, the skeleton shows the same type of preservation. However, relicts of the original aragonite exist at the periphery of the skeleton as visible by the black stain of Feigl´s solution. Crossed nicols. **(b-c)** SEM micrograph of recrystallized skeleton impregnated with epoxy resin (polished surface etched with dilute HCl). Blocky calcite spar seals skeletal porosity (SP) and molds (MP) formed by solution enlargement of the centres of calcification. Light grey fibrous elements tracing relicts of the skeleton and dissepiments (DI) represent moulds filled by epoxy resin. Mechanical compaction of the skeleton took place prior to cementation by calcite cement (white circles).

aragonite is present due to dissolution, leaving irregular empty skeletal molds with no documentation of the skeleton. Such voids are elongate bands (1-2 mm thickness), being a perfect reflection of the growth fabrics, where the skeleton have been preferentially destroyed by dissolution (Fig. 3.8). The pattern of centrifugal dissolution observed in thin-section is confirmed by SEM observation. In specimens impregnated with epoxy resin, some skeletal void space has been cemented by sparry calcite spar prior to final dissolution of the last aragonite relicts (Figs. 3.7b-c). Here, collapse of the skeleton weakened by dissolution (Fig. 3.7b) implies that both, skeletal molds and intraskeletal porosity remained unfilled prior to cementation by blocky spar. In a last stage after cementation, residual aragonite fibres were dissolved (Figs. 3.7b-c). However, the skeleton is not uniformly preserved or documented as ghost in calcite spar. Ramose corals show additional, altenative growth rhythms. Polished slabs exhibit stacks of convex upward light and dark bands formed of micrite and sparry calcite, or crescent-shaped empty voids (Fig. 3.8b). The micritic bands peripherally merge with an outer micritic envelope (few millimetres wide) which reflects the general growth form of the colonies. The convex micritic bands are laterally discontinuous and tend to become progressively thinner towards the centre of the colonies, which may be formed entirely of sparry calcite, or may even exhibit an open void lined by blocky calcite cement (Figs. 3.8b, 3.9a, d). Although, according to staining experiments of thin-sections with Feigl´s solution, no original aragonite is left, the architecture of the skeleton is clearly visible in the outer zones, because it is fully encased in micrite (Figs. 3.9c-e). The clear banding results from intercalations of micrite and micro-pelletoidal carbonate, which show a clear cut base and an irregular top (Figs. 3.9a-b). The pelletoidal layers tend to become thinner inward (Figs. 3.9a, c), because

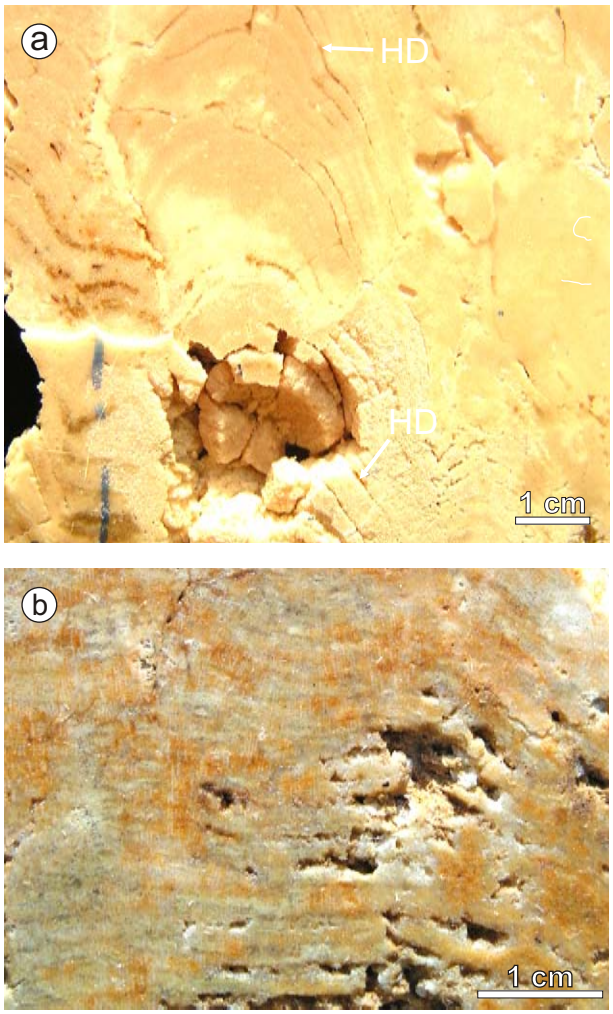

Fig. 3.8. Polished slabs of massive Porites. **(a)** Narrow, sheet-like empty voids (HD) resulting from preferential dissolution of the “light” bands. Moni Gorgolaini area, early Messinian. Unit 7. **(b)** Ghost structures of growth bands in a fully recrystallized *Porites* result from preferential dissolution and cementation of elongate void spaces interpreted to represent the original high density bands. Agios Antonios reef, Kroussonas area, Tortonian. Unit 5.

the fine-grained carbonate may have filtered into the skeleton as a sediment (Fig. 3.9e) or may have formed as a micropelletoidal cement (Fig. 3.9b; *cf.* Macintyre, 1977, 1985; Lighty, 1985). The structure of the skeleton may be enhanced by thin micrite envelopes separating drusy granular spar formed within intraskeletal pore space and skeletal molds (Fig. 3.9b).

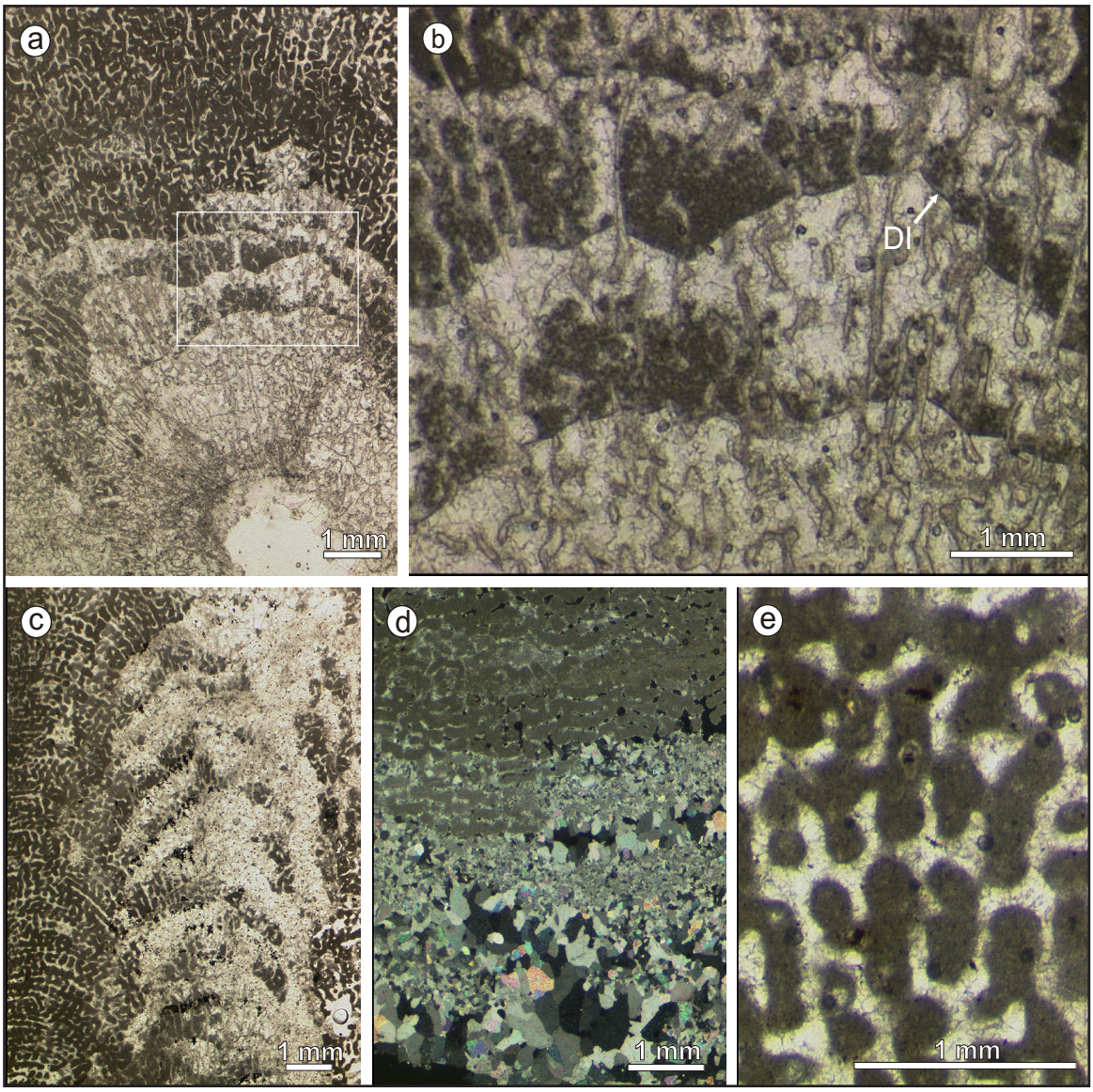

Fig. 3.9. Growth banding in recrystallized branching *Porites*. Apomarma outcrop, Tortonian. **(a)** Thin-section micrograph showing growth banding produced by alternating micropelletoidal micrite and sparry calcite cement. Intraskeletal void space at the periphery of the branch is filled with micrite (upper margin of photograph). The center of the branch is formed by open void space (lower margin of micrograph). Plane light. **(b)** Close-up from fig. 3.9a showing concentrations of micropelletoidal carbonate along tabulate dissepiments (DI). Thin section micrograph, plane light. **(c)** Longitudinal section of a branching *Porites* colony. Conspicuous ghost structures of growth banding are present within the center of a branch. The growth bands merge at the periphery of the branch to form a homogeneous layer. Thin-section micrograph, plane light. **(d)** Detail from peripheral zone of a *Porites* branch. Micrite occurs within the marginal intraskeletal void spaces only. Some segments of the skeleton are open void space (moldic porosity), preferentially along the outer surface of the colony (upper margin of picture). The center of the branch (lower half of picture) is formed by a mosaic of anhedral calcite cement increasing in size towards the center of the stick (drusy cement). Thin section micrograph, crossed nicols. **(e)** Thin section micrograph from peripheral zone of *Porites* branch. Skeleton replaced by drusy calcite spar. Plane light.

3.5 Retention of the original aragonite

The “aragonite corals” show some conspicuous banding, which is also visible on radiographs from coral slabs (Figs. 3.4b-c), and coincides with stable isotope signatures (Fig. 3.6). It resembles to annual density bands known from modern *Porites* (Knutson *et al.*, 1972). According to the isotopic composition of unaltered specimens (Fig. 3.6), these bands represent the high density bands (Rosenfeld *et al.*, 2003). “Aragonite *Porites*” were found in two specific geological settings: (1) blocks in debris flow deposits embedded in marl (Moni Gorgolaini), or (2) along the top surface of Psalidha builddup. In the latter, corals protruding into poorly classified sandstone have retained the original aragonite mineralogy, whereas all aragonite fauna has been dissolved and recrystallized in the well drained carbonate mass below. From these observations an inactive “stagnant” meteoric to shallow burial diagenetic environment with little/no pore water movement (*sensu* Longman, 1980) is inferred for the zone of aragonite preservation (no dissolution and cementation). Isolated fragments of aragonite corals encased in gypsum have been described from the Fortuna Basin (SE-Spain). Here, preservation of the original aragonite skeleton was suggested to result from its inclusion in evaporite minerals (Santisteban & Taberner, 1983).

3.6 Origin of the banding in recrystallized *Porites*

Relicts of the original aragonite skeleton encased in calcite cement at various stages of destruction by dissolution imply that preservation of the skeleton must have been a function of a high rate of cementation versus a lower rate of dissolution of the original skeleton, and that dissolution and cementation took place largely at the same time. It will be demonstrated, that retention of growth bands in the overall recrystallized skeleton is controlled by two independent processes: (1) dissolution processes dominating over cementation in the freshwater phreatic diagenetic/shallow burial environment (Fig. 3.10) and/or (2) growth rhythms expressed by tabulate dissepiments and cryptocrystalline marine cements.

3.6.1 Growth banding in massive *Porites* related to dissolution processes

The skeleton of massive and branching *Porites* from coral buildups in central Crete are generally recrystallized and transformed into calcite. Preservation of the growth banding in these corals appears to follow a basic scheme related to dissolution. Dissolution started at centers of calcification within the trabecular network. Corals that are only moderately affected by diagenesis document a preferential dissolution of the light band, i.e. the high density band (Fig. 3.8a). Increased dissolution rates in the high density bands as compared to the low density bands is interpreted to be a consequence of the smaller crystal forming the “light” high density band. With ongoing dissolution, many of the corals, therefore, display open, elongate voids (left over from dissolution), which are parallel to the growth bands and more or less filled with calcite cement (Fig. 3.8b). The presence of a banding formed by dissolution loss of the high density bands implies, that the first generation of micrite rims/micropelletoidal carbonate was not pervasive over the whole skeleton, and preservation of skeletal moulds is a function of relative dissolution rates vs. relative cementation rates in the marine and freshwater diagenetic environment (Fig. 3.10). Depending on the relative rate of cementation, the skeleton may be encased as a whole in a mosaic of sparry calcite (high relative cementation rate) or may be documented by stack of alternating couplets of voids skeletal layers filled by sparry calcite (Fig. 3.8b). The recrystallized corals exhibit ghost structures of the original skeleton (low relative rate of precipitation of calcite) formed by drusy calcite cement crystallized within molds of the original skeleton. Dissolution occurred through enlargement of the centers of calcification as evident from various stages of dissolution of aragonite and subsequent precipitation of blocky calcite. Prior to dissolution, the skeleton was encased in micrite envelopes or drusy calcite cement or a mixture of both. In this scenario, the bands with ghosts represent the high density bands. According to the type of cement formed (equant

blocky spar), cementation took place in a freshwater phreatic/shallow burial environment (*cf.* Folk, 1974; Longman, 1980).

Central parts of coral colonies tend to be empty voids, because no fine-grained carbonate reached/crytallized in the central segments of the colonies nor did any fibrous or blocky cements form within this zone before dissolution. Some segments of the moldic porosities were subsequently filled by blocky cement (Figs. 3.9a, d, 3.10).

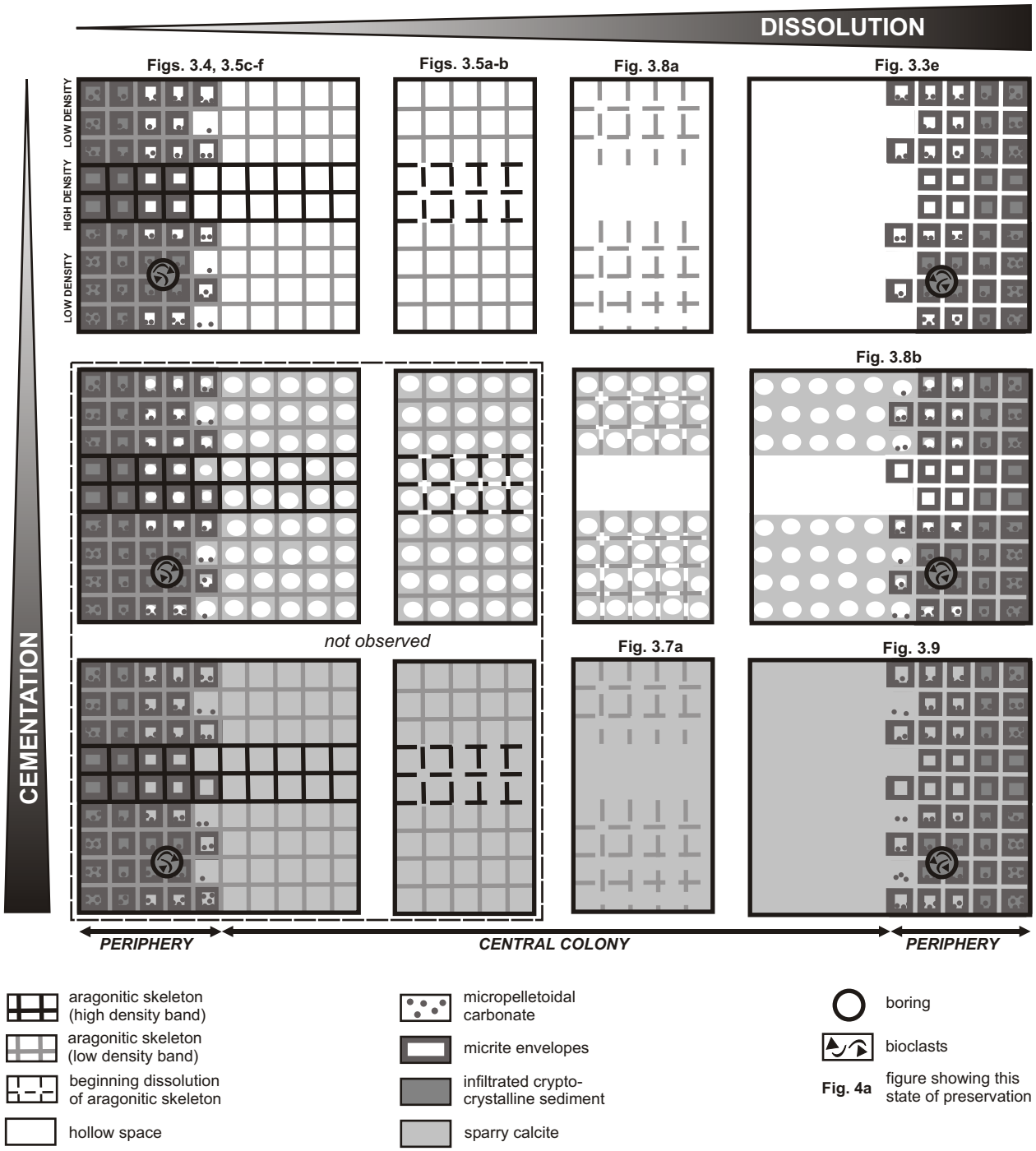

Fig. 3.10. Schematic representation of diagenetic pathways in *Porites* skeletons controlled by relative rates of dissolution and cementation in a freshwater/shallow burial environment. Marine sediment and micropelletoidal cements preferentially occur at the margins of the colonies.

3.6.2 Growth banding in ramose *Porites* controlled by dissepiments

In the more marginal zones of the colonies, infiltration of fine-grained sediment into the skeleton, or precipitation of pelletoidal cement was controlled and dammed by the presence of laterally continuous dissepiments (Figs. 3.9a-b). Marine microcrystalline carbonate occurs preferentially along the outer rims of the corals (Fig. 3.9c) or peripheral to borings and within discrete levels because connectivity of the intraskeletal porosity is partitioned by laterally continuous dissepiments (basal plates). Rhythmic changes of micropelletoidal carbonate and sparry calcite controlled by the presence of dissepiments must therefore mimic original growth increments. In modern *Porites*, dissepiments form according to lunar cycles (Barnes & Lough, 1993; Cohen & Sohn, 2004), which helps to explain the narrow spacings at ~1.8 mm. Nonetheless, the annual growth rates in ramose *Porites* remain difficult to reconstruct, because coral growth may have been strongly seasonal and, therefore, subannual, lunar cycles may have an incomplete record.

3.7 Banding in microsolenid corals (Late Jurassic)

Couplets of light and dark bands in mesozoic corals interpreted to represent annual growth bands, have been described from various taxa, including the Triassic *Ceriostella* and the Jurassic genera *Microsolena*, *Isastrea* and *Thamnasteria* (Ali, 1984; Geister, 1989; Insalaco, 1996; Nose, 1999). Microsolenid corals were chosen for comparison with *Porites*, because the complex 3D skeletal network of the microsolenids formed by confluent and porous septa, synapticulothecate corallites, and tabulate dissepiments has some general similarity with the poritid skeleton (Figs. 3.11b-c).

The corals investigated form massive, head-like colonies. Polished slabs show conspicuous black, grey and light grey patches and bands, which represent an almost perfect, but smaller, representation of the outer surface of the colonies (Fig. 3.11a). The conspicuous banding visible in polished slabs results from losses of skeletal documentation (black bands formed by mosaics of coarse calcite spar, no micrite linings present), from ghosts of the skeleton encased in fine drusy calcite spar (grey bands), and from elongate patches or bands made of micropelletoidal carbonate caught in the intraskeletal network along tabulate dissepiments (light grey bands; fig. 3.11a). The thickness of individual light/dark couplets (<5 mm) and their lateral continuity, however, is highly variable, and tends to decrease outward. In thin-section (Figs. 3.11b-c), the coral skeleton turns out to be fully transformed into calcite and no original aragonite is left. Thin micritic envelopes almost entirely cover the former skeleton, giving a perfect representation of skeletal architecture, including septa, synapticles and dissepiments, whereas the skeleton itself is replaced by drusy equant spar. This calcite cement nucleated along both sides of the micrite envelope as a cement, on the outer surfaces and in voids left from dissolution of the entire skeleton. Wherever the linings are not present, no trace of the original skeleton is left in an overall mosaic of coarse blocky calcite, which appears black in polished slabs (Fig. 3.11a). Patches of cryptocrystalline carbonate preferentially occur along the outer margin of the colony and along borings or other discontinuities. They may fuse laterally to form bands parallel to the growth fabrics of the skeleton, which show a distinct cut base and an irregular top, because the micropelletoidal carbonate accumulated along tabulate dissepiments (Figs. 3.11b-c). The cryptocrystalline carbonate accumulations represent early diagenetic precipitates of peloidal Mg-calcite (marine), because they do not contain any bioclasts and are fully equivalent with those described from modern scleractinian corals in terms of fabric and dimension (Lighty, 1985; Macintyre, 1985). In the microsolenid skeleton the most continuous accumulations of pelletoidal carbonate occur immediately above bands formed of coarse blocky spar without traces of the skeleton (interpreted to represent the high density band removed by dissolution) which further enhances the prominence of the banding. The reason for this rhythmic precipitation of marine cement remains obscure. However, it is tentatively suggested that it may correspond with a warmer

water temperature during summer. In analogy to the diagenetic scenario developed for Miocene *Porites*, the dark bands (reflected light) formed through preferential dissolution along discrete layers and subsequent cementation by coarse sparry calcite (no ghost structures preserved) represent the high density band.

In other Jurassic corals (*Thamnasteria concinna*, *Fungiastrea arachnoides*, I*sastrea explanata*) Ali (1984) found that the banding results from alternating regions with thicker and more numerous skeletal elements (septa, dissepiments = high density band), and regions of a thinner and less well developed skeleton (septa, dissepiments = low density band). This vertical variation in skeletonization was suggested to have been enhanced by differential diagenesis, leading to more intense recrystallization in high density bands and less recrystallization in low density bands, where relicts of the original skeleton are preferentially preserved in cryptocrystalline carbonate infilling intraskeletal void spaces (Ali, 1984; Insalaco, 1996). Although this study supports earlier identifications of high and low density bands, the observations obtained from various stages of diagenetic alteration in *Porites* show, that the banding is not an effect of more intense recrystallization of the high density bands. It is suggested, that the high density bands have little preservational potential, because dissolution rate of the skeleton is enhanced when compared to the low density band. During subsequent cementation, the skeleton may image stacks of elongate dissolution voids (representing the high density bands) filled by coarse blocky spar and bands formed by relicts of the skeleton encased in calcite spar (representing the low density band)

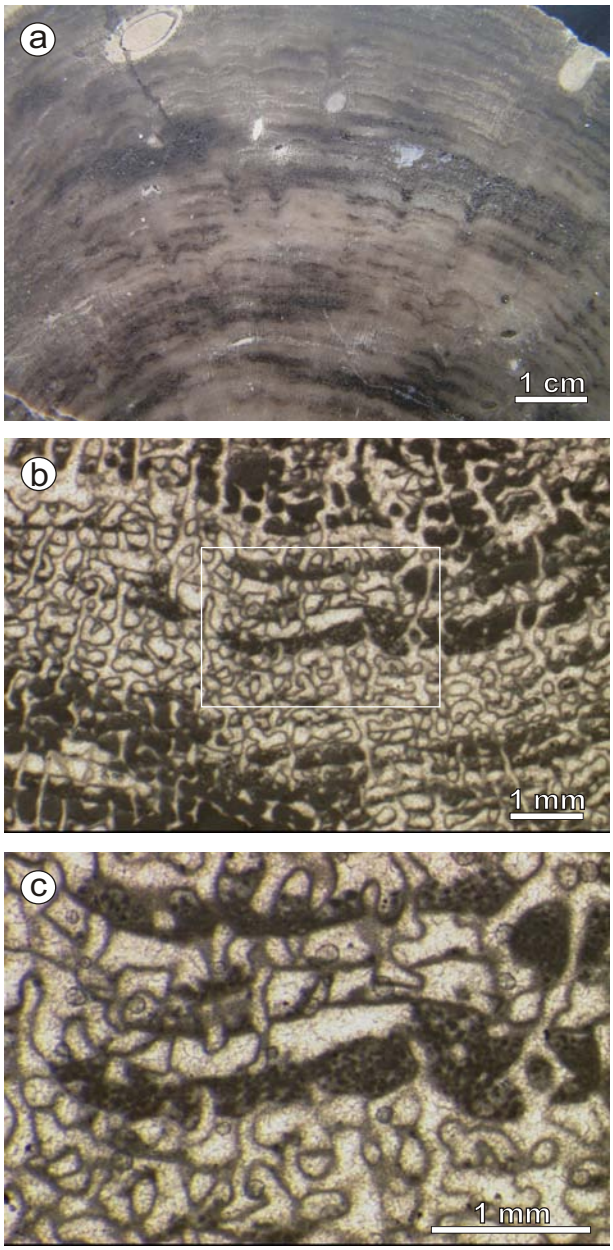

Fig. 3.11. Banding in a Late Jurassic microsolenid coral. Oxfordian, Hainholz Quarry, NW-Germany (see Helm *et al.*, 2003 for location). **(a)** Polished slab. Dark bands with white spots are coarse blocky calcite. Ghost structures of the skeleton exist in the medium grey bands (fine blocky spar) and light grey bands (micropelletoidal carbonate). **(b)** Thin-section view (plane light) of a microsolenid coral. Subsequent to the formation of a micrite envelope, the original skeleton has been leached and replaced by equant spar. Micropelletoidal carbonate settled or formed within skeletal cavities; it preferentially accumulated along tabulate dissepiments. Thin section micrograph, plane light. **(c)** Detail of fig. 3.11b. Thin-section micrograph, plane light.

3.8 Conclusions of chapter 3

(1) Coral limestone of Late Miocene age from the island of Crete (Greece) exhibits the typical pattern of preservation of the hermatypic coral skeleton: moldic porosity related to leaching of the original aragonite skeleton and partial or full replacement by sparry calcite cement. In some marl deposits and poorly classified sandstone/conglomerate, however, coral skeletons underwent no significant non-marine diagenesis and, correspondingly, have fully retained their original mineralogy, microstructures and porosity (stagnant diagenetic environment). Conspicuous couplets of “light” and “dark” bands in coral slabs represent annual growth increments because they are fully compatible with prominent density bands detected in X-ray radioographs and stable isotope variations ($\delta^{18}O$, $\delta^{13}C$).

(2) The conspicuous “light” and “dark” annual bands in corals result from slight variations in skeletonization and crystal size of the skeleton. In the active diagenetic environment, alteration and dissolution of the skeletons is induced at the centers of calcification, however, at higher rates in the “light” bands (the high density bands) because of the reduced crystal size. This process favours the formation of sheet-like voids, that reflect the growth bands. Were dissolution rates do not fully exceed cementation rates, leading to formation of a large mold, annual banding in massive, recrystallized *Porites* may be preserved in the freshwater/shallow burial diagenetic environment. Thickness of the banding is equivalent to the “aragonite *Porites*” (~4 mm), which demonstrates the potential use of growth bands in paleoclimatology and paleoecology. For instance, vertical extension rates of few millimetres per year in massive *Porites* are known from high latitude reefs in modern oceans only, and appear to be typical for the periphery of the present global tropical reef belt (Grigg, 1982; Lough & Barnes, 2000). In terms of the Late Miocene paleogeography, the Mediterranean area can be considered the „outpost“ of the global coral reef belt in the northern hemisphere (Esteban, 1996).

(3) Branching *Porites* exhibit growth banding formed by concentrations of pelletoidal micrite along tabulate dissepiments. The narrow spacing of this type of banding (~1.8 mm) and its association with dissepiments implies the possibility of reflecting a subannual, lunar rhythmicity (Lough & Barnes, 2000; Cohen & Sohn, 2004). Estimates of vertical extension rates in fossil corals, therefore, require proper documentation of the high and low density bands, whereas the existence of rhythmic growth bands alone is insufficient to detect annual growth and a possible photosymbiotic lifestyle.

(4) Conspicuous, millimetric couplets of light and dark bands are also present in Mesozoic corals. In the microsolenid skeleton continuous accumulations of pelletoidal carbonate along dissepiments immediately above bands formed of coarse blocky spar

(interpreted to represent the high density band removed by dissolution). The prominent banding present in these massive corals, therefore, results from the superposition of monthly and annual growth rhythms. This interpretation agrees with the reconstructed high latitude position for the sampled Late Jurassic (Oxfordian) coral reef from NW-Germany (Lower Saxony Basin), located at a transitional position between the warm Tethys and the temperate boreal faunal provinces during the Oxfordian (Helm *et al.*, 2001).

4 Late Miocene corals (10 Ma) from Crete (Greece) document interannual climate variability controlled by the Icelandic Low

The present knowledge of the global climate evolution during the Cenozoic era was unlocked principally from deep sea sedimentary archives using environmental proxy data reflecting global ice build-up (Miller *et al.*, 1991, Zachos *et al.*, 2002), water temperature (Billups *et al.*, 2002), weathering history (Raymo *et al.*, 1992), and carbonate patterns (Lear *et al.*, 2003a). For the Neogene period, this record allows to identify insolation changes as pacemakers of paleoenvironmental changes (Sierro *et al.*, 2003) and to establish a quantitative chronostratigraphic framework on orbital time scales (Hilgen *et al.*, 1995). In shallow water environments, carbonate secreting biota are highly sensible to sea surface temperature (SST), salinity and nutrient concentrations (Lees & Buller, 1972) and, therefore, have potential to document climate changes in the geological record (Betzler *et al.*, 1997b; James, 1997). However, systematic application of the method in palaeoclimatology is limited, because upon crossing certain critical environmental thresholds, the shallow water systems tend to switch from one stable condition into an other, and the paleoclimatic record of shallow water carbonates remains largely qualitative (Brachert *et al.*, 1996, 2001). In addition, Cenozoic carbonate platform data suffers from a discontinuous sedimentary record and limited precision in age models (Schlager, 1992, 1999). Notwithstanding these limitations, the environmental information stored in the skeleton of large scleractinian corals may add a new dimension to the understanding of the Cenozoic climate system, because the massive skeletons of colonial corals represent archives of past SST, salinity (SSS) and productivity that resolve up to interannual to subannual timescales. In historic and prehistoric time, the coral record has therefore proven to be an important source of information to study seasonality and climatic variations on interannual to interdecadal time scales (Druffel, 1997; Gagan *et al.*, 2000; Grottoli, 2001; Felis *et al.*, 2004). However, the aragonite coral skeletons are susceptible to various types of mineralogical and geochemical alteration, and corals older than the Pleistocene are generally recrystallized and transformed from original aragonite into secondary calcite (Constanz, 1986; Roulier & Quinn, 1995).

In chapter 4, seasonally-resolved environmental proxy records using fossil *Porites* corals found in sediments of early Late Miocene age (10 Ma, Tortonian) on the island of Crete (eastern Mediterranean Sea) are presented. The massive coral skeletons have retained their original aragonite mineralogy, microstructure and skeletal porosity. In cross sections, and X-ray radiographs, conspicuous growth increments represent annual density bands known from modern *Porites* (see chapter 3). Growth rates were ~4 mm/year^{-1} and similar to massive *Porites* from modern high-latitude reefs (Abram *et al.*, 2001), which reflects the position of Crete at the northern margin of the Late Miocene reef belt (Esteban, 1996), and the warmer than present Late Miocene greenhouse climate (Zachos et al. 2001). Although the Late Miocene paleoceanography and paleoclimatic evolution of the Mediterranean is well known on geological time-scales (Hilgen *et al.*, 1995; Lourens & Hilgen, 1997; Schenau *et al.*, 1999), little information exists with regard to the subannual and interannual climate variability. A Miocene tree ring record from central Europe has revealed highly significant variance at periods of 5-6 years (Kurths *et al.*, 1993). For the eastern Mediterranean and Middle East, the Arctic Oscillation/North Atlantic Oscillation (AO/NAO), the Northern Hemisphere's dominant mode of atmospheric variability (Hurrell, 1995; Thompson & Wallace, 2001), exerts not only a major impact on the present-day climate, but has also played a critical role during the Holocene and last interglacial, preferentially on interannual time scales of 5-6 years (D´Arrigo & Cullen, 2001; Rimbu *et al.*, 2001; Felis *et al.*, 2000, 2004). In order to evaluate the significance of the Miocene interannual climate signal from the terrestrial archive, and to put it into a large-scale climatic context, a marine coral stable isotope record ($\delta^{18}O$) from the Miocene of Crete that covers a time span of 69 years is analyzed. The combined approach based on the coral proxy data and model simulations for the Tortonian using the ECHAM4/ML climate model for a world without Greenland ice shield (Micheels, 2003; Steppuhn *et al.*, 2004) provides new insights into atmospheric variability at interannual time scales in the European/Mediterranean region 10 Ma ago.

4.1 Geological context

Following the greenhouse climate of the Middle Miocene, stepwise cooling and incipient glaciation of the northern hemisphere took place during the Late Miocene (Zachos *et al.*, 2001). During this period, 10-5 million years ago, the global paleogeography and plate mosaic arrived at the main traits of the present-day situation. Although situated at a somewhat more southward position (1-3° latitude; Perrin, 2002), the general paleogeography of the Mediterranean Sea was similar to the present-day: it formed a marginal sea of the Atlantic Ocean framed by uplifting mountain ranges. An ephemeral sea strait intermittently linked the eastern Mediterranean via the Aegean with the Paratethys to the north of the alpine orogen system (Rögl & Steininger, 1984). Coral reef growth over most shallow water zones of the ancient Mediterranean Sea and a subtropical vegetation (Sachse & Mohr, 1996), is the obvious local expression of a globally warm climate (Zachos *et al.*, 2001). During the earliest Tortonian, in the central Mediterranean province, almost no true reefs but only isolated non-framework communities of *Porites* and *Tarbellastrea* occurred. Neither zooxanthellate corals nor reefs existed to the west of the Betic-Rifan chain in the Atlantic, nor in the northernmost Mediterranean Sea and the Paratethys, whereas coral reef growth only has been documented in the western and eastern Mediterranean area. This biogeographic pattern and the remarkably low diversity of reef corals (dominance by *Porites* and *Tarbellastrea*) are generally supposed to reflect a position of the Mediterranean at the northern limit of the global coral reef belt (Brachert *et al.*, 1996; Esteban, 1996).

On astronomical time scales, the eastern Mediterranean oceanography was repeatedly affected by monsoon (Schenau *et al.*, 1999; Hilgen *et al.*, 2003). However, with regard to the overall similarity of the paleogeography with the present-day situation, there might have been a marked influence of the Atlantic domain on eastern Mediterranean climate via atmospheric teleconnections and ocean circulation patterns (D´Arrigo & Cullen, 2001; Felis *et al.*, 2000, 2004; Rimbu *et al.*, 2001; Meijer *et al.*, 2004; Cullen & deMenocal, 2000).

4.2 The island of Crete during the Late Miocene

The Tortonian rock section of central Crete starts with clastics of the Ambelousos Formation (Fig. 4.1; Meulenkamp *et al.*, 1979). Depositional environments were brackish lagoons and marginal marine environments. Coarse clastic sediments formed along the coastline, which were intermittently colonized by corals forming isolated reef patches and laterally extensive biostromes (see chapters 1-2). The coral constructions are taken as an indicator of winter SST not colder than 18°C (Abram *et al.*, 2001). Coral biostromes composed of large massive colonies of *Porites* and *Tarbellastrea* with minor contributions of *Acanthastrea* developed during episodes of low terrigenous input due to low precipitation, whereas thicket-like coral biostromes constructed by ramose branching *Porites* formed during episodes of high siliciclastic influx due to high precipitation (see chapter 2). Stratiform lignite concentrations within some segments of the formation (Fig. 4.1) strikingly document moist climatic conditions. However, a bed with pedogenic lenticular gypsum (Fig. 4.2) implies a shift from moist to dry climatic conditions over geological time scales during the Tortonian. Consistently, terrestrial floras document a warmer, but also a more humid climate than in present-day Crete, with a maximum of precipitation during the winter (Sachse & Mohr, 1996). The Ambelousos Formation is covered by the more calcareous Varvara Formation of late Tortonian - early Messinian age (Late Miocene). The Early

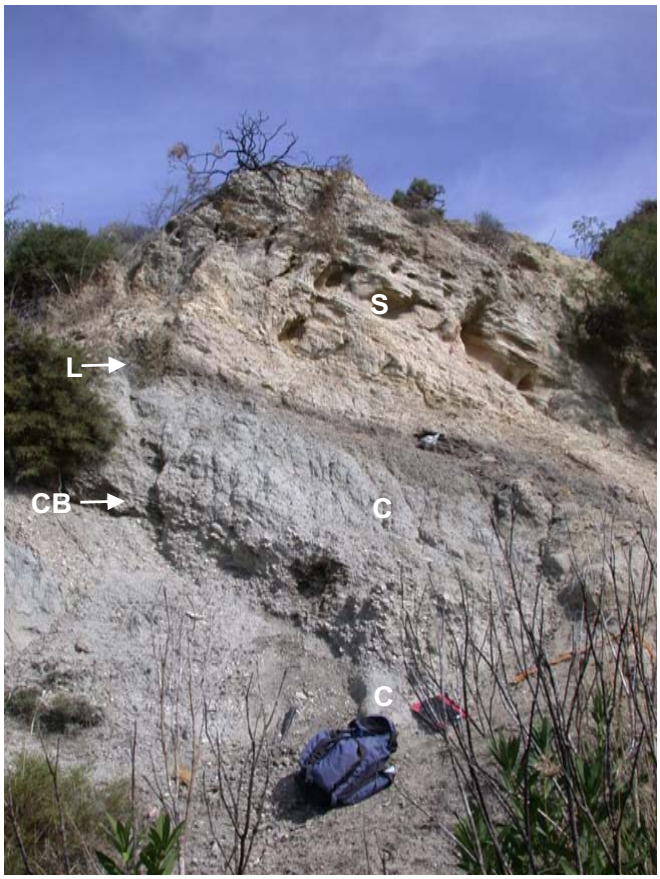

Fig. 4.1. *(left)* Clay and sandstone section beneath Psalidha buildup; basal Ambelousos Fm. Intercalated with dark grey clay (C) are a thin bed lignite (L) and a *Crassostrea*-bank (CB). Typical constituents of clay and oyster bed are gastropds (*Terebralia* cf. *bidentata*, *Melanopsis impressa*), ostracods (*Cyprideis*) and foraminifera (*Ammonia*), whereas the lignite includes *Theodoxus, Cyprideis* and gyrogonites. The hanging sandstone (s) contain no fossils. The biotic composition point to a restricted marginal marine environment with lowered salinity and fluvial discharge. N 35.08274°, E 024.95983°.

Fig. 4.2. *(above)* Lenticular gypsum crystall (length 1,5 cm). Such idiomorph gypsum crystals are common in dark grey clay on top of the exposed section in fig.4.1, where they are associated with fossil rootlets. They are pedogenic and were formed under arid conditions (Demicco & Hardie, 1994).

Messinian paleobotanical record documents successive climatic drying (Sachse, 1997; Zidianakis *et al.*, 2004), but temperatures remained sufficiently warm to sustain reef growth (see chapter 1.4). Finally, a thick gypsum unit present at the top of Varvara Formation implies environmental restriction in a very dry environment for the late Early Messinian (Meulenkamp *et al.*, 1979).

4.3 Methods

Two sites with aragonite corals have been found in central Crete near the ancient town of Psalidha (Figs. 2.1, 2.6, tab. 4.1). Site 1.3A is located in a grove with olive-trees, where recently ploughing has exposed abundant centimetric fragments of corals (*Porites*, minor T*arbellastrea*). Site 1.3B is an outcrop at the top of the Psalidha coral buildup with decimetric corals preserved in growth position (Fig. 3.3a). A geological section was measured at the latter site (Fig. 3.2A) and lithologies were classified according to biofacies and primary sedimentary textures. According to fine-scale geological mapping, both coral sites are in the same stratigraphic position at the top of Psalidha buildup (Fig. 2.9).

Location	Latitude	Longitude
Coral Site 1.3A	N 35.08446°	E 024.96668°
Coral Site 1.3B	N 35.08424°	E 024.96094°

Tab. 4.1. GPS coordinates of the Coral Sites 1.3A and B, top of Psalidha coral buildup (Fig. 2.6). Rouvas municipality, central Crete (Greece).

The fragile aragonite coral skeletons from Site 1.3B were embedded in polyurethane foam to prevent disintegration during sampling, transportation and splitting. Large specimens were split with a simple pad saw in the laboratory. Slabs and thin-sections of corals were stained with Feigl´s solution to reveal the distribution of aragonite and calcite (Füchtbauer, 1988). Under the SEM, broken and polished surfaces of the corals were analysed for ultrastructures. X-ray radiographs were taken from slabs cut to an equal thickness of 6 mm at the Research Center for Ocean Margins, University of Bremen, to reveal the annual density bands and potential recrystallization effects or cements. X-ray diffraction for aragonite and calcite was carried out at the Institut für Geowissenschaften, Mainz (H.-D. Werner) using a Seifert XRD 3000 diffractometer and were scanned from 2Φ of 20° to 60°.

From a total of 32 coral specimens, three samples were selected for a detailed stable isotope study according to visibility and thickness of the growth bands (P2, P3 and P4). Sampling for stable isotope analysis was performed along continuous transects following the most rapidly extending primary growth axes in order to minimize variation through po-

tential kinetic isotope effects (McConnaughey, 1989). Coral specimens P3 and P4 were mounted on a scaled movable table below a micro miller to allow for accurate, continuous equidistant sampling (distance 1.0 mm, diameter of drill bit 1.0 mm). The largest coral fragment (P2) was sampled along a continuous transect using a fine-scale chisel, to avoid for sliding effects of a hand-hold microdrill (sampling distance 1.22 mm). Stable isotope analysis was performed by M.M. Joachimski (Erlangen University, Germany). Carbonate powders were reacted with 100% phosphoric acid at 75°C using a Kiel III online carbonate preparation line connected to a ThermoFinnigan 252 masspectrometer. All values are reported in per mil relative to V-PDB by assigning a $\delta^{13}C$ value of +1.95‰ and a $\delta^{18}O$ value of -2.20‰ to NBS19. Reproducibility was checked by replicate analysis of laboratory standards and is better than ±0.03‰ (1σ). SST and SSS (sea surface salinity) variations were calculated according to published equations (Gagan & Chivas, 1994; Felis *et al.*, 2004; Craig, 1966). Measured coral isotope data sets are listed in the Appendix (A2-4). Age models were based on banding couplets and were calibrated against the most positive oxygen isotope values measured per annual cycle. The longest coral record (69 years) was selected for spectral analysis to detect potential interannual cyclicity. Prior to spectral analyses (Ghil *et al.*, 2002), the original data set was transformed into an equally spaced time series of four samples per year (Paillard *et al.*, 1996; quarterly resolution), detrended and normalized.

To investigate the physical mechanisms behind the documented interannual climate variability in the coral proxy records from Crete and to intergrate it into a large-scale climatic context, a simulation with a complex atmospheric general circulation model coupled to a mixed-layer ocean model (ECHAM4/ML) for Tortonian conditions is analyzed (Micheels, 2003; Steppuhn *et al.*, 2004). The resolution of the spectral ECHAM model was T30 (3.75°×3.75°) with 19 levels for the vertical domain. The set of surface boundary conditions of the Tortonian simulation included a generally lower orography and a reconstructed vegetation which was characterized by a generally larger forest cover than today (Micheels, 2003; Steppuhn *et al.*, 2004). Moreover, continental ice was removed on the northern hemisphere (e.g. no Greenland ice shield), the land-sea distribution referred to modern conditions, and the atmospheric CO_2 was set to the present-day value of 353 ppm (Micheels, 2003; Steppuhn *et al.*, 2004; Pearson & Palmer, 2000; van der Burgh *et al.*, 1993). To account for a generally weaker paleooceanic heat transport such as represented in Miocene ocean model studies (Bice *et al.*, 2000; Mikolajewicz *et al.*, 1993), the flux correction of the constant depth 50 m-slab ocean model was adjusted for the Tortonian simulation (Steppuhn *et al.*, 2004). Miocene surface ocean circulation was not affected by the shape of the Mediterranean basin (Meijer *et al.*, 2004).

4.4 Preservation of the coral skeletons selected for stable isotope study

Corals were sampled for detailed petrographic and geochemical investigation at two locations of Psalidha buildup, (Coral Sites 1.3A-B; fig. 2.6, tab. 4.1). At Site 1.3B of Psalidha locality, a massive *Porites* has been found, which measures 1x1x2 m in size and which has fully retained its original aragonite mineralogy and skeletal microstructures. The massive skeleton consits of smaller, 5-10 cm wide, laterally fused columns with convex-upward hemispheric growth surfaces. It exhibits fractures, which preferentially were formed parallel to the contacts of the individual columns. Some of the fractures are filled with light grey, fine-grained limestone, whereas a second generation of fractures has remained open (Fig. 4.3).

In reflected light, conspicuous “light” and “dark” bands with a wavy form reflect the fused-columnar to protuberant growth form of the massive colony. According to X-ray radiographs, the couplets of “light” and “dark” bands correspond with alternating zones of high and low skeletal density (Figs. 4.3, 4.4a-b, tab. 3.1). The banding couplets seen in reflected light and x-radiographs, therefore, have been assigned to the annual growth increments, well documented from modern *Porites* corals (Knutson *et al.*, 1972). Correspondingly, the various pieces of the present coral span periods of 4 years to a maximum

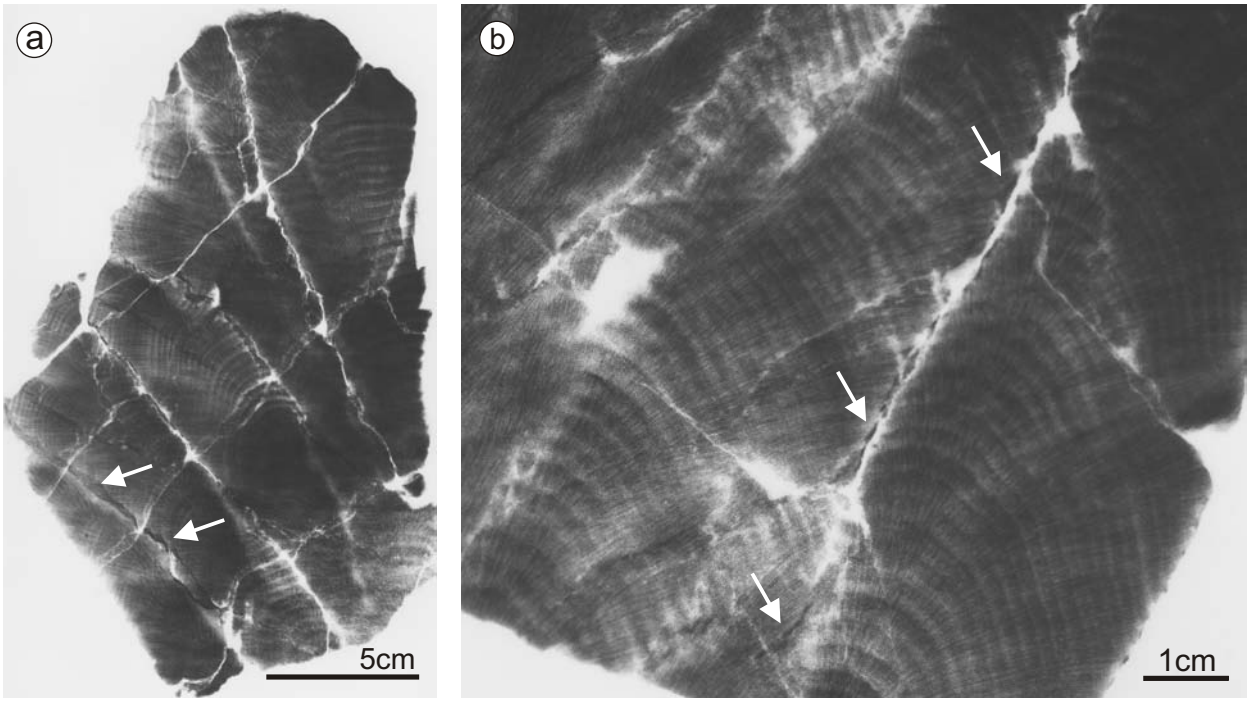

Fig. 4.3. X-ray photograph (positive print) from coral P2. Alternating bands of high (dark colour) and low skeletal density (light colour) are visible. One year is represented by one density couplet. The high density band appears “light” in reflected light, the low density band “dark” (Tab. 3.1). Irregular white lines crossing the growth fabrics represent fractures. White arrows mark fractures filled with cryptocrystalline carbonate (dark shade).

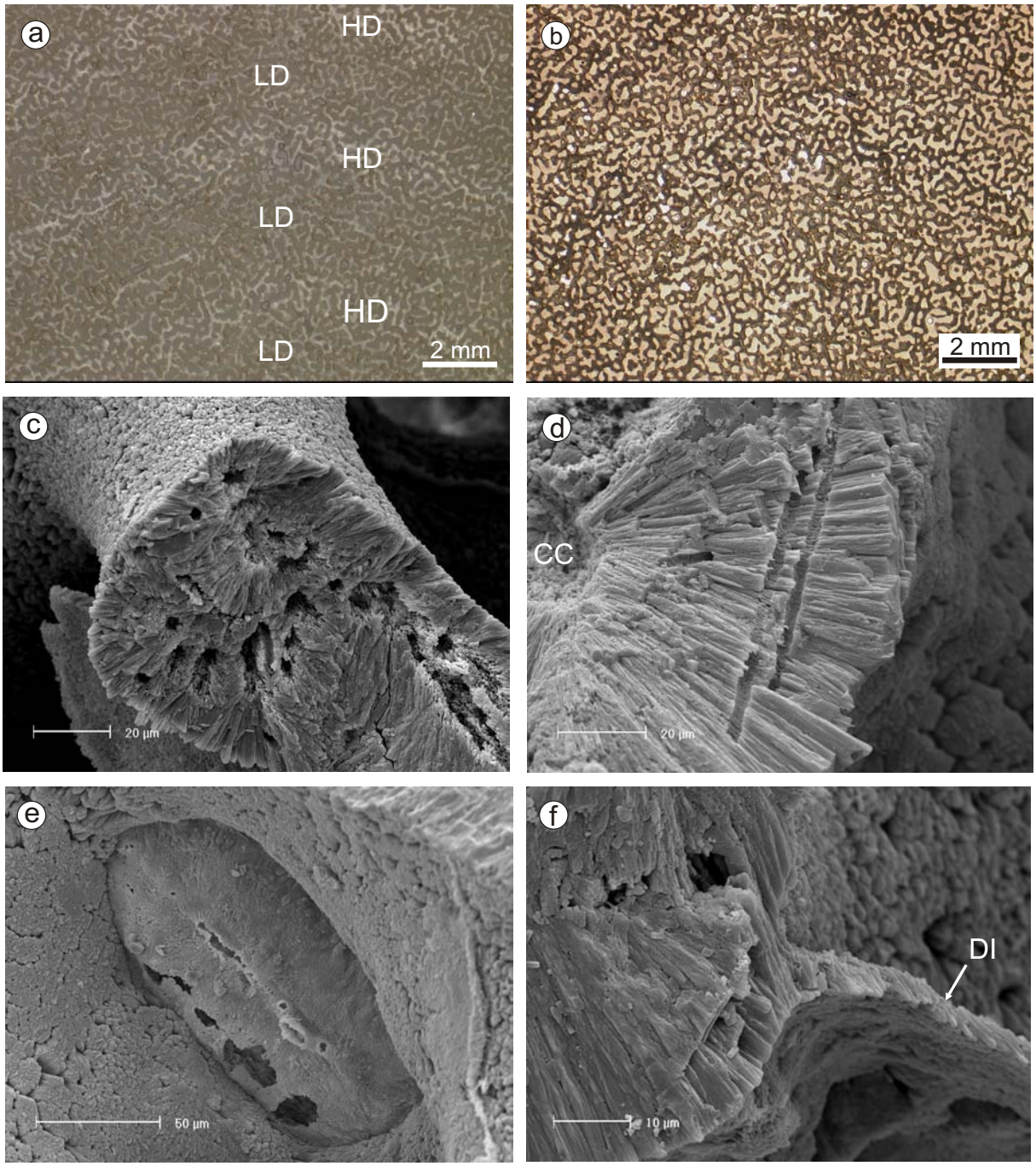

Fig. 4.4. Microscopic aspects of the coral skeleton. Thin section photomicrographs of the skeleton in reflected (**a**) and transmitted (**b**) light showing conspicuous couplets of dark and light bands. **(a)** The light material in this photograph is the coral skeleton. The skeleton is compact and thick in the light bands (HD) and comparatively more delicate and thinner in the dark bands (LD). Dark reflection between skeleton results from impregnation with epoxy resin. **(b)** In transmitted plane light, the growth banding is hardly visible. Diagenetic overgrowths and recrystallizations are not visible at this magnification and are therefore volumetrically not significant. Both photographs show same segment of coral P 2. **(c-f)** SEM micrographs of fresh fracture surfaces of the skeleton of coral P2. **(c)** Radial arrangement of trabecular fans. Centers of calcification were enlarged by partial dissolution. **(d)** Radial arrangement of trabecular fibres. The skeleton is riddled with abundant microborings of the siphonaceous green algae *Ostrobium quekettii* (*Ichnoreticulina elegans*; *det.* G. Radtke, Wiesbaden), which have not been filled by subsequent cementation. CC = centre of calcification. **(e)** Well preserved dissepiment in contact to a smooth skeleton surface. This side of the dissepiment shows no overgrowth by marine cements. The smooth surfaces remained in that areas, where the tissue stayed in prolonged contact with the skeleton. **(f)** The tiny crystallites of the dissepiments (DI) form meniscate diaphragms in continuity with trabecular fans and therefore represent an original growth fabric.

of 69 years. Growth rates remained at ~4 mm/year^{-1} and compare well with *Porites* from modern high-latitude reefs (Lough & Barnes, 2000, Abram *et al.*, 2001).

In thin-section (Figs. 4.4a-b), the skeleton exhibits a pristine type of preservation, with radially arranged trabeculae. Thin basal diaphragms (dissepiments) forming meniscate bridges within the skeleton are clearly visible. Diagenetic overgrowths and recrystallizations are not visible at this magnification and are therefore volumetrically not significant. SEM micrographs of fresh fracture surfaces of the skeleton, reveal the pristine aragonite texture of the skeleton with radial arrangement of trabecular fans showing no significant signs of dissolution nor recrystallization, even within the centres of calcification (Figs. 4.4c-f). The tiny aragonite crystals (1-2 µm) of the dissepiments do not exhibit any evidence for dissolution. The surface of the skeleton is either smooth or ragged, the latter due to some crystal growth. Planned-smooth surfaces show blunt crystal terminations, which were not subsequently overgrown by cement (Figs. 3.5e, 4.4e). These surfaces are interpreted to have formed in immediate contact with the calcioblastic tissue of the coral (Constantz, 1986), and were not later overgrown by cements. Tips of syntaxial aragonite cements (1-2 µm) forming thin crusts are interpreted to represent marine cement crystallized deeper in the coral, after withdrawal of the calcioblastic tissue from the skeleton during growth (Fig. 3.5f; Enmar *et al.*, 2000). Apart from cryptocrystalline carbonate infilling fractures calcite cements are not visible within the skeleton, (Fig. 4.3). Consequently, calcite concentrations remained below the detection limits of the X-ray diffraction method in all samples (1-2%), which reflects a very pristine stage of preservation of the corals studied, despite the fact that the age of these corals is 10 Ma.

4.5 Environmental interpretation of the coral stable isotope records

From both coral sites (Fig. 2.6, tab. 4.1), a total of three corals (P2, P3, P4) was selected and sampled for stable oxygen ($\delta^{18}O$) and carbon ($\delta^{13}C$) isotope analysis. The small coral fragments P3 and P4 were sampled at 1 mm increments allowing for a quarterly (P4) and bi-monthly (P3) resolution, and time series of 12 and 4 years duration, respectively. For technical reasons, a 69 years record (coral P2) was analysed at an average sampling resolution of 3 samples/year (~1.3 mm sampling increments), providing a near-quarterly resolution time series. In all records, the stable isotope patterns are within the same spectrum of variation: The mean $\delta^{18}O$ composition found within the short records of corals P3 (-2.59‰) and P4 (-2.96‰) are within the variation present in the 69 years record of coral P2 (-2.83‰; figs. 4.5, 4.6).

4.5.1 Annual variation

The coral $\delta^{18}O$ signatures exhibit a cyclic signal which consistently reflects the annual growth band couplets: maxima coincide with thin white bands, minima with thick dark bands. In the highest-resolution record (coral P3), the $\delta^{18}O$ signal is commonly a series of U-shaped arcs and is not necessarily a sinusoidal curve, because the maxima form narrow peaks (Fig. 4.5A). Coral $\delta^{13}C$ shows a correlation with the density couplets as well, but is usually phase-shifted relative to $\delta^{18}O$ by about a half isotope cycle. However, the minima in $\delta^{13}C$ consistently precede the maxima in $\delta^{18}O$ by one data point, i.e. ~2 months (Fig. 4.5A).

Interpretation: The couplets of light and dark bands are consistent with the density banding detected in X-ray radiographs (Figs. 3.4, 4.3) and the stable isotope patterns (Fig. 4.5): The thin light bands (observation in reflected light) of high skeletal density (inferred from X-ray radiographs) correspond to the more positive $\delta^{18}O$ values of an annual cycle and therefore reflect the suboptimal growth season, i.e. the winter. On the other hand, the thick dark bands of low skeletal density correspond to the more negative $\delta^{18}O$ values and therefore represent the summer. The asymmetric, series of arc-type oxygen isotope patterns implies, that the cold season is underrepresented due to slow growth (Wefer & Berger, 1991; fig. 4.5). The relationships between coral $\delta^{18}O$, $\delta^{13}C$ and the density banding pattern are identical to those of modern, shallow-water *Porites* from the nearby northernmost Red Sea (Felis *et al.*, 1998, 2000; Rosenfeld *et al.*, 2003). This arid region is the nearest modern analogue to the Tortonian reefs from Crete and is assumed to represent similar climatic/oceanographic conditions (high-latitude reefs, maximum sunshine in

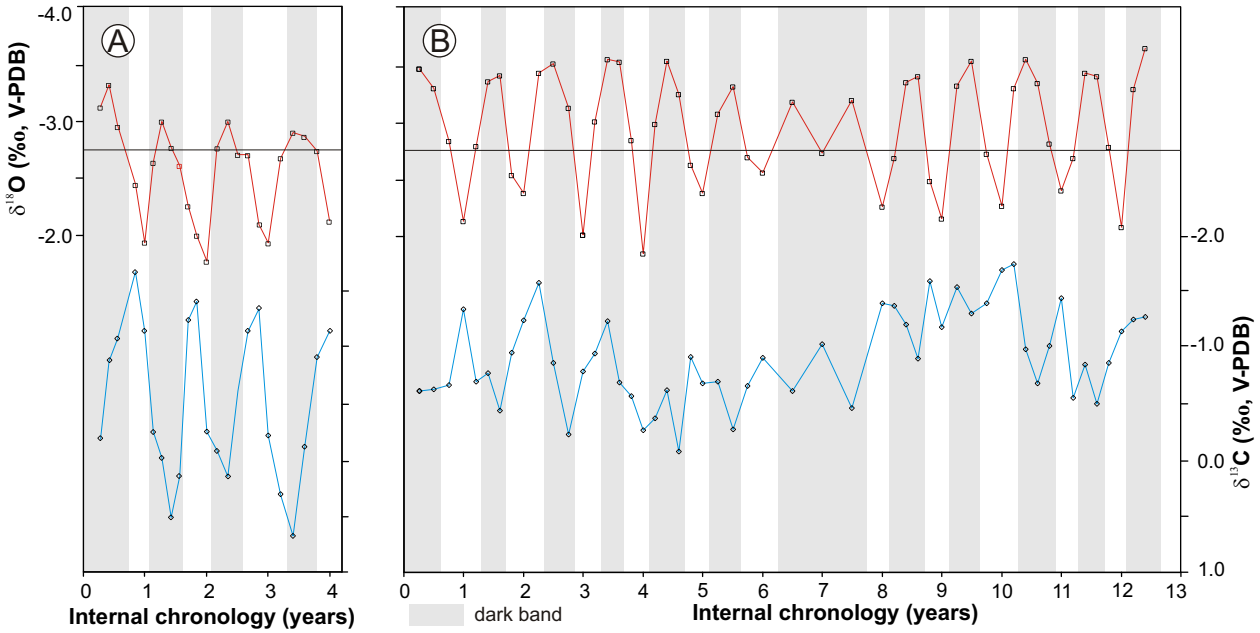

Fig. 4.5. High-resolution *Porites*-coral records of stable oxygen and carbon isotopic variations ($\delta^{18}O$ and $\delta^{13}C$ vs. V-PDB) from Psalidha Coral Site 1.3A. Gray bars show the dark bands visible in reflected light, black horizontal line shows mean $\delta^{18}O$ composition of the coral P2 shown in fig. 4.6. **(A)** coral P3, **(B)** coral P4.

summer, and clouds and rain in winter). Although paleobotanical records and lithological information from the Ambelousos Formation document extreme environmental variation over geological time scales, pure carbonate sediments preferentially formed in a rather dry climatic context (see chapter 1.4.1). Therefore, and because mean coral $\delta^{18}O$ seasonality in the Crete record (1.16‰) is in the same order of magnitude as from *Porites* from the last interglacial from the northernmost Red Sea (1.27‰/8.4°C; Felis *et al.*, 2004), it is assumed that the $\delta^{18}O$ seasonality in the Crete corals is largely controlled by temperature, which would suggest an SST seasonality of 7.7°C (Felis et al. 2004) for the eastern Mediterranean during the Tortonian (Fig. 4.5). According to Hofrichter (2002), the present-day eastern Mediterranean undergoes minor seasonal salinity changes as well (<0.5 ‰, equivalent with ~0.14‰ $\delta^{18}O$ V-PDB seawater change; Craig, 1966), but has a slightly more pronounced SST seasonality (~9°C equivalent with ~1.4‰ $\delta^{18}O$ V-PDB change in *Porites*; Felis *et al.*, 2004). The minor discrepance in SST seasonality could be explained in terms of a more southward position of the Mediterranean and a globally warmer climate during the Tortonian (Zachos *et al.*, 2001; Perrin, 2002).

The seasonal range of variation in coral $\delta^{13}C$ and phase shift relative to $\delta^{18}O$ is interpreted to reflect changes in autotrophy of the coral (Fairbanks & Dodge, 1979), i.e. less photosynthesis due to less sunshine in the suboptimal season and, second, a shallow water setting (Rosenfeld *et al.*, 2003). The latter reconstruction fits the general concepts of Miocene Mediterranean coral zonations with a maximum water depth for large massive

Porites of 10 m (Pomar *et al.*, 1996; Perrin *et al.*, 1995). Although on an annual scale, light intensity and SST are positively correlated, minimum winter temperatures lagged behind the minimum in light intensity by about two months (one sample increment). An analogous pattern has been described from the northernmost Red Sea, where annual light minima exist in winter (December-February), whereas the lowest SST have been encountered during March (Felis *et al.*, 1998).

All in all, these findings rule out the possibility of significant diagenetic modifications of the skeleton with respect to stable isotope ratios, because diagenesis tends to homogenize isotope signatures (McGregor & Gagan, 2003).

4.5.2 Interannual variation

One large coral (P2) provides a near-quarterly resolution $\delta^{18}O$ time series for a time window of 69 years. Apart from an overall $\delta^{18}O$ decrease in the order of -0.5‰ over the 69 years, the interannual coral $\delta^{18}O$ variations are in the order of 0.3 to 0.7‰ (Fig. 4.6). A compatible pattern of interannual $\delta^{18}O$ variation has been reproduced in the short (12 years) high-resolution record of coral P4 from Coral Site 1.3A (Fig. 4.5B).

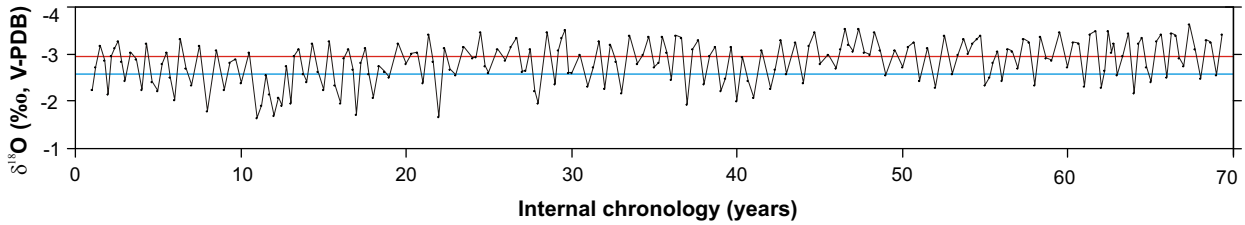

Fig. 4.6. Multidecadal (69 years) record of coral $\delta^{18}O$ with a near quarterly resolution. *Porites* P2, Coral Site 1.3B. Horizontal lines show mean $\delta^{18}O$ of corals P3 (blue line) and P4 (red line).

Interpretation: The $\delta^{18}O$ long-term trend and interannual variability may reflect not solely variations in SST but also in $\delta^{18}O_{seawater}$ as a result of variations in the hydrologic balance and related discharge in the marginally marine environment where the corals were growing. The presence of a consistent pattern of interannual variation in records from both coral sites suggests constraints by a specific climatic system variation during growth of the Psalidha buildup in the eastern Mediterranean area. Interannual $\delta^{18}O$ changes of the same order of magnitude were documented in Quaternary *Porites* from the northernmost Red Sea and the western tropical Pacific (Felis *et al.*, 2004).

4.6 Spectral analysis

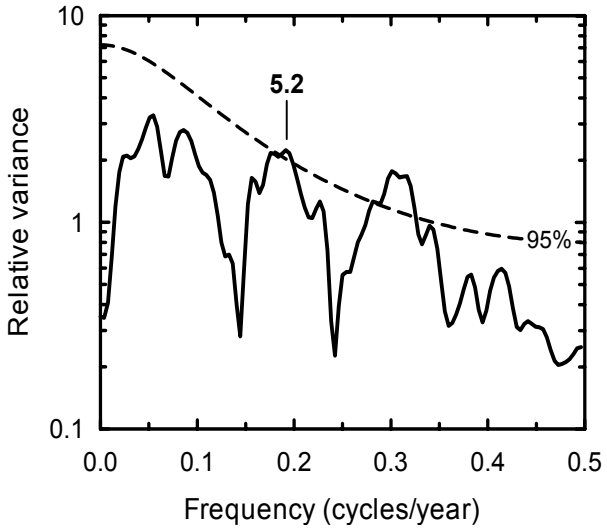

Fig. 4.7. Spectral properties of the 69-year Late Miocene coral $\delta^{18}O$ time series from coral P2. Multitaper method spectral analysis with red noise null hypothesis (Ghil *et al.*, 2002; number of tapers: 3, bandwidth parameter: 2, 95% significance level is indicated) of the quarterly interpolated, detrended and normalized coral $\delta^{18}O$ time series.

Multitaper method spectral analysis of the coral $\delta^{18}O$ time series (P2) reveals significant variance at periods of 5-6 years (with a peak at 5.2 years) reflecting interannual variations in SST and hydrologic balance in the eastern Mediterranean during growth of the Psalidha buildup (Fig. 4.7). These time scales could indicate a link with El Niño-Southern Oscillation (ENSO)-related monsoon activity, such as the long-term Neogene sapropel records from the eastern Mediterranean document monsoon discharge variation on geological time scales (Schenau *et al.*, 1999; Hilgen *et al.*, 2003). However, dominant interannual variability within the same frequency band (with a peak at 5.6 years) has been found previously in Miocene tree ring-width records from central Europe, Germany (Kurths *et al.*, 1993). The presence of enhanced variance at similar interannual periods in proxy records from both, central Europe and the eastern Mediterranean area, implies that both regions were linked to the same climatic system, and that a 5-6 years variability seems to be representative for the early Tortonian. Proxy records of eastern Mediterranean/Middle East climate for the last interglacial, the late Holocene, past centuries, and instrumental data from the present-day consistently show significant variance at periods of 5-6 years. In this region, these time scales of interannual variability are indicative of AO/NAO-like atmospheric variability over the Northern Hemisphere (D´Arrigo & Cullen, 2001; Felis *et al.*, 2000, 2004). Although the AO/NAO is most pronounced during winter, enhanced variance at these time scales is reflected in the region's climate variability throughout the year (Felis et al. 2004), as the AO/NAO is present throughout the year (Barnston & Livezey, 1987; Rogers & Hugh, 2002). On the other side, ENSO teleconnections in the eastern Mediterranean/Middle East region are weak, non-stationary, and modulated by higher latitude atmospheric circulation regimes (Felis *et al.*, 2000; Rimbu *et al.*, 2003). The coral-based results from Crete therefore suggest that time scales of interannual climate variability in the eastern Mediterranean during growth of Psalidha buildup were similar to the present, and furthermore are interpreted as an indication of AO/NAO-like atmospheric variability 10 million years ago. This scenario does not rule out the possibility of changes in eastern Mediterranean climate variability during the Tortonian on geological time scales that are related to insolation changes and indirect monsoon influence (Schenau *et al.*, 1999; Hilgen *et al.*, 2003).

4.7 Modelling Tortonian climate

The modelled surface air temperature anomalies indicate warmer winters during the Tortonian relative to the present in northern Europe and in the western and eastern parts of the Mediterranean basin, but cooler winters over the Atlantic. This result is consistent with the spatial distribution of earliest Tortonian coral reefs, non-framework colonial coral communities and cool-water carbonates (Fig. 4.8A; Guernet, 1978; Braga & Martín, 1990; Franseen *et al.*, 1996; Wrobel, 2000; Kroeger, 2004). The interannual variability of modelled eastern Mediterranean winter SST during the Tortonian is linked to a spatial pattern in the modelled sea level pressure field that resembles the present-day Icelandic Low (Fig. 4.8B), one of the centres of action of the AO/NAO. The model is consistent with the coral-based results from Crete that suggest AO/NAO-like interannual variability during the Tortonian. Compared to today, the Icelandic Low in the model is displaced southwards and more pronounced relative to the Azores High, the AO/NAO´s subtropical center. The model suggests that interannual SST variability in the eastern Mediterra-

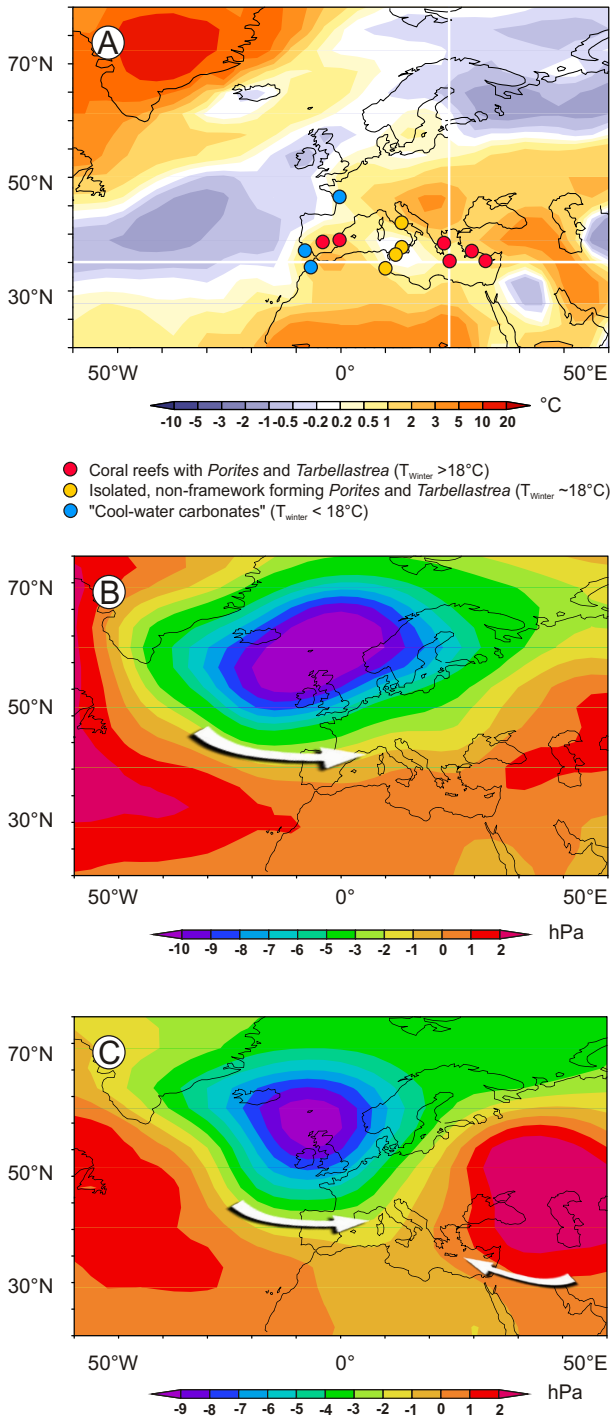

Fig. 4.8. (A) Near-surface air temperature anomaly showing the difference between Tortonian (Late Miocene) and modern winter climate (December, January, February; DJF), based on simulations with the ECHAM4/ML atmospheric circulation model coupled to mixed layer ocean model (Micheels, 2003; Steppuhn *et al.*, 2004). Earliest Tortonian reefs (red dots) indicate winter SST >18°C and single coral colonies in non-reefal carbonates (orange dots) are assumed to reflect winter SST of ~18°C. White cross marks Crete **(B-C)** Relationship between modelled interannual eastern Mediterranean climate variability and modelled North Atlantic-European air temperature and sea level pressure (SLP) during the Tortonian, based on the ECHAM4/ML model (Micheels, 2003; Steppuhn *et al.*, 2004). Near surface wind anomaly is schematically represented as white arrows. **(B)** Composite map for modelled Tortonian sea surface temperature in the eastern Mediterranean (20°-30° E; 35°-40° N) and modelled SLP for winter (DJF). **(C)** Same as in (B), but for modelled Tortonian evaporation in the eastern Mediterranean (DJF).

nean during the Tortonian was linked to the variability of the Icelandic Low, which controlled the intensity of the westerlies bringing warm air from the Atlantic ocean to the Mediterranean (Fig. 4.8B).

The interannual variability in the Tortonian coral $\delta^{18}O$ record does not solely reflect variations in SST but also in the hydrologic balance. Consistent with the coral-based results, the interannual variability of modelled eastern Mediterranean winter evaporation is linked to the variability of the Icelandic Low (Fig. 4.8C). The model suggests that the physical mechanism is provided by a high-pressure anomaly over southern Eurasia that in turn is related to variations of the Icelandic Low. The high-pressure anomaly controls the advection of dry continental air from northern Arabia towards the eastern Mediterranean.

4.8 Conclusions of chapter 4

(1) Corals recovered from the top of the Psalidha buildup (early Tortonian, 10 Ma, central Crete) have fully retained their original microstructure, aragonite mineralogy and stable isotope composition. Variations of coral $\delta^{18}O$ and $\delta^{13}C$ are compatible with annual growth bands visible in polished slabs and annual density bands observed in X-ray radiographs, and reflect seasonal environmental variability.

(2) On the interannual time scale, the coral $\delta^{18}O$ variations exhibit a 5-6 years cyclicity, which matches the present-day eastern Mediterranean climate variability controlled by the AO/NAO (Felis *et al.*, 2004), that has previously been documented in Miocene tree ring records from central Europe (Kurths *et al.*, 1993). This identical signal of climate variability at interannual time scales suggests that both, the eastern Mediterranean area and central Europe, were coupled to the same climatic system, and according to a simulation with a climate model, were controlled by atmospheric variability associated with the Icelandic Low.

(3) The combined coral- and model-based study suggests AO/NAO-like atmospheric variability over the Northern Hemisphere 10 million years ago, in a period when the Greenland ice sheet did not exist. The possible future retreat of the Greenland ice sheet (Dethloff *et al.*, 2004; Gregory & Huybrechts, 2004) along with an expected global temperature increase of 1-2K within the next centuries (IPCC, 2001) might provide a possible analogoue situation to the Tortonian, for which a similar temperature difference from today has been estimated (Crowley & Zachos, 2000).

(4) Clearly, more proxy records that resolve seasonal to interannual climate variability, allowing to separate temperature from seawater effects on coral $\delta^{18}O$, are needed to establish Late Miocene climate patterns. However, this study highlights the sinificant contribution of the analysis of shallow water carbonate systems can make to Neogene paleoclimatology and paleoceanography, and supports the idea of the Tortonian as a period for cross-validation of paleoclimate reconstructions and climate models to successfully predict future climate.

5 Coral growth bands: an efficient and easy to use paleothermometer in paleoenvironment analysis and paleoclimatology

Zooxanthellate scleractinian corals represent high-resolution archives of past climates. It is mostly the geochemical signature of the skeleton, that is explored for proxy records of atmospheric variations and carbon budgets of the ocean (Felis & Pätzold, 2004). The method is limited in use for the more distant geological past, because the scleractinian aragonite skeleton is subject to rapid textural change and chemical alteration in most diagenetic environments (see chapter 3). Consequently, geochemical proxy records of corals older than Pleistocene are rare (2005; Roulier & Quinn, 1995). Beyond geochemical paleoenvironmental data, calcification rates and annual vertical extension rates are directly linked to ambient water temperature and, to a lesser extent, to factors such as nutrient concentration or wave exposure (Barnes & Lough, 1993; Lough & Barnes, 2000). Paleoenvironmentally, the annual growth increments are of particular significance, because in diagenetically altered scleractinian skeletons they are commonly preserved as ghost structures and easy to measure in the field or in the laboratory (see chapter 2). Nonetheless, only few studies have explored the potential of growth bands in fossil corals in comparative paleoenvironment analyses, or for tracing the history of algal symbiosis (Ali, 1984; Insalaco, 1996; Helmle & Stanley, 2003). In chapter 5, massive *Porites* of Late Miocene age from the island of Crete (eastern Mediterranean) are described, that are useful for testing the potential of the growth band approach in paleoenvironment analysis and paleoclimatology.

Cenozoic plate movements transformed the central Teyths ocean into the Mediterranean Sea. By the end of the Middle Miocene, the sea straits connecting the Indopacific and the Mediterranean had closed, and the Mediterranean now formed a deep marginal sea of the Atlantic ocean. However, these marine passages in the Betic and Rifan domain were increasingly restricted in the course of the Late Miocene, perhaps leading to complete Mediterranean isolation during the Messinian Salinity Crisis (Hsü *et al*., 1977). In the Mediterranean, a sea strait linked the eastern Mediterranean with the Paratethys to the north of the alpine orogen system via the Aegean Sea. Finally, the new Gibraltar passage into the Atlantic was established by the early Pliocene (Meulenkamp & Sissingh, 2003; Rögl & Steininger, 1984). Correspondingly, the modern Mediterranean Sea represents a deep

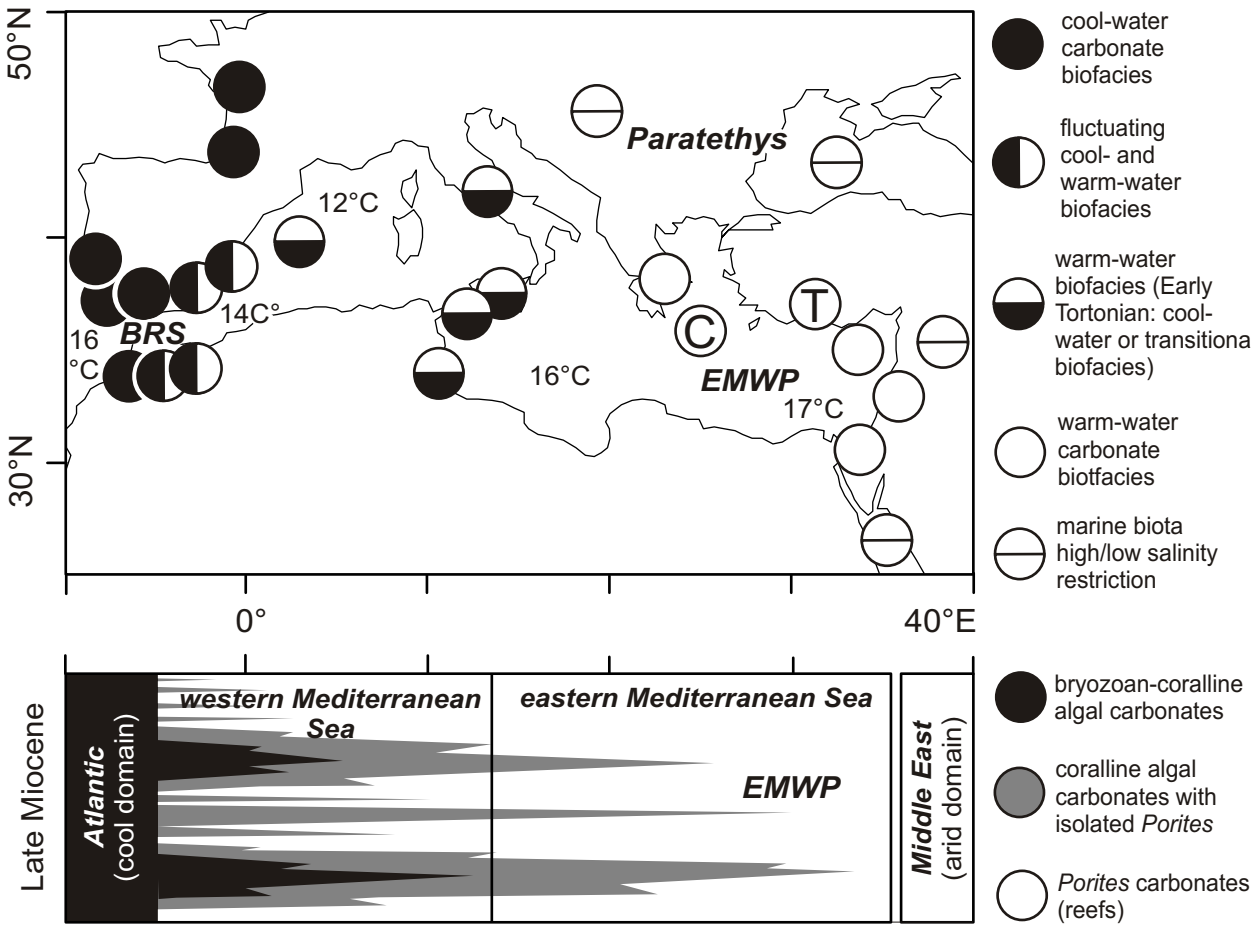

Fig. 5.1. Late Miocene shallow marine biofacies of the Mediterranean region. Numbers show modern February water temperatures at 10 m depth (from Levitus database). EMWP is the Eastern Mediterranean Warm Pool and BRS the Betic-Rifan Sill. C and T give the locations of Crete and Turkey.

marginal basin of the Atlantic. Incoming surface waters from the Atlantic get more saline and warmer towards the east, where they form the oligotrophic Eastern Mediterranean Warm Pool (EMWP, new term) with SST_{winter} remaining warm-temperate (above 17°C at 10 m depth, from Levitus database; fig. 5.1). A shallow sill at Gibraltar prevents inflow of cool deep water into the basin, which allows for the formation of a remarkably homiothermal Mediterranean water column. Atmospheric variability of the Mediterranean region and Middle East is controlled by the Arctic Oscillation/Nordatlantic Oscillation (AO/NAO; D'Arrigo & Cullen, 2001; Hurrell, 1995).

Late Miocene climate was transitional from the Middle Miocene greenhouse towards the icehouse state of the late Neogene (Zachos *et al.*, 2001). In addition to the Late Miocene warm climatic situation, the Mediterranean area was positioned slightly more to the south and has subsequently moved into the present location (Perrin, 2002). Late Miocene warm surface temperatures in the Mediterranean area are documented by widespread coral reef growth, but no reefs existed in the northern Mediterranean Sea (Gulf of Lyons, Adri-

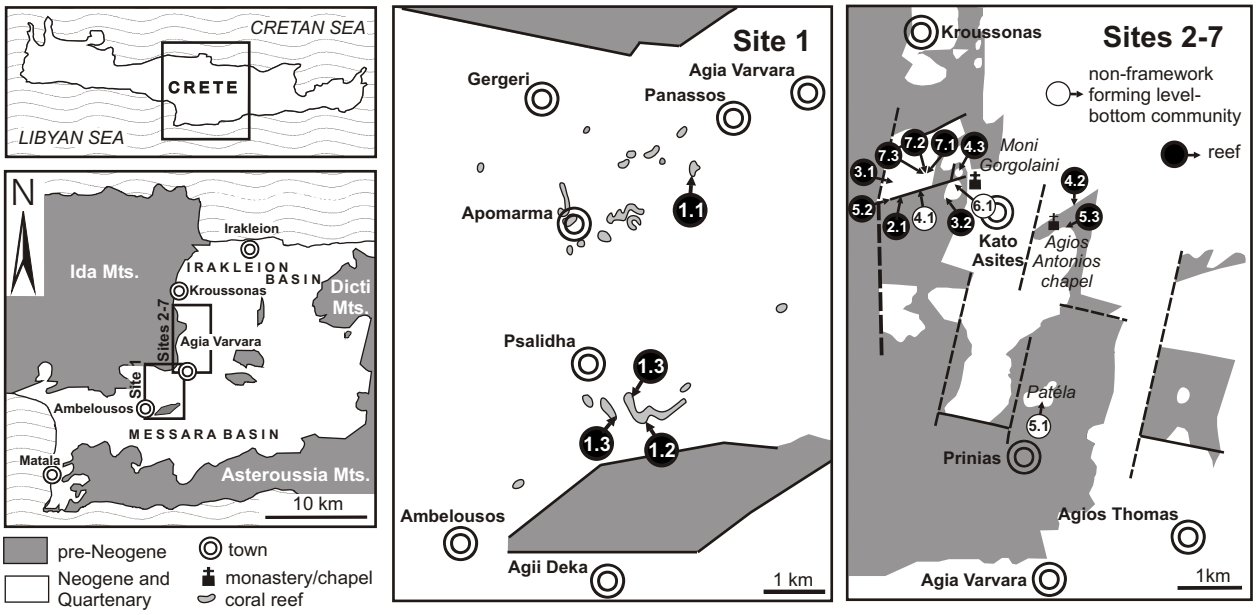

Fig. 5.2. Location of sampling sites.

atic Sea, northern Aegean Sea) or in the epicontinental Paratethys and to the west of the Betic-Rifan chain in the eastern Atlantic (Esteban, 1996). Reef growth was intermittent in the west, where constructional coral communities alternate with level-bottom carbonate communities (Brachert *et al.*, 1996; Martín & Braga, 1994; Montenat, 1990). Towards the east, carbonates formed by non-reefal level bottom communities become less abundant (Fig. 5.1). The Mediterranean reef biogeography, the remarkably low diversity of reef corals and the discontinuous growth patterns of the reefs is generally believed to reflect a position of the Mediterranean at the northern margin of the global coral reef belt (Brachert *et al.*, 1996; Esteban, 1996). In this context, final extinction of the reef ecosystem in the Mediterranean area by the Pliocene is supposed to be a consequence of climatic cooling (Esteban, 1996; Martín & Braga, 1994). Recently, this view of late Neogene carbonate ecosystem change has been challenged by a concept that infers fluctuating nutrient concentrations (Pomar *et al.*, 2004).

Systematic assessments of skeletal growth rates in Indo-Pacific *Porites* have demonstrated a clear calcification or growth rate over sea surface temperature relationship, whereas other factors, such as nutrient concentrations are subordinate or insignificant as control of growth rates (Barnes & Lough, 1993; Lough & Barnes, 2000). In this chapter, the potential that systematic documentations of vertical skeletal extension rates of Late Miocene massive *Porites* may have for the ongoing discussion on Mediterranean coral growth and paleoclimatic or paleoenvironmental reconstructions is discussed. The corals analysed in this study were selected from Late Miocene sediments of the island of Crete (Greece), located in the centre of the Eastern Mediterranean Warm Pool (Figs. 5.1, 5.2). Coral reefs

and level bottom coral communities occurred in the coastal zone, where they were a part of mixed clastic-carbonate ramp systems. Within the topographically isolated centre of the basin, they formed a pure carbonate realm that exhibits ramp and escarpment-type depositional systems (see chapter 1.4). The presence of massive *Porites* in these contrasting environments represents a perfect pre-requisite for testing the effects of water transparence, water depth, sediment load, terrestrial nutrients and sea floor physiography on coral growth rates beyond temperature effects. It is shown, that annual growth bands provide basic information pertaining to past sea surface temperatures (SST) and give new clues for understanding the ongoing debate on the Late Miocene paleoceanography of the Mediterranean area. The growth rate data have the potential to back-up and calibrate previous $\delta^{18}O$, Mg/Ca or Sr/Ca SST reconstructions.

5.1 Material and Methods

Field work for this study is based on detailed measurements of annual growth increments in massive skeletons of the coral *Porites*. Preservation of the original aragonite mineralogy and microstructures is rather unusual in the geological record of scleractinian corals (see chapter 3). In central Crete, aragonitic preservation of corals is restriced to the uppermost reef level in Psalidha outcrop (Site 1.3; fig. 3.2A) and to debrites in Moni Gorgolaini-North outcrop (Sites 7.1, 7.2, 7.3; figs. 3.2C, 5.2, A7). The vast majority of corals from the Ambelousos and Varvara Formations are leached or transformed and recrystallized into coarse blocky calcite spar. This is the typical state of preservation of zooxanthellate corals from Neogene carbonate sediments (Brachert *et al.*, 2001; Martín *et al.*, 1989). However preservation of corals transitional between original aragonite and secondary calcite, reveals that conspicuous banding in recrystallized corals represents ghost structures of the original annual density bands (see chapter 3). This type of preservation is omnipresent in massive *Porites* from the Late Miocene of Crete and allows for reliable measurements of growth rates of corals in the field (Fig. 5.3).

Fig. 5.3. Field aspect of growth bands in a recrystallized coral from Coral Site 4.2. Sheet-like empty voids represent the original high density bands.

Coral growth rates were measured at 16 sites that have been assigned to 7 chronostratigraphic coral levels based on stratigraphic geometries that are equivalent to the depositional units in chapter 1 (Fig.1.2). The coral levels cover the Tortonian and early Messinian period of time (Figs. 5.4, 5.5). Coral growth rates were measured in the field on natural cross sections of massive heads of *Porites*. Three dimensional weathering surfaces of the corals allowed for a reliable detection of the axes of maximum growth. Extension rates were determined as annual means by counting the annual growth bands within a given segment of the corals that was measured with a digital caliper. This method allowed for sufficient precision in the determination of the thickness of growth bands on a submillimetre scale. Measurements were made in outcrops with a well documented chronostratigraphic position (see chapter 1.3, fig. 5.4, A5-6).

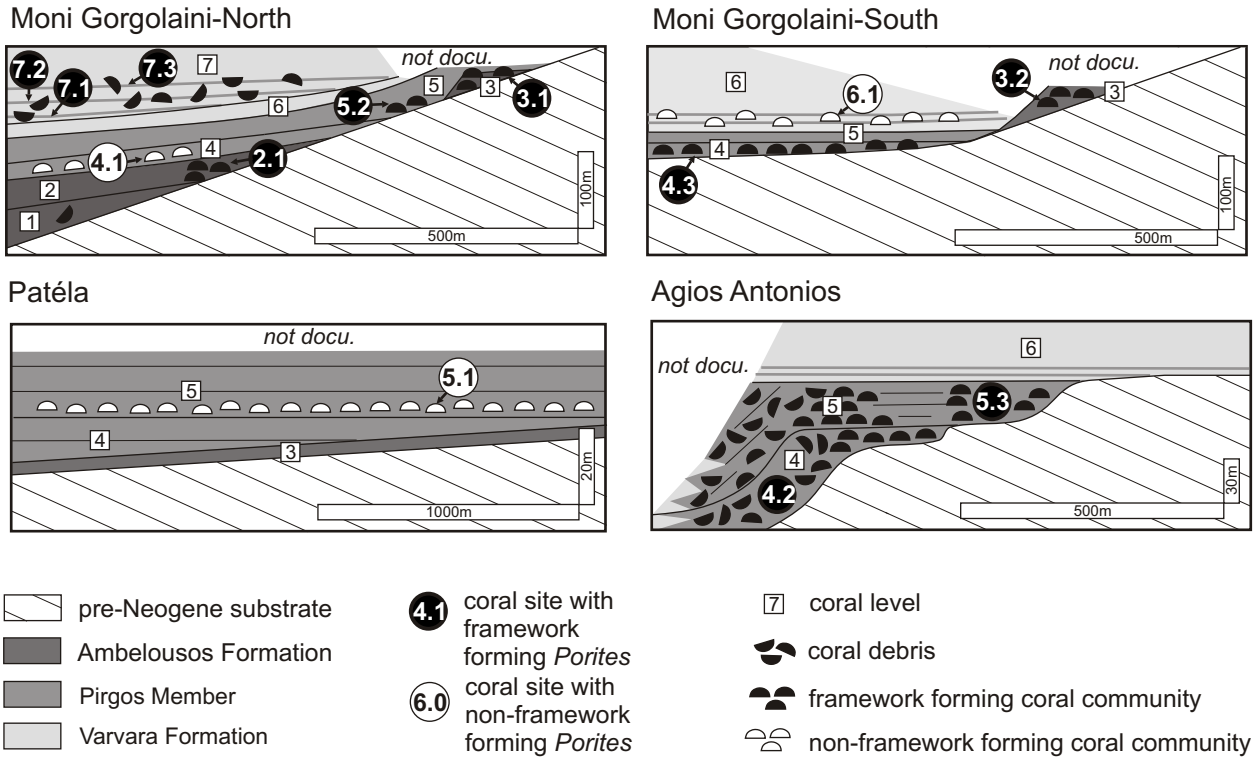

Fig. 5.4. Schematic representations of stratal geometries and chronostratigraphy of measured coral sites and levels in the Kroussonas - Asites area (central Crete).

5.2 The case study: central Crete, eastern Mediterranean

The Neogene basins of central Crete were formed by extensional tectonics during the late Middle Miocene (Meulenkamp & Sissingh, 2003; Rahl, 2004). Subsequent to an episode of non-marine sedimentation during the late Middle Miocene, the basins of Irakleion and Messara in central Crete became inundated by the sea (Meulenkamp *et al.*, 1979). After an early episode of clastic sedimentation during the early Tortonian, climatic aridification led to an increasing sediment starvation of the basin, where the remaining alluvial sediment load was trapped in the marginal zone of the basin (see chapter 1.4).

The Upper Miocene section of central Crete has been assigned to three lithostratigraphic units, the Ambelousos Formation and Pirgos Member of Tortonian age, and the Varvara Formation of late Tortonian - Messinian age (Krijgsman *et al.*, 1999; Meulenkamp *et al.*, 1979; Santarelli *et al.*, 1998; ten Veen & Postma, 1996; ten Veen & Postma, 1999; fig. 5.5). The chronostratigraphic classification and age model for Late Miocene shallow-water deposits of the western margin of Irakleion Basin relies on stratal architectures and stacking patterns of seven unconformity bound depositional units ("coral levels"), grouped into three larger-scale depositional sequences (see chapter 1.2, figs. 5.4, 5.5). According to the given time-frame constraints (Kroeger, 2004; ten Veen & Postma, 1999), these sequences are a reflection of 3rd order eustatic changes (see chapter 1.2, figs. 1.2, 5.5) and therefore represent a suitable age model for the coral growth rate analyses. Depositional Units 1-3 were assigned to the Early Tortonian sea level cycle, Units 4-6 to the

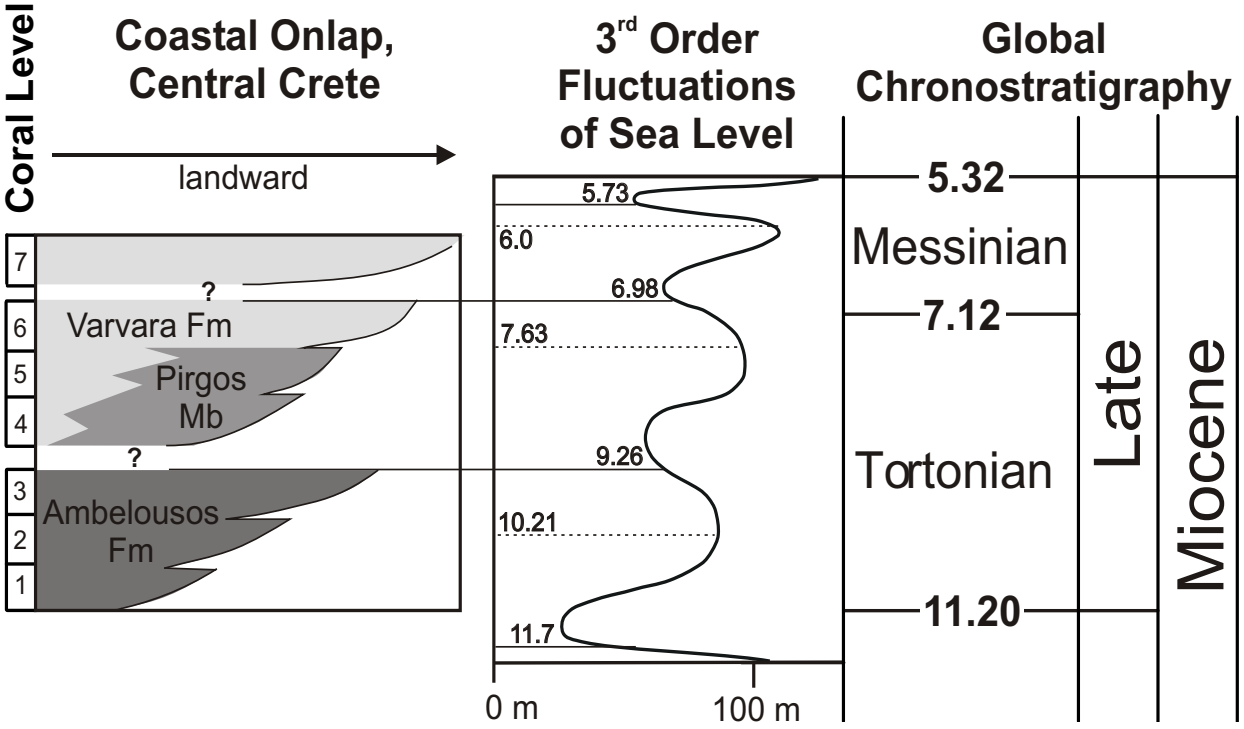

Fig. 5.5. Age model for measured coral levels in central Crete. 3rd order sea level curve from Hardenbol *et al. (*1998) as a reference frame.

late Tortonian, and Unit 7 to the Early Messinian eustatic cycle (Fig. 5.5; Haq *et al.*, 1988; Hardenbol *et al.*, 1998).

For this study, coral outcrops were selected in the Asites - Kroussonas area in the western Irakleion Basin (Fig. 5.2, A7). Outcrop conditions in this area allow for an exact calibration of the coral levels in the chronostratigraphic scheme (Figs. 5.4, 5.5). A detailed account on depositional geometries and lithologies of the transects has been presented in chapter 1.3 exempt from transect Moni Gorgolaini-South that is additionally choosen because it contains a level-bottom coral community in Coral Level 6 and a coral reef in Coral Level 4 (A5-6). Except for small fragments, no *in situ* coral fauna or reef is present in the coastal conglomerates of Unit 1. To cover the earliest Tortonian time, additional outcrops have been chosen from the Ambelousos - Apomarma area (northern Messara Basin; fig. 5.2). Outcrop conditions in this area were not good enough to document stratal geometries. All coral sites from this area used for this study interfinger with coastal conglomerates and are grouped in one single coral level, equivalent with Coral Level 1 (Fig. 5.4). Such a classification is consistent with the Sr-chronostratigraphy of central Crete (Kroeger, 2004).

5.2.1 Corals from Coral Level 1

In the Ambelousos – Apomarma area (Fig. 5.2), the lower Ambelousos Formation exhibits spectacular outcrops of coral biostromes and reefs formed in clastic coastal environments of early Tortonian age (see chapter 2). Dense stands of ramose branching *Porites* with minor contents of *Siderastrea* (Fig. 2.8b) or massive *Porites* and *Tarbellastrea* with minor amounts of *Acanthastrea* (Fig. 3.3a, d) form sheet-like biostromes of meter thickness that are laterally continuous over hundreds of metres (Sites 1.1, 1.2 and 1.3). At Psalidha locality, the biostromes are stacked vertically to form a low mounded coral buildup (Sites 1.2 and 1.3). Along the top of Psalidha buildup (earliest Tortonian; Site 1.3), corals are of exceptional size with the largest domical colonies of *Porites* measuring 2x1x1 m. This last growth stage of the buildup is also notably, because most corals have retained the original aragonite mineralogy and microstructure of the skeleton (see chapters 3-4).

5.2.2 Corals from Coral Levels 2-7

In the Asites - Kroussonas area of central Crete (Fig. 5.2) patch reefs predominate (Figs.1.5, 4.6a). Reef frameworks result from mutual coral incrustations of massive *Porites* and *Tarbellastrea* (decimetre to metre size) with some patchy intergrowths of ramose branching *Porites* (0.7 m high; figs. 5.6b-c). Binding by coralline algae or boring by sponges and bivalves is insignificant.

Nearshore reefs formed on ramps in a mixed carbonate–clastic environment. Colonies with an inverted or oblique orientation interpreted to be reworked are rare (Sites 2.1, 3.1, 3.2, 4.3 and 5.2). Nonetheless, some isolated heads of coral (*Porites*, *Tarbellastrea*) occur basinward from nearshore reefs in a poorly classified, muddy fossiliferous sandstone. Here, the massive corals (*Porites*, *Tarbellastrea*) exhibit ragged outlines and complex intergrowths with sediment, non-geniculate coralline algae and encrusting bryozoa. They are considered to represent a par-autochthonous level-bottom coral association in the muddy nearshore zone (Site 4.1).

On top of uplifted fault blocks located within Irakleion Basin, the Ambelousos Formation is either truncated by limestone of the Pirgos Member (Fig. 1.9e) or absent. Coralline red algae with additions of bryozoans, bivalves and larger foraminifers represent the principal constituents of the limestone (Figs.1.9a, c). Locally, non-constructional coral associations of *Porites* and *Tarbellastrea* may be present (Site 5.1; figs. 1.9b, 2.3e, 5.6d). In a few locations positioned along fault scarps of tilted blocks, the red algal facies changes into reefal talus and coral bioherms (Sites 4.2 and 5.3; see chapter 1.3.5).

The Varvara Formation is situated on top of the Ambelousos Formation and Pirgos Member. It copnsits of rhythmically bedded light grey marl and limestone (Fig.1.9d), grading into a unit of laminated gypsum. Non-framework coral associations occur at the base of the Varvara Formation (Site 6.1). The nearshore zone and a coral reef environment is not documented, probably due to young erosion of the Neogene sediments. Up-section, in proximal settings (Moni Gorgolaini-North) the Varvara Formation contains massive beds with angular lithic and skeletal fragments supported by a fine-grained matrix (debrites), and graded calcarenites (calciturbidites). The debrites contain decimetric angular fragments of massive *Porites* and *Tarbellastrea* (Fig. 3.3c), thus documenting reef growth in an upslope direction in shallow water (Sites 7.1, 7.2 and 7.3).

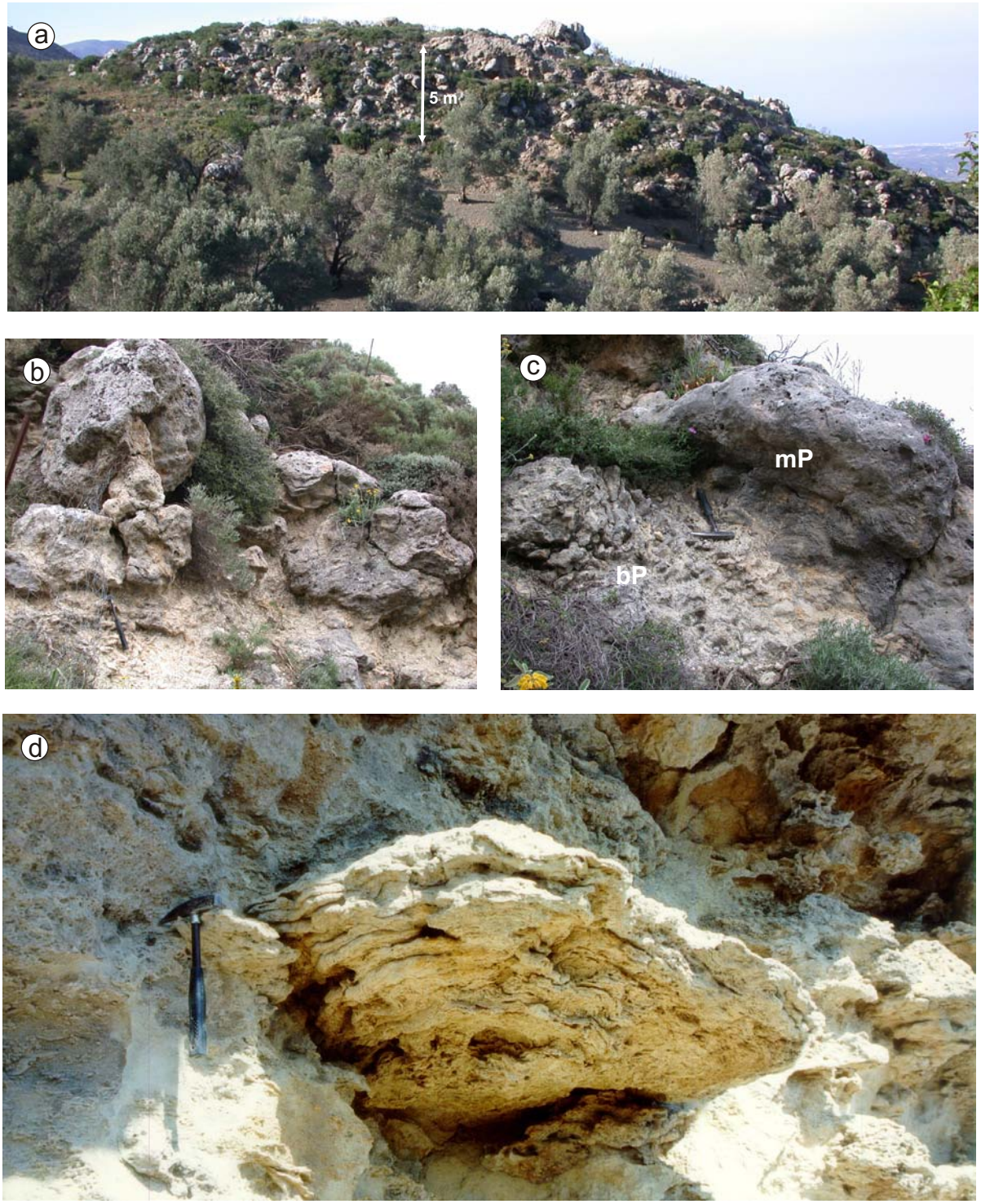

Fig. 5.6. Field aspects of late Tortonian coral growth patterns. Coral Level 5. **(a)** Mound-shaped coral patch reef in nearshore mixed cabonate-siliciclasic environment. Transect Moni Gorgolaini 1, Coral Site 5.2. The framework is build-up by massive *Porites* and *Tarbellastrea* with minor contribution of ramose branching *Porites*. **(a-b)** Mutual coral incrustations of colonies in live position. Transect Moni Gorgolaini 1, Coral Site 5.2. **(b)** Main framework builders are massive *Porites*. **(c)** Patchy ingrowth of ramose branching *Porites* (bP) between massive corals. The branching colony hamper a massive coral (mP) in its lateral extension, probably because it growths faster (see chapter 3). Later, the massive *Porites* was able to overgrew the *Porites*-bush due to its longer life span. Such interactions document synchroneous growth of massive and branching *Porites* in the coral habitat. **(d)** Isolated *Porites* colony from an offshore non-framework froming coral community that developed in deeper and pure carbonate environment of a isolated dip-slope ramp. The ragged margins of the massive coral are conspicous. Patéla transect, Coral site 5.1; figs b-d: hammer for scale.

5.3 Annual extension rates in Late Miocene *Porites* from central Crete (Fig. 5.7)

In Coral Level 1, mean growth rates were low at rates of 2.1-2.6 mm/yr^{-1} (mean) with a maximum of 3.8 mm/yr^{-1}. With a mean of 4.3 mm/yr^{-1} and a maximum of 5.2 mm/yr^{-1}, growth rates encountered are substantially higher in the stratigraphically topmost biostrome of the Ambelousos - Apomama area.

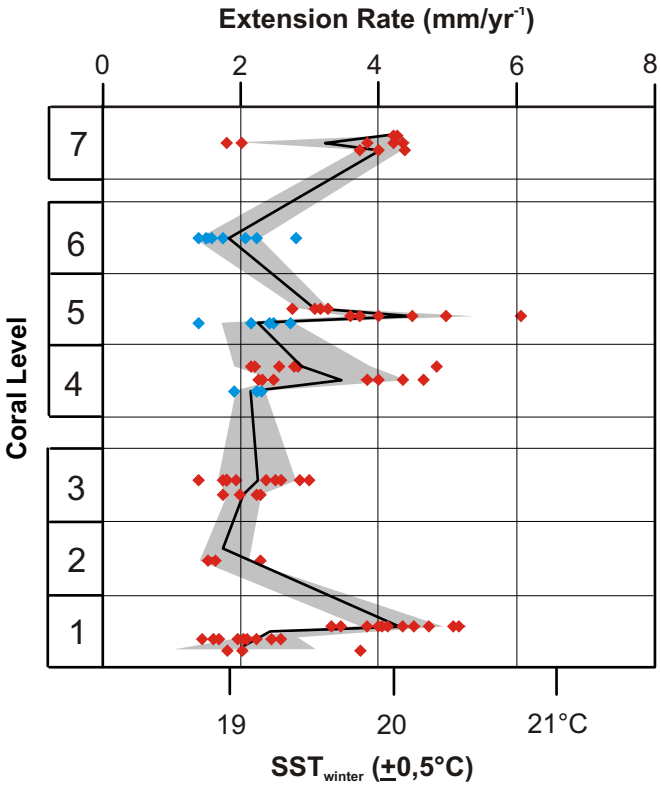

Fig. 5.7. Growth rates of massive *Porites* in central Crete and indicated paleotemperatures. Blue dots: non-framework forming *Porites*; red dots: framework forming *Porites*.

From Coral Levels 2 and 3, massive *Porites* from small patch reefs within clastic nearshore environments were analysed, exhibiting low growth rates at 1.8-2.3 mm/yr^{-1} (2.3-3.0 mm/yr^{-1} maximum). Low growth rates of massive *Porites* (mean 2.2 mm/yr^{-1}, maximum 2.3 mm/yr^{-1}) occur in a level-bottom coral association of a nearshore environment of Level 4. In coral reefs from the same stratigraphic level, in positions proximal to the paleocoast and on an uplifted block in an offshore position, growth rates of 2.9 and 3.5 mm/yr^{-1} (maxima 4.9 and 4.4 mm/yr^{-1}) were found. In Coral Level 5, there is again significant variation between massive *Porites* from reefs and level-bottom communities: Growth rates were comparatively low in isolated *Porites* from a level-bottom community (mean = 2.3 mm/yr^{-1}, maximum = 2.8 mm/year^{-1}), and high in coral reefs from both, nearshore clastic environment and offshore carbonate environment. In the former, mean growth rates were 4.5 mm/yr^{-1} (maximum = 5.0 mm/yr^{-1}), in the latter 3.1 mm/yr^{-1} (maximum = 3.3 mm/yr^{-1}). In Coral Level 6, massive *Porites* from a level-bottom community in a distal paleogeographic setting exhibit low mean annual growth rates of 1.8 mm/year^{-1} (maximum = 2.3 mm/yr^{-1}), similar to the older level-bottom communities. Coral fragments recovered from three successive debris flow deposits of Coral Level 7 of early Messinian age are consistently at a mean of 4.0 to 4.3 mm/yr^{-1} (maximum 4.3 to 4.4 mm/yr^{-1}) respectively. The source area for the debrites has been destroyed by sub-recent erosion. However, the overall paleogeography of the basin suggests a reefal source (see chapter 1).

5.4 Paleoenvironmental significance of the annual growth increments

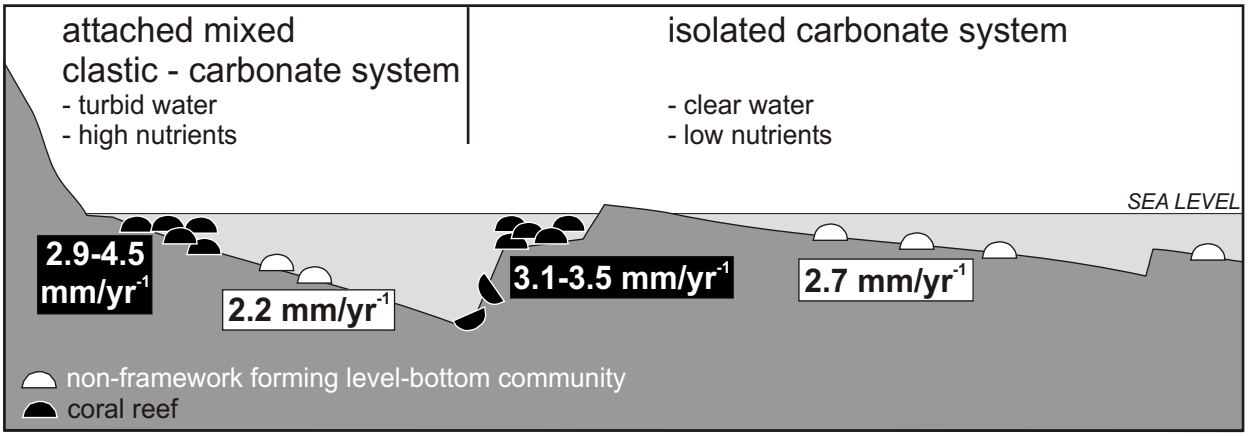

Fig. 5.8. Late Tortonian coral environments, central Crete.

Although some reworked coral material was encountered in association with steep submarine scarps, the rock record of Late Miocene coral environments in Crete displays mostly corals preserved *in situ*, both in the attached mixed clastic-carbonate systems (Figs. 5.6 a-c) and isolated carbonate environments of the central basin (Figs. 5.6d). Reef debris is subordinate in growth-framework pores and peripheral to the reefs, and reefs do not exhibit any ecological zonations. The geological record of the particular coral communities therefore appears to be not significantly biased by incomplete preservation (Fig. 5.6). Given the preserved mutual coral incrustations and small thickness, the reef outcrops cover a short time interval, lasting a few thousands of years at most (*cf.* Shinn, 2001; Geister, 1989). The growth rate data collected were thus assumed to be representative for any given outcrop and representing a specific paleoenvironment.

During the late Tortonian (Coral Levels 4 and 5) coral reefs and level bottom coral communities occurred synchronously in mixed clastic carbonate and pure carbonate environments (Fig. 5.8). Growth rates in massive *Porites* were low in level-bottom communities as compared to reefal communities. In consequence, low growth rates in the level-bottom corals can be referred to low light conditions (water depth, turbidity) and not to SST at the lower reef threshold value (*cf.* Abram *et al.*, 2001; Betzler *et al.*, 1997). Surprisingly, extension rates of massive *Porites* were high in coeval reefs from the clastic nearshore environments as compared to the pure carbonate environments located offshore. Hence, clastic turbidity in the nearshore zone did not have a negative effect on growth rates of the corals (Figs. 5.7, 5.8), but high nutrient availability in the nearshore zone appears to have stimulated coral growth (*cf.* Barnes & Lough, 1993; Lough & Barnes, 2000).

5.5 *Porites* thermometry

As noted in studies on modern *Porites*, calcification rates and vertical extension rates are principally a function of minimum SST in shallow water. In the present-day Indo-Pacific, average annual extension rates in massive *Porites* change by 3.1 mm/year^{-1} per 1°C change in average annual SST (over a range of 22-29°C: Lough & Barnes, 2000; fig. 5.9). Because the modern data set combines measurements from different parts of the ocean and from various species of the genus *Porites*, it is assumed that the growth rate over temperature relationship for the modern ocean also applies to the Late Miocene. Growth rates in fossil *Porites* from Crete systematically fall into the lowest distributional spectrum of their modern counterparts, an observation that is compatible with previous conclusions of the Mediterranean area being positioned at the northern margin of the Late Miocene reef belt (Brachert *et al.*, 1996; Esteban, 1996; Perrin, 2002). With regard to Late Miocene SST, and given the growth rate over temperature relationship (Lough & Barnes, 2000), the Cretan corals analysed reflect fairly constant average winter temperatures of 19-21°C (Fig. 5.9). For this reconstruction, data from level bottom communities were left out, in cases where they were outpaced by values from other reef localities, that fall into the same time-slice, because here slow growth is suggested to have been a low-light effect (Figs. 5.7, 5.8). Based on the modern analogue (Lough & Barnes, 2000), the Cretan corals reflect ~6°C of SST seasonality (Fig. 5.9). This is compatible with oxygen isotope data (Fig. 4.5), but less than in the present-day Mediterranean (Hofrichter, 2002).

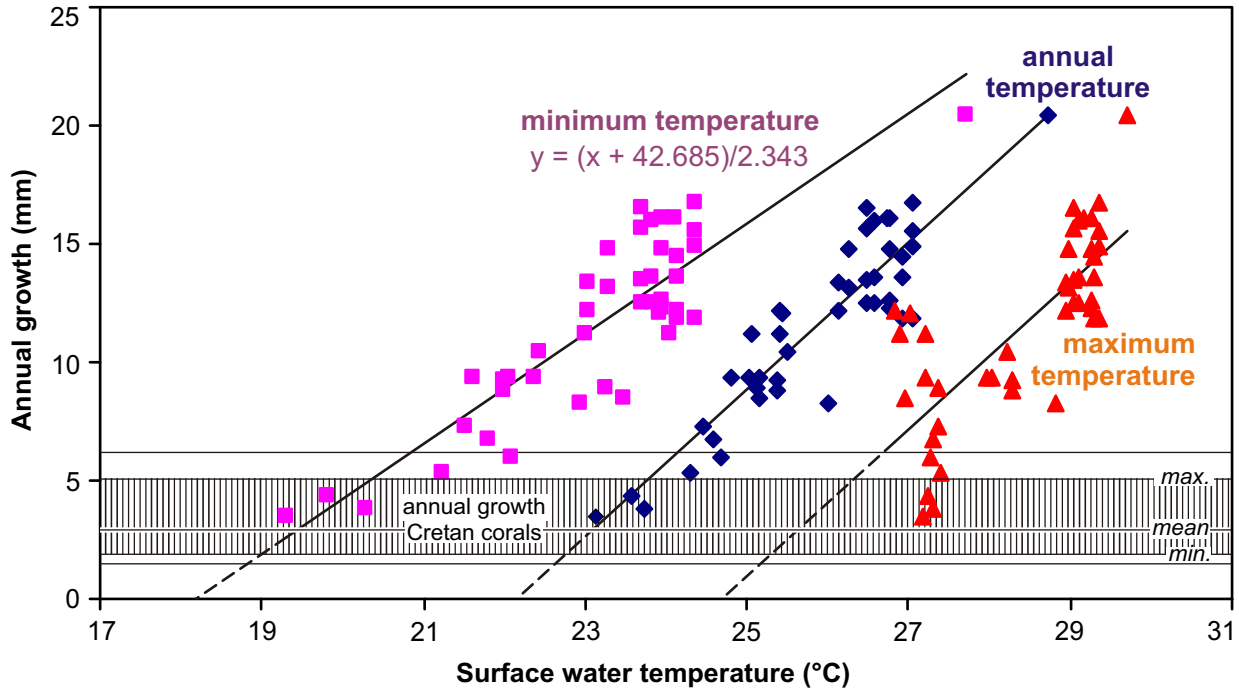

Fig. 5.9. Growth rates of various species of the genus *Porites* from the Indopacific (data from J. Lough, AIMS). Equation used: SST [°C_{winter}] = (annual growth rate + 42.685)/2,343

The *Porites* thermometer fails to document SST below the lower threshold temperature of modern *Porites* at 17.5°C (Fig. 5.9; Lough & Barnes, 2000). Relative SST changes during the Late Miocene inferred from coralline red algal associations suggest episodic cooling of the surface waters below the reef threshold level (Kroeger, 2004). However, according to the larger foraminifer fauna (*Amphistegina*, *Heterostegina*), SST remained within the warm-temperate spectrum (>14.5°C SST_{winter} *sensu* Betzler et al., 1997; Kroeger, 2004). Temperature changes within Cretan coral levels were therefore <6°C, but still sufficiently high as to episodically shut-off and on coral growth, even though the island was located in the EMWP. SST changes of the same magnitude have been documented for early Holocene reefs (Beck *et al.*, 1997). However, located well in the tropical Pacific, SST were not below the threshold for zooxanthellate corals.

5.6 Cretan SST in the light of Mediterranean reef patterns and global temperatures

Zooxanthellate corals (i.e. *Porites*) in reefs or level-bottom communities are a common feature of the Late Miocene of the Mediterranean area, and clearly document a warm-water domain (Esteban, 1996). The absence of these corals to the west of the Betic-Rifan Sill (BRS) suggests SST below the reef threshold level in the eastern Atlantic (Fig. 5.1) related to low tropical heat export into the eastern Atlantic before the Pliocene (*cf.* Haug & Tiedemann, 1998). Consistently, computer modelling predicts a negative surface air anomaly in the eastern Atlantic and a positive anomaly in the western Mediterranean (see chapter 4.7). Fluctuating inflow of cool Atlantic surface waters into the western sector of the Mediterranean is therefore plausible to explain episodic turnovers of warm- and cool-water shallow benthic communities (Martín & Braga, 1994). Modern surface waters in the Mediterranean originate from Atlantic surface waters via the Gibraltar passage. Winter mixing and cooling in the western sector, however, forms a modified water mass, that upon travelling eastward warms-up again and increases salinity (Hofrichter, 2002; fig. 5.1). The presence of transitional carbonate systems (level-bottom coral associations of largely Early Tortonian age) in the central Mediterranean (*cf.* Pedley, 1996), and reefs in the EMWP (Fig. 5.1) suggests the existence of analogous, anti-estuarine surface currents that were driven by westerly winds and dry climates in the Middle East (see chapter 4.7; Meijer *et al.*, 2004; Rögl & Steininger, 1984). Late Miocene Mediterranean surface water, therefore has to have been strongly oligotrophic and to have had some east-west temperature gradient. In the eastern sector and EMWP, non-reefal episodes (Kroeger, 2004) were short, and corals or coral reefs are almost omnipresent over the Late Miocene section here (see chapter 1). Nonetheless, stable oxygen isotope records in Cretan *Porites*

(early Tortonian) strongly suggest a significant Atlantic control on eastern Mediterranean climate variability (see chapter 4.7) as in the present day (D'Arrigo & Cullen, 2001). Because coral growth rates in the EMWP document Late Miocene winter SST at 19-20°C close to the lower reef threshold level (Fig. 5.10), weak Mediterranean temperature gradients are inferred in those episodes when reef growth took place almost over the entire Mediterranean (Fig. 5.1).

Little SST variation over the Late Miocene documented in the Cretan coral record is in agreement with the deep-sea oxygen isotope and Mg/Ca record (Billups & Schrag, 2003; Lear *et al.*, 2003b; Zachos *et al.*, 2001) and terrestrial archives (pollen spectra, Utescher *et al.*, 2000; fig. 5.10). However, coral growth rates significantly above those found in *Porites* from Crete have been detected in Langhian (Middle Miocene) patch reefs with a high diverse coral fauna (28 genera: Karabiyikoglu *et al.*, 2005) in southern Turkey. According to measurements from field photographs in Karabiyikoglu *et al.* (2005: fig. 6c), growth rates were ~6 mm/yr^{-1}, and equivalent with ~21°C winter SST (Fig. 5.9). Own measurements on Late Miocene massive *Porites* (4 corals measured;Tortonian-Messinian) from two localities with low diverse coral associations (6 coral genera: Karabiyikoglu *et al.*, 2005) in southern Turkey (Kargi dam: N 37.29904°, E 030.81446°, Gebiz: N 37.10464°, E 030.94747°; both localities Antalya Basin, Aksu Sub-Basin) show mean extension rates between 3.75 and 4.23 mm/yr^{-1} (mean 4.02 mm/yr^{-1}), that are in the range of the Cretan *Porites*. Correspondingly, during the Middle Miocene climatic optimum (Zachos *et al.*, 2001) winter SST in the eastern Mediterranean were ~1°C higher than during the Late Mi-

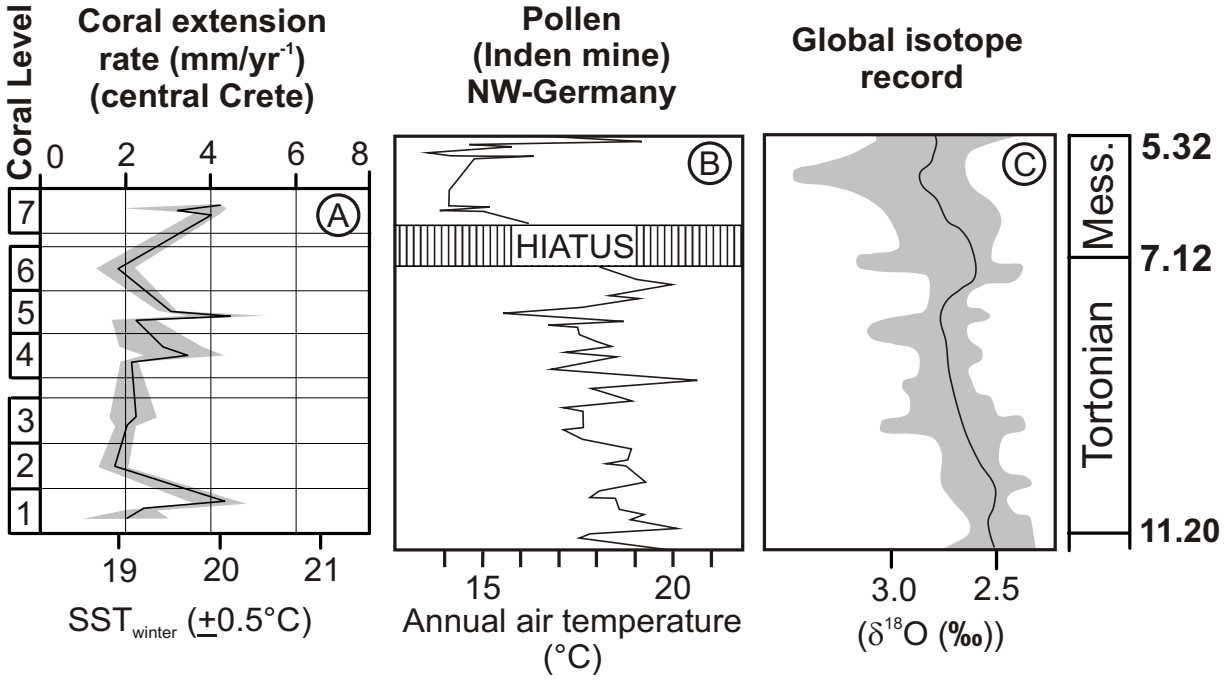

Fig. 5.10. *Porites* growth rates from Crete **(A)** compared with global climate proxies. **(B)** Utescher *et al.*, 2000; **(C)** Zachos *et al.*, 2001

ocene (Fig. 5.9) but 4-5°C higher than at present (from Levitus data base). In the middle as well as Late Miocene of southern Turkey, reefs developed on fan-deltas and alluvial fans, that show no distinct facies variations over the time, which explain the drastic decline of coral diversity by regional processes (Karabiyikoglu *et al.*, 2005). Moreover, the decrease of coral taxa from the Middle to Late Miocene is a global phenomenon and reflect the Late Miocene cooling (Veron, 1995), which corrresponds to the *Porites*-thermometer results.

5.7 Conclusions of chapter 5

(1) Late Miocene *Porites* corals from the island of Crete (Greece) exhibit clearly visible ghost structures of the original annual growth bands. The thickness of the annual growth increments was measured in *Porites* from seven chronostratigraphic units covering the Tortonian and early Messinian.

(2) From constant growth rates with 2.4 mm/yr$^{-1,}$ little SST variation over the Late Miocene is deduced a reconstruction that is in line with global paleoclimatic trends. In terms of modern *Porites*, the Miocene growth rates are compatible with a high-latitude reef setting, and - according to the growth over temperature relationship found for Indo-Pacific *Porites* - suggests that winter SST did not exceed 19-21°C.

(3) In a given time-slice, SST can be considered spatially uniform on a basin scale. Correspondingly, spatial growth vartions in massive *Porites* provide intriguing additional information as to light levels and nutrient concentrations.

(4) On a Mediterranean scale, the eastern segment appears to have been a coral refuge, where SST were subject to less variation as compared the western Mediterranean, termed the Eastern Mediterranean Warm Pool (EMWP).

(5) The *Porites*-thermometer described in this chapter is a new and easy to use tool in paleoenvironment analysis, that is based on the thickness of annual growth increments, and not sensitive to diagenetic alteration such as geochemical proxy records.

6 Summary

For the Late Miocene section of the tectonically mobile Irakleion Basin (Crete, Greece), the recognition of block movements and eutstatic sea level fluctuations is the basis for a chronostratigraphic frame and for a new facies model for carbonates in the transition of the tropical and temperate climate zones. By the combination of the facies model with the reconstructed coastal onlap curve, it is demonstrated that coral reefs are common over the entire Late Miocene, normal-marine succession of central Crete (SW Irakleion Basin). Thus SSTs in winter of >18°C and oligotroph conditions for the Tortonian and early Messinian are indicated.

Since the late Tortonian, the terrigenuous supply from the mainland („central Cretan landmass“) increased notably. It was independent from relative sea level changes and hinterland uplift and is interpreted as the result of aridification consistent with Late Miocene terrestrial floras from Crete.

The thickness of ghost structrures of coral growth increments from fully recrystallized, massive *Porites* (light and dark bands) were measured and compared with those of modern *Porites* from the Indopacific that exhibit a clear correlation of coral growth rate and water temperature („*Porites*-thermometer“). This represents a new approach to quantify the Late Miocene water temperatures and requires the identification of coral growth bands in fully recrystallized corals and the comprehension of their modes of preservation. A model for the diagenesis of growth bands in poritid corals is developed, allowing their confident recognition and assignment to light and dark bands in transformed skeletons of massive *Porites* corals. The analysis of the thicknesses of ghost structures of coral growth increments from seven chronostratigraphic units reveals that in the Tortonian and early Messinian SSTs in winter stayed continuously near the lower treshold temperature for coral reefs (19-21°C). Cool phases in which coral reef development collapsed, as well known from the western Mediterranean, are hard to recognize in the SW Irakleion Basin and only reflected in reduced coral growth rates. Therefore, the presence of an „Eastern Mediterranean Warm Pool“ is suggested, that acted as refuge for corals during the cool episodes.

The climatic data from coral growth bands are specified by high-resolution timeseries of stable oxygen isotopes that are stored in early Tortonian *Porites* skeletons in aragonite preservation. They document a SST saisonality of 6-7°C. In addition, the spectral analyses of a 69 year $\delta^{18}O$ timeseries shows a significant 5-6 years variance. Late Miocene

tree ring records from middle Europe document an remarkable analogous temporal variability of 5-6 years. From the uniform atmospheric variability in middle Europe and the eastern Mediterranean it is concluded, that in the Late Miocene both areas were affected by the the same climate system. At present-day, a comparable situation exist with the AO/NAO variability that controls the European climate and that is linked to the Icelandic Low activity in the northern Atlantic. The 69 year stable isotope record from Crete is therefore used in a simulation with a complex atmospheric general circulation model that is coupled to a mixed layer ocean model (ECHAM4/ML), adapted for the Tortonian conditions (vegetation, orography, atmospheric CO_2, continental ice volume, paleooceanic heat transport). The result gives evidence that atmospheric variability in the eastern Mediterranean was coupled to the Icelandic Low already in the Late Miocene and is consistant with the spatial distribution patterns of coral reefs, non-framework forming coral communities and cool-water carbonates in the Mediterranean.

7 Acknowledgements

8 References

Abram, N.J., Webster, J.M., Davies, P.J. and **Dullo, W.C.** (2001) Biological response of coral reefs to sea surface temperature variation: evidence from the raised Holocene reefs of Kikai-jima (Ryukyu Islands, Japan). *Coral Reefs*, **20**, 221-234.

Ali, O.E. (1984) Sclerochronology and carbonate production in some Upper Jurassic reef corals, *Paleontology*, **27**, 537-548.

Barnes, D.J. and **Lough, J.M.** (1993) On the nature and causes of density banding in massive coral skeletons. *Journal of Experimental Marine Biology and Ecology*, **167**, 91-108.

Barnston, A.G. and **Livezey, R.E.** (1987) Classification, seasonality and persistence of low-frequency atmospheric circulation patterns. *Monthly Weather Review*, **115**,1083-1126.

Beck, J.W., Récy, J., Taylor, F., Edwards, R.L. and **Cabioch, G.** (1997) Abrupt changes in early Holocene tropical sea surface temperature derived from coral records. *Nature*, **385**, 705-707.

Benda, L., Meulenkamp, J.E. and **Zachariasse, W.J.** (1974) Biostratigraphic correlations in the Eastern Mediterranean Neogene. 1. Correlation between planktonic, uvigerinid, sporomorphal, and mammal zonations of the Cretan and Italian Neogene. *Newsletter of Stratigraphy*, **3**, 205-217.

Betzler, C., Brachert, T.C., Braga, J.C. and **Martín, J.M.** (1997a): Nearshore, temperate, carbonate depositional systems (Lower Tortonian, Agua Amarga Basin, southern Spain): Implications for sequence stratigraphy. *Sedimentary Geology*, **113**, 27-53.

Betzler, C., Brachert, T.C. and **Nebelsick, J.** (1997b) The warm-temperate carbonate province - A review of the facies, zonations and deliminations. *Courier Forschungsinstitut Senckenberg*, **201**, 83-99.

Betzler, C., Martín, J. M. and **Braga J. C.** (2000) Non-tropical carbonates related to rocky submarine cliffs (Miocene, Almería, southern Spain). *Sedimentary Geology*, **131**, 51-65.

Bice, K.L., Scotese, C.R., Seidov, D. and **Barron, E.J.** (2000) Quantifying the role of geographic change in Cenozoic ocean heat transport using uncoupled atmosphere and ocean models. *Paleogeography, Paleoclimatology, Paleoecology*, **161**, 295-310.

Billups, K. and **Schrag, D.P.** (2002) Paleotemperatures and ice volume of the past 27 Myr revisited with paired Mg/Ca and $^{18}O/^{16}O$ measurements on benthic foraminifera. *Paleoceanography*, **17**/1, 1-3.

Billups, K. and **Schrag, D.P.** (2003) Application of benthic foraminiferal Mg/Ca ratios to questions of Cenozoic climate change. *Earth and Planetary Science Letters*, **209**, 181-195.

Bosellini, F.R., Russo, A. and **Vescogni, A.** (2002) The Messinian Reef Complex of the Salento Peninsula (Southern Italy): Stratigraphy, Facies and Paleoenvironmental Interpretation. *Facies*, **47**, 91-113.

Brachert, T.C., Betzler, C., Braga, J.C. and **Martín, J.M.** (1996) Record of climatic change in neritic carbonates: Turnovers in biogenic associations and depositional modes (Upper Miocene, southern Spain). *Geologische Rundschau*, **85,** 327-337.

Brachert, T.C., Betzler, C., Braga, J.C. and **Martín, J.M.** (1998) Microfacies of a warm-temperate carbonate ramp (Uppermost Tortonian/Lowermost Messinian, southern Spain). *Palaios*, **13**, 459-475.

Brachert, T.C., Hultzsch, N., Knoerich, A.C., Krautworst, U.M.R. and **Stückrad, O.** (2001) Climatic signatures in shallow water carbonates: High-resolution stratigraphic correlation in structurally controlled carbonate buildups (Late Miocene, S-Spain). *Paleogeography, Paleoclimatology, Paleoecology*, **175**, 211-237.

Brachert, T. C., Krautworst, U. M. R. and **Srückrad O. M.** (2002) Tectono-climatic evolution of a Neogene intramontane basin (Late Miocene Carboneras subbasin, SE Spain): revelations from basin mapping and biofacies analysis. *Basin Research*, **14**, 503-521.

Brachert, T.C., Forst, M.H., Pais, J.J., Legoinha, P. and **Reijmer, J.J.G.** (2003) Lowstand carbonates, highstand sandstones?. *Sedimentary Geology*, **155**, 1-12.

Braga, J.C., Martín, J.M. and **Alcala, B.** (1990): Coral reefs in coarse-terrigenous sedimentary environments (Upper Tortonian, Granada Basin, southern Spain). *Sedimentary Geology*, **66**, 135-150.

Braga, J.C. and **Martín, J.M.** (1996) Geometries of reef advance in response to relative sea level changes in a Messinian (uppermost Miocene) fringing reef (Caratiz reef, Sorbas Basin, SE Spain). *Sedimentary Geology*, **107**, 61-81.

Brenchley, P. J. and **Harper, D. A. T.** (1998) Paleoecology, 402 pp.. Chapman and Hall, London.

Buchbinder, B. (1996) Middle and Upper Miocene reefs and carbonate plattforms in Israel. In: Models for carbonate stratigraphy from Miocene reef complexes of Mediterranean regions (Eds. E.K. Franseen, M. Esteban, W.C. Ward and J.-M. Rouchy), *Concepts in Sedimentology and Paleontology*, **5**, 333-347. Society for Sedimentary Geology, Tulsa.

Carannante, G., Esteban, M., Millman, J.D. and **Simone, L.** (1988) Carbonate lithofacies as paleolatitude indicators: problems and limitations. *Sedimentary Geology*, **60**, 333-346.

Collins, L. B., Wyrwoll, K.-H. and **France, R. E.** (1991) The Abrolhos carbonate platforms: geological evolution and Leeuwin Current activity. *Journal of the Royal Society of Western Australia*,**74**, 47-57.

Cohen, A.L. and **Sohn, R.A.** (2004) Tidal modulation of Sr/Ca ratios in a Pacific coral. *Geophysical Research Letters* ,**31**, 4.

Constantz, B.R. (1986) The primary surface area of corals and variations in their susceptibility to diagenesis. In: Reef Diagenesis (Eds. J.H. Schroeder and B.H. Purser), 53-76. Springer, New York.

Craig, H. (1966) Isotopic composition and origin of the Red Sea and Salton Sea geothermal brines. Science, **154**, 1544-1548.

Crowley, T.J. and **Zachos, J.C.** (2000) Comparison of zonal temperature profiles for past warm time periods. In: Warm Climates in Earth History (Eds. B. Huber, K.G. MacLeod and S.L. Wing), pp. 50-76. Cambridge University Press, Cambridge.

Cullen, H.M. and **de Menocal, P.B.** (2000) North Atlantic influence on Tigris-Euphrates streamflow. *International Journal of Climatology*, **20**, 853-863.

Dabrio, C.J., Esteban, M. and **Martín, J.M.** (1981) The coral reef of Nijar, Messinian (Uppermost Miocene), Almeria Province, S. E. Spain. *Journal of Sedimentary Petrology*, **51**/2, 521-539.

D'Arrigo, R. and **Cullen, H.M.** (2001) A 350-year (AD 1628-1980) reconstruction of Turkish precipitation. *Dendrochronologia*, **19**, 169-177.

Demicco, R.V. and **Hardie, L.A.** (1994) Sedimentary structures and early diagenetic features of shallow marine carbonate deposits. *SEPM Atlas Series*, **1**, 265 pp.. Society of Sedimentary Geology, Tulsa.

Dethloff, K., Dorn, W., Rinke, A., Fraedrich, Junge, K.M., Roeckner, E., Gayler, V., Cubasch, U. and **Christensen, J.H.** (2004) The impact of Greenland´s deglaciation on the Arctic circulation. *Geophysical Research Letters*, **31**, 19201-19204.

Druffel, E.R.M. (1997) Geochemistry of corals: Proxies of past ocean chemistry, ocean circulation, and climate. *Proceedings National Academy of Sciences USA*, **94**, 8354-8361.

Dullo, W.-C. (1986) Variations in diagenetic sequences: and example from Pleistocene coral reefs, Red Sea, Saudi Arabia. In: Reef Diagenesis (Eds. J.H. Schroeder and B.H. Purser), 77-90. Springer, New York.

Dullo, W.-C. and **Mehl, J.** (1989) Seasonal growth lines in Pleistocene scleractinians from Barbados: record potential and diagenesis. *Paläontologische Zeitschrift*, **63**, 207-214.

Dullo, W.-C., Moussavian, E. and **Brachert, T.C.** (1990) The foralgal crust facies of the deeper fore reefs in the Red Sea: a deep diving survey by submersible. *Geobios*, **23**, 261-281.

Dunham, R. J. (1970) Stratigraphic reefs versus ecologic reefs. *American Association of Petroleum Geologists Bulletin*, **54**, 1931-1932.

Enmar, R., Stein, M., Bar-Matthews, M., Sass, E., Katz, A. and **Lazar, B.** (2000) Diagenesis in live corals from the Gulf of Aqaba. I. The effect on paleo-oceanography tracers. *Geochimica et Cosmochimica Acta*, **64**, 3123-3132.

Esteban, M. (1996) An overview of Miocene reefs from Mediterranean areas: General trends and facies models. In: Models for carbonate stratigraphy from the Miocene reef complexes of Mediterranean regions (Eds. E.K. Franseen, M. Esteban, W.C. Ward and J.-M. Rouchy), *Concepts in Sedimentology and Paleontology*, **5**, 3-54. Society for Sedimentary Geology, Tulsa.

Fairbanks, R.G. and **Dodge, R.E.** (1979) Annual periodicity of the $^{18}O/^{16}O$ and $^{13}C/^{12}C$ ratios in the coral *Montastrea annularis*. *Geochimica et Cosmochimica Acta*, **43**, 1009-1020.

Fassoulas, C. (2001) The tectonic development of a Neogene basin at the leading edge of the active European margin: the Heraklion Basin, Crete, Greece. *Journal of Geodynamics*, **31**, 49-70.

Felis, T., Pätzold, J., Loya, Y. and **Wefer, G.** (1998) Vertical water mass mixing and plankton blooms recorded in skeletal stable carbon isotopes of a Red Sea coral. *Journal of Geophysical Research*, **103**, 30731-30739.

Felis, T., Pätzold, J., Loya, Y., Fine, M., Nawar, A.H. and **Wefer, G.** (2000) A coral oxygen isotope record from the northern Red Sea documenting NAO, ENSO, and North Pacific teleconnecions on Middle East climate variability since the year 1750. *Paleoceanography*, **15**, 679-694.

Felis, T., Lohmann, G., Kuhnert, H., Lorenz, S.J., Scholz, D., Al-Rousan, S.A. and **Al-Moghabi, S.M.** (2004) Increased seasonality in Middle Eastern temperatures during the last interglacial period. *Nature*, **429**,164-168.

Felis, T. and **Pätzold, J.** (2004) Climate reconstructions from annually banded corals. In: Global environmental change in the ocean and on land (Eds. M. Shiyomi, H. Kawahata, H. Koizumi, A. Tsuda and Y. Awaya), pp. 205-227. Terrapub, Tokyo.

Folk, R.L. (1974) The natural history of crystalline calcium carbonate: effect of magnesium content and salinity. *J. Sediment. Petrol.*, **44**, 40-53.

Franseen, E.K., Esteban, M., Ward, W.C. and **Rouchy, J.-M.** (1996), Models for carbonate stratigraphy from Miocene reef complexes of Mediterranean regions. *Concepts in Sedimentology and Paleontology*, **5**, 391 pp.. Society for Sedimentary Geology, Tulsa.

Franseen, E.K., Goldstein, R.H. and **Farr, M.R.** (1997) Substrate-Slope and Climate Controls on Carbonate Ramps: Revelations from Upper Miocene Outcrops, SE Spain. In: Cool-water Carbonates (Eds. N.P. James and J. Clarke), *SEPM Special*

Publication, **56**, 271-290. Society for Sedimentary Geoplogy,Tulsa.

Frakes, L.A., Francis, J.E. and **Syktus, J.I.** (1993) The history of the Earth´s climate over the past 600 million years. Cambridge University Press, Cambridge, 270 p.

Frydas, D. and **Keupp, H.** (1992) Kieseliges und kalkiges Phytoplankton aus dem Neogen von NW- und W-Kreta/Griechenland. *Berliner geowissenschaftliche Abhandlungen*, **E3**, 97-111.

Frydas, D. and **Keupp, H.** (1996) Biostratigraphical results in Late Neogene deposits of NW Crete, Greece, based on calcareous nannofossils. Berliner geowissenschaftliche Abhandlungen, **E18**, 169-189.

Frydas, D., Keupp, H. and **Bellas, S.M.** (1999) Biostratigraphical research in Late Neogene marine deposits of the Chania Province, western Crete, Greece. Berliner Geowissenschaftliche Abhandlungen, **E30**, 55-67.

Füchtbauer, H. (1988) Sedimente und Sedimentgesteine. Sediment-Petrologie, Teil II, E, 1141 pp.. Schweizerbart´sche Verlagsbuchhandlung (Nägele u. Obermiller), Stuttgart.

Gagan, M.K., Chivas, A.R. and **Isdale, P.J.** (1994) High-resolution isotopic records from corals using ocean temperature and mass-spawning chronometers. *Earth and Planetary Science Letters*, **121**, 549-558.

Gagan, M.K., Ayliffe, L.K., Beck, J.W., Cole, J.E., Druffel, E.R.M., Dunbar, R.B. and **Schrag, D.P.** (2000) New views of tropical paleoclimates from corals. *Quaternary Science Reviews*, **19**, 45-64.

Gawthorpe, R.L. and **Leeder, M.R.** (2000) Tectono-sedimentary evolution of active extensional basins, *Basin Research*, **12**, 195-218.

Geister, J. (1989) Quantitative aspects of coral growth and carbonate production in a Middle Jurassic reef. In: Fossil Cnidaria 5. (Eds. P.A. Jell and J.W. Pickett), *Association of Australasian Paleontology*, **8**, 425-432. Brisbane.

Ghil, M., Allen, M.R., Dettinger, M.D., Ide, K., Kondrashov, D., Mann, M.E., Robertson, A.W., Saunders, A., Tian, Y. Varadi, F. and **Yiou, P.** (2002) Advanced spectral methods for climate time series. *Review of Geophysics*, **40**/1, 3-41.

Grasso, M. and **Pedley, H.M.** (1989) Paleoenvironment of the Upper Miocene coral build-ups along the the northern margins of the Caltanissetta Basin (Central Sicily) - Atti 3° Simposio di Ecologia e Paleoecologia delle Communitá Bentoniche, Taomina, 373-389.

Gregory, J.M., Huybrechts, P. and **Raper, S.C.B.** (2004) Threatened loss of the Greenland ice-sheet. *Nature*, **428**, 616.

Grigg, R.W. (1982) Darwin Point: a threshold for atoll formation. *Coral Reefs*, **1**, 29-34.

Grottoli, A. (2001) Past climate from corals. In: Encyclopedia of ocean sciences (Eds J. Steele, S. Thorpe and K. Turekian), 2098-2107. University of Pennsylvania,

Department of Earth and Environmental Science, Philadelphia.

Guernet, C. (1978) L´évolution paléogéographique et tectonique de la Grèce au Miocène: Un essai de synthèse. *Revue de Géographie Physique et de Géologie Dynamique*, **20**, 95-108.

Halfar, J., Godinez-Orta, L., Mutti, M., Valdez-Holguin, J. and **Borges, J.** (2004) Nutrient and temperature controls on modern carbonate production: an example from the Gulf of California, Mexico. *Geology*, **32**/3, 213-216.

Hallock, P. and **Schlager, W.** (1986**)** Nutrient excess and the demise of coral reefs and carbonate platforms. *Palaios*,**1**, 389-398.

Hallock, P. (1987) Fluctuations in the trophic resource continuum: a factor in global diversity cycles?. *Paleoceanography*, **2**, 457-471.

Haq, B.U., Hardenbol, J. and **Vail, P.R.** (1988) Mesozoic and Cenozoic chronostratigraphy and cycles of sea level change. In: Sea level changes: An integrated approach (Eds. K.C. Wilgus, B.S. Hastings, C.G.S.C. Kendall, H.W. Posamentier, C.A. Ross and J.C.V. Wagoner), *SEPM Special Publications*, **42**, 71-108. Society for Sedimentary Geology, Tulsa.

Hardenbol, J., Thierry, J., Farley, M.B., Jacquin, T., de Graciansk i, P.-C. and **Vail, P.R.** (1998) Mesozoic and Cenozoic sequence stratigraphic framework of European Basins. In: Mesozoic and Cenozoic sequence stratigraphy of European basins (Eds. P.-C. de Graciansk i, J. Hardenbol, J. Thierry and P.R. Vail), *SEPM Special Publications*, **60**, 3-14. Society for Sedimentary Geology, Tulsa.

Hatcher, B.G. (1991) Coral reefs in the Leeuwin current - an ecological perspective. *Journal of the Royal Society of Western Australia*, **74**, 115-127.

Haug, G.H. and **Tiedemann, R.** (1998) Effect of the formation of the isthmus of Panama on Atlantic Ocean thermohaline circulation. *Nature*, **393**, 673-676.

Hayward, A.B. (1982) Coral reefs in a Clastic sedimentary Environment: Fossil (Miocene, S.W. Turkey) and Modern (Recent, Red Sea) Analogues. *Coral Reefs*, **1**, 109-114.

Helm, C., Schülke, I. and **Fischer, R.** (2001) Paläobiogeographie des Korallenooliths (Mittleres Oxfordium - Unteres Kimmeridgium): Tethyale Faunen- und Florenelemente auf höherer Paläobreite (Niedersächsisches Becken, NW-Deutschland). *Geologische Beiträge Hannover*, **2**, 51-64.

Helm, C., Reuter, M. and **Schülke, I.** (2003) Der Korallenoolith (Oberjura) im Osterwald (NW-Deutschland, Niedersächsisches Becken): Fazielle Entwicklung und Ablagerungsdynamik. *Zeitschrift der Deutschen Geologischen Gesellschaft*, **153**, 159-186.

Helmle, K.P. and **Stanley, G.D.** (2003) Oldest coral bands in the triassic of North America and the evolution of photosynthesis. *9th Int. Symp. fossil Cnidaria Porifera*, 1-6.

Henry, L.-A. and **Hart, M.** (1999) Regeneration from injury and resource allocation in

sponges and corals. *J. Exp. Mar. Biol. Ecol.*, **234**, 29-39.

Hilgen, F.J., Krijgsman, W., Langereis, C.G., Lourens, L.J., Santarelli, A. and **Zachariasse, W.J.** (1995) An astronomical (polarity) time scale for the Late Miocene. *Earth and Planetary Science Letters*, **136**, 495-510.

Hilgen, F.-J., Abdul-Aziz, H., Krijgsman, W., Raffi, I and **Turco, E.** (2003) Integrated stratigraphy and astronomical tuning of the Serravallian and lower Tortonian at Monte dei Corvi (middle-upper Miocene, northern Italy). *Paleogeography, Paleoclimatology, Paleoecology*, **199**, 229-264.

Hofrichter, R. (2002) Das Mittelmeer. Fauna, Flora, Ökologie. Spektrum Akademischer Verlag, Heidelberg, 607 pp..

Hsü, K.J., Montadert, L., Bernoulli, D., Cita, M.B., Ericson, A., Garrison, R.E., Kidd, R.B. and others (1977) History of the Mediterranean salinity crisis. *Nature*, **267**, 399-403.

Hurrell, J.W. (1995) Decadal trends in the North Atlantic Oscillation: regional temperatures and precipitation. *Science*, **269**, 676-679.

Insalaco, E. (1996) The use of Late Jurassic coral growth bands as paleoenvironmental indicators. *Paleontology*, **39**, 413-431.

IPCC (2001) The scientific basis - contribution of Working Group I to the third assessment report of the Intergovernmental Panel on Climate Change. Cambridge University Press, Cambridge.

James, N.P. and **von der Borch, C.C.** (1991) Carbonate shelf edge off southern Australia: a prograding open-platform margin, *Geology*, **19**, 1005-1008.

James, N.P., Boreen, T.D., Bone, Y and **Feary, D.A.** (1994) Holocene carbonate sedimentation on the west Eucla Shelf, Great Australien Bight: a shaved shelf. *Sedimentary Geology*, **90**, 161-177.

James, N.P. (1997) The cool-water carbonate depositional realm. *Society for Sedimentary Geology, Special Publication*, **56**, 1-20.

James, N.P., Bone, Y., Collins, L.B. and **Kyser, T.K.** (2001) Surficial sediments of the Great Australian Bight: facies dynamics and oceanography on a vast cool-water carbonate shelf. *Journal of Sedimentary Researc*h, **71**, 549-567.

Karabıyıkoğlu, M., Tuzcu, S., Çiner, A., Deynoux, M., Örçen, S. and **Hakyemez, A.** (2005) Facies and environmental setting of the Miocene coral reefs in the late-orogenic fill of the Antalya Basin, western Taurids,Turkey: implications for tectonic control and sea level changes. *Sedimentary Geology*, **173**, 345-371.

Kershaw, S. (1994) Classification and geological significance of biostromes. *Facies*, **31**, 81-92.

Keupp, H., Bellas, S.M., Frydas, D. and **Kohring, R.** (1994) Aghia Irini, ein Neogenprofil auf der Halbinsel Gramvoússa/NW-Kreta. *Berliner Geowissenschaftliche*

Abhandlungen, **E13**, 469-481.

Knutson, D.W., Buddmeier, R.W. and **Smith, S.V.** (1972) Coral chronometers: seasonal growth bands in reef corals. *Science*, **177**, 270-272.

Krijgsman, W., Hilgen, F.J., Raffi, I., Sierro, F.J. and **Wilson, D.S.** (1999) Chronology, causes and progression of the Messinian salinity crisis. *Nature*, **400**, 652-655.

Krijgsman, W., Garcés, M., Agustí, J., Raffi, I., Taberner, C. and **Zachariasse, W.J.** (2000). The „Tortonian Salinity Crisis" of the eastern Betics (Spain). *Earth and Planetary Science Letters*, **181**, 497-511.

Kroeger K.F. (2004) Sedimentary environments and climate change: a case study (late Miocene, central Crete). *PhD thesis, Johannes Gutenberg-Universität*, 224 pp..

Kurths, J., Spiering, C., Müller-Stoll, M. and **Striegler, U.** (1993) Search for periodicities on Miocene tree ring widths. *Terra Nova*, **5**, 359-363.

Langer, M.R. and **Hottinger, L.** (2000) Biogeography of selected „larger" foraminifera. *Micropaleontology*, **46** (1), 105-126.

Lear, C.H., Elderfield, H. and **Wilson, P.A.** (2003a) A Cenozoic seawater Sr/Ca record from benthic foraminiferal calcite and its application in determining global weathering fluxes. *Earth and Planetary Science Letters*, **208**, 69-84.

Lear, C.H., Rosenthal, Y. and **Wright, J.D.** (2003b) The closing of a seaway: ocean water masses and global climate change. *Earth and Planetary Science Letters*, **210**, 425-436.

Leeder, M.R. and **Gawthorpe, R.L.** (1987) Sedimentary models for extensional tilt-block/half-graben basins. In: Continental extensional teconics (Eds. M.P. Coward, J.F. Dewey and P.L. Hancock), *Geological Society Special Publication*, **28**, 139-152. Blackwell, Oxford.

Lees, A. and **Buller, A.T.** (1972) Modern temperate-water and warm-water shelf carbonate sediments contrasted. *Marine Geology*, **13**, M67-M73.

Lighty, R.G. (1985) Preservation of internal reef porosity and diagenetic sealing of submerged early Holocene barrier reef, southeast Florida shelf. In: Carbonate Cements (Eds. N. Schneidermann, P.M. Harris), *SEPM Special Publication*, **36**, 123-151. Society for Sedimentary Geology, Tulsa.

Lirman, D., Manzello, D. and **Macia, S.** (2002) Back from the dead: the resilience of *Siderastrea radians* to severe stress. *Coral Reefs*, **21**, 291-292.

Longman, M.A. (1980) Carbonate diagenetic textures from nearsurface diagenetic environments. *American Association of Petroleum Geologists Bulletin*, **64**, 461-487.

Lough, J.M. and **Barnes, D.J.** (2000) Environmental controls on growth of the massive coral *Porites*. *Journal of Experimental Marine Biology and Ecology*, **245**, 225-243.

Lourens, L.J. and **Hilgen, F.J.** (1997) Long-periodic variations in the earth´s obliquity

and their relation to third-order eustatic cycles and late Neogene glaciations. *Quaternary International*, **40**, 43-52

Macintyre, I.G. (1977) Distribution of submarine cements in a modern Caribbean fringing reef, Galeta Point, Panama. *Journal of Sedimentary Petrology*, **47**, 503-516.

Macintyre, I.G. (1985) Submarine cements - the peloidal question. In: Carbonate Cements (Eds. N. Schneidermann and P.M. Harris), *SEPM Special Publication*, **36**, 109-116. Society for Sedimentary Geology, Tulsa.

Martín, J.M., Braga, J.C. and **Rivas, P.** (1989) Coral successions in Upper Tortonian reefs in SE Spain. *Lethaia*, **22**, 271-286.

Martín, J.M. and **Braga, J.C.** (1994) Messinian events in the Sorbas basin in southeastern Spain and their implications in the recent history of the Mediterranean. *Sedimentary Geology*, **90**, 257-268.

Martín, J.M., Braga, J.C., Betzler, C. and **Brachert, T.C.** (1996) Sedimentary model and high-frequency cyclicity in a Mediterranean, shallow shelf, temperate-carbonate environment (uppermost Miocene, Agua Amarga Basin, southern Spain). *Sedimentology*, **43**, 263-277.

McConnaughey, T. (1989) ^{13}C and ^{18}O isotopic disequilibrium in biological carbonates: I. Patterns. *Geochimica Cosmochimica Acta*, **53**, 151-162.

McGregor, H.V. and **Gagan, M.K.** (2003) Diagenesis and geochemistry of *Porites* corals from Papua New Guinea: Implications for paleoclimate reconstruction. *Geochimica et Cosmochimica Acta*, **67**, 2147-2156.

Meijer, P.T., Slingerland, R. and **Wortel, M.J.R.** (2004) Tectonic control on past corculation of the Mediterranean Sea: A model study of the Late Miocene. *Paleoceanography*, **19**, 19.

Meulenkamp, J.E., Dermitzakis M., Georgiadou-Dikeoulia, E., Jonkers, H.A. and **Böger, H.** (1979) Field guide to the Neogene of Crete. *Publications of the Department of Geology and Paleontology. University of Athens*, p. 32.

Meulenkamp, J.E., van der Zwaan, G.J. and **van Wamel, W. A.** (1994) On Late Miocene to Recent vertical motions in the Cretan segment of the Hellenic arc. *Tectonophysics*, **234**, 53-72.

Meulenkamp, J.E. and **Sissingh, W.** (2003) Tertiary paleogeography and tectonostratigraphic evolution of the northern and southern Peri-Tethys platforms and the intermediate domains of the African-Eurasian convergent plate boundary zone. *Paleogeography, Paleoclimatology, Paleoecology*, **196**, 209-228.

Micheels, A. (2003) Late Miocene climate modelling with ECHAM4/ML - The effects of the paleovegetation on the Tortonian climate. *Dissertation Universität Tübingen*, 135 pp..

Mikolajewicz, U., Maier-Reimer, E., Crowley, T.J. and **Kim, K.J.** (1993) Effect of Drake

and Panamanian gateways on the circulation of an ocean model. *Paleoceanography*, **8**, 409-426.

Miller, K.G., Wright, J.D. and **Fairbanks, R.G.** (1991) Unlocking the ice house: Oligocene-Miocene oxygen isotopes, eustasy, and margin erosion. *Journal of Geophysical Research*, **96**, 6829-6848.

Moisette, P., Delrieu, B. and **Tsagaris, S.** (1993) Bryozoaires du Bassin néogène d´Héraklion (Crète centrale, Grèce). Le Miocène Supérieur: premiers résultats. *Neues Jahrbuch für Geologie und Paläontologie, Abhandlungen*, **190**, 75-123.

Montenat, C. (1990) Les bassins néogènes du domaine bétique oriental (Espagne) Documens et Travaux Institut Géologique Albert-de-Lapparent, 12-13. Institut Géologique Albert -de-Lapparent, Paris, 392 pp.

Nelson, C.S. (1988) An introductory perspective on non-tropical shelf carbonates. *Sedimentary Geology*, **60**, 3-12.

Nose, M. (1999) Environmental control on the morphology and the linear growth rate of *Microsolena agariciformis* Étallon (Scleractinia) from the Upper Jurassic of Portugal. *Profil*, **16**, 125-133.

Pätzold, J. (1984) Growth rhythms recorded in stable isotopes and density bands in the reef coral *Porites lobata* (Cebu, Philippines). *Coral Reefs*, **3**, 87-90.

Paillard, D., Labeyrie, L. and **Yiou, P.** (1996) Macintosh program performs time-series analysis. *EOS Transactions of the American Geophysical Union*, **77**, 1-379.

Pearson, P.N. and **Palmer, M.R.** (2000) Atmospheric carbon dioxide concentrations over the past 60 million years. *Nature*, **406**, 695-699.

Pedley, M. (1996) Miocene reef distributions and their associations in the central Mediterranean region: an overview. In: Models for carbonate stratigraphy from Miocene reef complexes of Mediterranean regions (Eds. E.K. Franseen, M. Esteban, W.C. Ward and J.P. Rouchy), *Concepts in Sedimentology and Paleontology,* **5**, 73-88. Society for Sedimentary Geology, Tulsa.

Perrin, C., Bosence, D.W.J. and **Rosen, B.** (1995) Quantitative approaches to paleozonation and paleobathymetry of corals and coralline algae in Cenozoic reefs. In: Marine paleoenvironmental analysis from fossils (Eds. D.W.J. Bosence and P.A. Allison), *Geological Society Special Publication*, **83**, 181-229. Geological Society Publishing House, London.

Perrin, C. (2002) Tertiary: The emergence of modern reef ecosystems. In: Phanerozoic reef patterns (Eds. W. Kiessling and E. Flügel), *SEPM Specal Publication*, **72**, 587-621. Society for Sedimentary Geology, Tulsa.

Perry, C.T. (2003) Coral reefs in a high latitude, siliciclastic barrier island setting: reef framework and sediment production at Inhaca Island, southern Mozambique. *Coral Reefs*, **22**, 485-497.

Playford, P. A. (1988) Guidebook to the geology of Rottnest Island. *Excursion guidebook*, **2**, 67 pp.. Geological Society of Australia, WA Division and the Geological Survey of Western Australia, Perth.

Pomar, L., Ward, W.C. and **Green, D.G.** (1996) Upper Miocene reef complexes of the Llucmajor area, Mallorca, Spain. In: Models for carbonate stratigraphy from Miocene reef complexes of Mediterranean regions (Eds. E.K. Franseen, M. Esteban, W.C. Ward and J.-M. Rouchy), *Concepts in Sedimentology and Paleontoogy,* **5**, 191-225. Society for Sedimentary Geology, Tulsa.

Pomar, L. (2001) Types of carbonate platforms: a genetic approach. *Basin Research*, **13**, 313-334.

Pomar, L., Brandano, M. and **Westphal, H.** (2004) Environmental factors influencing skeletal-grain sediment associations: A critical review of Miocene examples from the Western Mediterranean. *Sedimentology*, **51**, 627-651.

Raymo, M.E. and **Ruddiman, W.F.** (1992) Tectonic forcing of late Cenozoic climate. *Nature*, **359**, 17-122.

Pomoni-Papaioannou, F., Drinia, H. and **Dermitzakis M.D.** (2002) Neogene non-tropical carbonate sedimentation in a warm temperate biogeographic province (Rethymnon formation, Eastern Crete, Greece). *Sedimentary Geology*, **154**, 147-157.

Postma, G., Fortuin, A.R. and **van Wamel, W.A.** (1993) Basin-fill patterns controlled by tectonics and climate: the Neogene „fore-arc" basins of eastern Crete as a case history. *Special Publication, International Association of Sedimentologists*, **20**, 335-362.

Quade, J., Cater, J.M.L., Ojha, T.P., Adam, J. and **Harrison, T.M.** (1995) Late Miocene environmental change in Nepal and the northern Indian subcontinent: Stable isotope evidence from paleosols. *Geological Society of America Bulletin*, **107**, 1381-1397.

Rahl, J. M. (2004) Exhumation of high-pressure metamorphic rocks within an active convergent margin, Crete, Greece. *Field-trip guide book, 32nd International Geological Congress*, 36 pp.

Rasser, M.W. and **Riegl, M.** (2002) Holocene coral reef rubble and its binding agents. *Coral Reefs*, **21**, 57-72.

Reuter, M., Fischer, R., Helm, C. and **Schülke, I.** (2001) Entwicklung und Faziesverteilung eines Riffkomplexes im Korallenoolith (Oberjura) des Osterwaldes (Niedersachsen). *Geologische Beiträge Hannover*, **2**, 31-50.

Riding, R., Martín, J.M. and **Braga, J.C.** (1991) Coral-stromatolite reef framework, upper Miocene, Almeria, Spain. *Sedimentology*, **38**, 799-818.

Riegl, B. (2001) Inhibition of reef framework by frequent disturbance: examples from the Arabian Gulf, South Africa, and the Cayman Islands. *Palaeogeography, Palaeoclimatology, Palaeoecology*, **175**/1-1, 79-102.

Rimbu, N., Lohmann, G., Felis, T. and **Pätzold, J.** (2001) Arctic oscillation signature in a Red Sea coral. *Geophysical Research Letters*, **28**, 2959-2962.

Rimbu, N., Lohmann, G., Felis, T. and **Pätzold, J.** (2003) Shift in ENSO teleconnections recorded by a northern Red Sea coral. *Journal of Climate*, **16**, 1414-1422.

Rogers, J.C. and **McHugh, M.J.** (2002) On the separability of the North Atlantic Oscillation and Arctic Oscillation. *Climate Dynamics*, **19**, 599-608.

Rögl, F. and **Steininger, F.** (1984) Neogene Paratethys, Mediterranean and Indo-Pacific seaways: Implications for the paleobiogeeography of marine and terrestrial biotas. In: Fossils and climate (Ed. P. Brenchley), 171-179. Wiley and Sons Ltd., New York.

Rosen, B.R. (1977) The depth distribution of recent hermatypic corals and its paleontological significance. *Mémoires R.R.G.M.*, **89**, 507-517.

Rosenfeld, M., Yam, R.,Shemesh, A. and **Loya, Y.** (2003) Implication of water depth on stable isotope composition and skeletal density patterns in a *Porites lutea* colony: results from a long-term translocation experiment. *Coral Reefs*, **22**, 337-345.

Roulier, L.M. and **Quinn, T.M.** (1995) Seasonal- to decadal-scale climatic variability in southwest Florida during the middle Pliocene: Inferences from a coralline stable isotope record. *Paleoceanography*, **10**, 429-443.

Sachse, M. and **Mohr, B.** (1996) Eine obermiozäne Makro- und Mikroflora aus Südkreta (Griechenland), und deren paläoklimatische Interpretation - Vorläufige Betrachtungen. *Neues Jahrbuch für Geologie und Paläontologie, Abhandlungen*, **200**, 149-182.

Sachse, M. (1997) Die Makrilia Flora (Kreta, Griechenland) - Ein Beitrag zur neogenen Klima- und Vegetationsgeschichte des östlichen Mittelmeergebietes. *PhD thesis Eidgenössische Technische Hochschule, Zürich*, 311 pp.

Saint Martin, J.P. (1990) Les formations récifales coralliennes du Miocéne supérieur d´Algérie du Maroc. *Mém. Mus. Nat. Hist. Nat. (C)*, **56**, 1-366, Paris.

Santarelli, A., Brinkhuis, H., Hilgen, F.J., Lourens, L.J., Versteegh, G.J.M. and **Visscher, H.**(1998) Orbital signatures in a Late Miocene dinoflagellate record from Crete (Greece). *Marine Micropaleontology*, **33**, 273-297.

Santisteban, C. (1981) Petrologia y sedimentologia de los materiales del Mioceno superior de la cuenca de Fortuna (Murcia) a la luz de la Teoria de la Crisis de Salinidad. *PhD thesis, University of Barcelona*, 722 pp..

Santisteban, C. and **Taberner, C.** (1983) Shallow marine and continental conglomerates derived from coral reef complexes after desiccation of a deep marine basin: the Tortonian-Messinian deposits of the Fortuna basin, southeast Spain. *Journal of the Geological Society*, **140**, 401-411.

Santisteban, C. and **Taberner, C.** (1988) Sedimentary models of siliciclastic deposits and coral reefs interrelation. In: Carbonate-Clastic Transitions (Eds. L.J. Doyle and H.H. Roberts), *Developments in Sedimentology*, **42**, 35-76. Elsevier, Amsterdam.

Schenau, S.J., Antonarakou, A., Hilgen, F.J., Lourens, L.J., Nijenhuis, I.A., van der Weijden, C.H. and **Zachariasse, W.J.** (1999) Organic-rich layers in the Metochia section (Gavdos, Greece): evidence for a single mechanism of sapropel formation during the last 10My. *Marine Geology*, **153**, 117-135.

Schlager, W. (1992) Sedimentology and sequence stratigraphy of reefs and carbonate platforms, a short course. *The American Association of Petroleum Geologists, Continuing Education Course Note Series*, **34**, 1-71.

Schlager, W. (1999) Scaling of sedimentation rates and drowning of reefs and carbonate platforms. *Geology*, **27**, 183-186.

Sierro, F.J., Flores, J.A., Francés, G., Vazquez, A., Utrilla, R., Zamarreno, I., Erlenkeuser, H. and **Barcena, M.A.** (2003) Orbitally controlled oscillations in planktic communities and cyclic changes in western Mediterranean hydrography during the Messinian. *Paleogeography, Paleoclimatology, Paleoecology*, **190**, 289-316.

Shinn, E.A. (2001) Coral reefs as shoreline dipsticks. In: *Geological perspectives of global climate change* (Eds. L.C. Gerhard, W.E. Harrison and B.M. Hanson), *AAPG Studies in Geology*, **47**, 251-264. American Association of Petroleum Geologists, Tulsa.

Steppuhn, A., Micheels, A., Geiger, G. and **Mosbrugger, V.** (accepted): Reconstructing the Late Miocene climate and oceanic heat flux using the AGCM ECHAM4 coupled to a mixed-layer ocean model with adjusted flux correction. *Paleogeography, Paleoclimatology, Paleoecology*.

ten Veen, J.H. and **Postma, G.** (1996) Astronomically forced variations in gamma-ray intensity: Late Miocene hemipelagic successions in the eastern Mediterranean basin as a test case. *Geology*, **24**, 15-18.

ten Veen, J. H. and **Postma, G.** (1999) Neogene tectonics and basin fill patterns in the Helenic outer-arc (Crete, Greece). *Basin Research*, **11**, 223-242.

ten Veen, J.H. and **Kleinspehn, K.I.** (2000) Quantifying the timing and sense of fault dip slip: new application of biostratigraphy and geohistory analysis. *Geology*, **28**, 471-474.

Thompson, D.W.J. and **Wallace, J.M.** (2001) Regional climate impacts of the Northern Hemisphere Annular Mode. *Science*, **293**, 85-89.

Utescher, T., Mosbrugger, V. and **Ashraf, A.R.** (2000) Terrestrial climate evolution in Northwest Germany over the last 25 Million years. *Palaios*, **15**, 430-449.

van der Burgh, J., Visscher, H., Dilcher, D.L. and **Kürschner, W.M.** (1993) Paleoatmospheric Signatures in Neogene Fossil Leaves. *Science*, **260**, 1788-1790.

van Woesik, R. (1998) Lesion healing on massive *Porites* spp. corals. *Marine Ecology Progress Series*, **164**, 213-220.

Veron, J.E.N. (1995) Corals in space and time: biogeography and evolution of the Scleractinia, 321 pp.. Comstock/Cornell, Ithaca and London.

Wefer, G. and **Berger, W.H.** (1991) Isotope paleontology: growth and composition of extent calcareous species. *Marine Geology*, **100**, 207-248.

Wrobel, F. (2000) Das Lorca-Becken (Obermiozän, SE-Spanien). *Geologische Beiträge Hannover*, **1**, 1-141.

Zachariasse, W.J. (1975) Planctonic foraminiferal biostratigraphy of the Late Neogene of Crete (Greece). *Utrecht Micropaleontological Bulletin*, **11**, 1-143.

Zachos, J., Pagani, M., Sloan, L., Thomas, E. and **Billups K.** (2001) Trends, rhythms, and aberrations in global climate 65 Ma to present. *Science*, **292**, 686-693.

Zachos, J.C., Arthur, M.A., Bralower, T.J. and **Spero, H.J.** (2002) Paleoclimatology: tropical temperatures in greenhouse episodes. *Nature*, **419**, 897-898.

Zidianakis, G., **Mohr, B.** and **Fassoulas, C.** (2004) The Late-Miocene flora Vrysses, Western Crete - A contribution to the climate and vegetation history. *5th International Symposium on Eastern Mediterranean Geology, Thessaloniki, Greece*, S5-S9.

9 Appendix

Coral	Identifier	Sampling interval (mm)	Growth band (reflected light)	Age model (years)	$\delta^{13}C$ (V-PDB)	$\delta^{13}C$ standard deviation (1σ)	$\delta^{18}O$ (V-PDB)	$\delta^{18}O$ standard deviation (1σ)
P1	**01**	**1,53**	**light**	**1.00**	**-1.72**	**0.01**	**-2.39**	**0.02**
	02	3.06	dark	1.50	-1.09	0.01	-3.10	0.02
	03	**4.59**	**light**	**2.00**	**-1.72**	**0.01**	**-2.66**	**0.02**
	04	6.12	dark	2.50	-1.71	0.02	-3.06	0.06
	05	**7.65**	**light**	**3.00**	**-2.07**	**0.01**	**-2.59**	**0.02**
	06	9.18	dark	3.50	-1.51	0.02	-2.74	0.02
	07	**10.71**	**light**	**4.00**	**-1.74**	**0.02**	**-2.27**	**0.02**
	08a	12.24	dark	4.33	-1.45	0.02	-3.07	0.02
	08b	13.77	dark	4.66	-2.28	0.01	-2.73	0.03
	09	**15.30**	**light**	**5.00**	**-1.88**	**0.01**	**-2.48**	**0.02**
	10a	16.83	dark	5.33	-1.58	0.02	-3.05	0.04
	10b	18.36	dark	5.66	-1.80	0.02	-3.17	0.03
	11	**19.89**	**light**	**6.00**	**-2.29**	**0.01**	**-2.17**	**0.04**
	12a	21.42	dark	6.33	-2.16	0.02	-3.01	0.04
	12b	22.95	dark	6.66	-1.63	0.03	-3.10	0.03
	13	**24.48**	**light**	**7.00**	**-1.83**	**0.01**	**-2.12**	**0.03**
	14a	26.01	dark	7.33	-1.17	0.01	-2.81	0.03
	14b	27.54	dark	7.66	-1.54	0.03	-2.88	0.02
	15	**29.07**	**light**	**8.00**	**-1.67**	**0.01**	**-2.33**	**0.02**
	16a	30.60	dark	8.33	-1.24	0.02	-3.30	0.03
	16b	32.13	dark	8.66	-1.74	0.01	-2.99	0.01
	17	**33.66**	**light**	**9.00**	**-1.62**	**0.02**	**-2.24**	**0.02**
	18a	35.19	dark	9.33	-1.09	0.03	-3.20	0.04
	18b	36.20	dark	9.66	-1.25	0.02	-2.78	0.04
	19	**38.25**	**light**	**10.00**	**-1.52**	**0.02**	**-2.15**	**0.04**
	20a	39.78	dark	10.33	-0.28	0.02	-2.81	0.04
	20b	41.31	dark	10.66	-0.52	0.02	-3.08	0.02
	21	**42.84**	**light**	**11.00**	**-0.90**	**0.01**	**-2.11**	**0.02**
	22a	44.37	dark	11.33	0.24	0.02	-2.66	0.04
	22b	45.80	dark	11.66	-0.40	0.01	-3.12	0.02
	23	**47.43**	**light**	**12.00**	**-1.89**	**0.02**	**-1.98**	**0.04**
	24a	48.96	dark	12.33	-1.88	0.01	-3.09	0.02
	24b	50.49	dark	12.66	-1.70	0.02	-2.98	0.04
	25	**52.02**	**light**	**13.00**	**-3.06**	**0.02**	**-3.02**	**0.06**
	26a	53.55	dark	13.33	-0.90	0.03	-2.99	0.05
	26b	55.08	dark	13.66	-1.39	0.02	-2.83	0.03
	27	**56.61**	**light**	**14.00**	**-2.55**	**0.03**	**-2.80**	**0.04**
	28a	58.14	dark	14.33	-0.89	0.02	-2.76	0.02
	28b	59.67	dark	14.66	-1.24	0.02	-3.05	0.04
	29	**61.20**	**light**	**15.00**	**-2.25**	**0.02**	**-2.23**	**0.03**
	30a	62.73	dark	15.33	-1.16	0.03	-2.86	0.05
	30b	64.26	dark	15.66	-1.72	0.03	-3.04	0.05
	31	**65.79**	**light**	**16.00**	**-2.47**	**0.02**	**-2.73**	**0.03**

A1. Coral stable isotope data set ($\delta^{13}C$ and $\delta^{18}O$). Sample P1, Psalidha, Coral Site 1.3A, Coral Level 1, early Tortonian.

Coral	Identifier	Sampling interval (mm)	Growth band (reflected light)	Age model (years)	$\delta^{13}C$ (V-PDB)	$\delta^{13}C$ standard deviation (‰)	$\delta^{18}O$ (V-PDB)	$\delta^{18}O$ standard deviation (‰)
	01		**dark**	**1.00**	**-0.50**		**-2.24**	
	02		dark	1.25	-0.25		-2.72	
	03		light	1.50	-0.82		-3.19	
	04		dark	1.75	-1.08		-2.88	
	05		**dark**	**2.00**	**-0.86**		**-2.16**	
	06		dark	2.20	-0.49		-2.96	
	07		dark	2.40	-0.28		-3.14	
	08		light	2.60	-0.30		-3.27	
	09		light	2.80	-0.85		-2.84	
	10		**light**	**3.00**	**-0.36**		**-2.45**	
	11		light	3.33	-0.36		-3.03	
	12		dark	3.66	-0.17		-2.89	
	13		**dark**	**4.00**	**-0.69**		**-2.24**	
	15		light	4.33	-0.39		-3.24	
	16		dark	4.66	-1.18		-2.41	
	17		**dark**	**5.00**	**-0.50**		**-2.22**	
	18		dark	5.25	-0.13		-2.81	
	19A		light	5.50	0.34		-3.04	
	20		dark	5.75	-0.66		-2.50	
	21		**dark**	**6.00**	**-0.34**		**-2.02**	
	22		light	6.33	0.05		-3.33	
	23		dark	6.66	-0.31		-2.71	
	24		**dark**	**7.00**	**-0.24**		**-2.35**	
	025 (1)A		light	7.50	0.31		-3.19	
P2	**26**	1.22	**dark**	**8.00**	**-0.46**	<±0.03	**-1.80**	<±0.03
	27		dark	8.50	0.12		-3.08	
	28		**light**	**9.00**	**0.12**		**-2.25**	
	29		dark	9.33	0.26		-2.83	
	30		dark	9.66	0.87		-2.90	
	31		**light**	**10.00**	**0.15**		**-2.39**	
	32		dark	10.50	0.44		-3.03	
	34		**light**	**11.00**	**-0.07**		**-1.65**	
	35		dark	11.25	0.34		-1.90	
	36		dark	11.50	0.83		-2.55	
	37		light	11.75	0.28		-2.15	
	38		**light**	**12.00**	**0.07**		**-1.69**	
	40		light	12.25	0.20		-2.08	
	41		dark	12.50	0.44		-1.92	
	42		dark	12.75	0.57		-2.74	
	43		**light**	**13.00**	**-0.18**		**-1.97**	
	44		dark	13.25	-0.27		-2.97	
	45		dark	13.50	-0.01		-3.12	
	46		light	13.75	-0.49		-2.58	
	47		**dark**	**14.00**	**0.06**		**-2.41**	
	48		dark	14.33	0.03		-3.22	
	49A		light	14.66	-0.73		-2.64	
	50		**dark**	**15.00**	**-0.71**		**-2.25**	
	51		dark	15.33	0.15		-3.27	
	52		dark	15.66	0.14		-2.35	

	53		**light**	**16.00**	**-0.54**		**-1.95**	
	54		dark	16.25	0.26		-2.91	
	55		dark	16.50	0.61		-3.10	
	56		light	16.75	-0.82		-2.67	
	57		**dark**	**17.00**	**-0.82**		**-1.72**	
	58		dark	17.25	0.61		-2.83	
	59		dark	17.50	0.90		-3.13	
	60		light	17.75	0.05		-2.59	
	61		**dark**	**18.00**	**-0.44**		**-2.08**	
	62		dark	18.33	0.69		-2.75	
	63		light	18.66	-0.48		-2.62	
	64		**dark**	**19.00**	**-0.03**		**-2.51**	
	65		dark	19.50	0.21		-3.22	
	66		**light**	**20.00**	**-0.06**		**-2.79**	
	67		dark	20.33	0.23		-3.02	
	68		dark	20.66	0.57		-3.05	
	69		**light**	**21.00**	**-0.04**		**-2.40**	
	70		dark	21.33	0.04		-3.43	
	71		dark	21.66	0.35		-2.84	
	72		**light**	**22.00**	**0.37**		**-1.66**	
	73		dark	22.33	0.24		-3.13	
	74		light	22.66	0.17		-2.69	
	75		dark	**23.00**	**-0.01**		**-2.57**	
	76		dark	23.50	0.15		-3.16	
P2	**77A**	1.22	**light**	**24.00**	**-0.33**	<±0.03	**-2.91**	<±0.03
	78		dark	24.25	-0.14		-2.94	
	79		dark	24.50	0.13		-3.46	
	80		light	24.75	-0.15		-2.74	
	81		**dark**	**25.00**	**-0.54**		**-2.61**	
	82		dark	25.50	0.38		-3.11	
	83		**light**	**26.00**	**-0.59**		**-2.87**	
	84		dark	26.33	-0.24		-3.16	
	85		dark	26.66	0.21		-3.35	
	86		**light**	**27.00**	**-0.36**		**-2.64**	
	87		dark	27.25	-0.57		-2.65	
	88		dark	27.50	0.46		-3.12	
	89		light	27.75	-0.08		-2.23	
	90		**dark**	**28.00**	**-0.64**		**-1.97**	
	91		dark	28.50	0.39		-3.46	
	92		**light**	**29.00**	**-0.17**		**-2.36**	
	93		dark	29.20	-0.17		-3.09	
	94		dark	29.40	0.36		-3.36	
	95		dark	29.60	-0.31		-3.52	
	96		light	29.80	-0.75		-2.61	
	97		**dark**	**30.00**	**0.20**		**-2.60**	
	98		dark	30.50	0.35		-3.00	
	99		**light**	**31.00**	**-0.99**		**-2.32**	
	100		dark	31.33	-0.41		-2.72	
	101		dark	31.66	0.45		-3.29	

	102		**light**	**32.00**	**-0.18**		**-2.27**	
	103		dark	32.33	0.41		-3.20	
	104		light	32.66	-0.02		-2.84	
	105		**dark**	**33.00**	**-0.42**		**-2.18**	
	106A		dark	33.50	-0.13		-3.41	
	107		**light**	**34.00**	**-0.34**		**-2.80**	
	108		dark	34.33	-0.49		-3.00	
	109		dark	34.66	-0.09		-3.38	
	110B		**light**	**35.00**	**0.14**		**-2.72**	
	110A		light	35.25	-0.62		-2.82	
	111		dark	35.50	0.70		-3.37	
	112		dark	35.75	0.25		-3.03	
	113		**light**	**36.00**	**0.12**		**-2.47**	
	114		dark	36.33	0.49		-3.39	
	115		dark	36.66	0.53		-3.35	
	116		**light**	**37.00**	**-0.04**		**-1.94**	
	117		dark	37.33	-0.40		-3.12	
	118		dark	37.66	0.68		-3.30	
	119		**light**	**38.00**	**0.17**		**-2.36**	
	120		dark	38.33	0.19		-2.96	
	121		dark	38.66	0.62		-3.16	
	122		**light**	**39.00**	**0.07**		**-2.22**	
	123		dark	39.33	0.54		-2.48	
	124		dark	39.66	1.19		-3.16	
P2	**125**	1.22	**light**	**40.00**	**0.97**	<±0.03	**-2.00**	<±0.03
	126		dark	40.33	0.82		-2.94	
	127		light	40.66	0.34		-2.45	
	128		**light**	**41.00**	**0.87**		**-2.08**	
	129		dark	41.50	0.80		-3.09	
	130		**light**	**42.00**	**0.50**		**-2.26**	
	131		dark	42.33	0.11		-2.67	
	133		light	42.66	0.59		-3.30	
	134		**dark**	**43.00**	**0.57**		**-2.59**	
	135		dark	43.50	0.15		-3.25	
	136		**light**	**44.00**	**-0.19**		**-2.39**	
	137		dark	44.33	-0.38		-3.18	
	138		dark	44.66	0.17		-3.47	
	139		**light**	**45.00**	**0.15**		**-2.81**	
	140		dark	45.50	0.32		-2.99	
	141		**light**	**46.00**	**0.47**		**-2.71**	
	142		dark	46.25	-0.61		-3.10	
	143		dark	46.50	-0.18		-3.54	
	144		light	46.75	-0.87		-3.20	
	145		**dark**	**47.00**	**-0.64**		**-3.06**	
	146		dark	47.33	-0.45		-3.55	
	147		light	47.66	-1.14		-3.04	
	148		**dark**	**48.00**	**-0.66**		**-2.99**	
	149		dark	48.33	-0.12		-3.47	
	150		light	48.66	-0.20		-3.09	

	151		**dark**	**49.00**	**-0.62**		**-2.56**	
	152		dark	49.50	0.01		-3.09	
	153		**light**	**50.00**	**-1.22**		**-2.73**	
	154		dark	50.33	0.13		-3.17	
	155		light	50.66	-0.48		-3.25	
	156		**dark**	**51.00**	**-0.35**		**-2.45**	
	157		dark	51.50	-0.67		-3.13	
	159		**light**	**52.00**	**-0.83**		**-2.29**	
	160		dark	52.50	-0.56		-3.39	
	161		**dark**	**53.00**	**-0.13**		**-2.80**	
	162		dark	53.33	-0.71		-2.98	
	163		light	53.66	-1.67		-3.32	
	164		**dark**	**54.00**	**-1.63**		**-3.01**	
	165		light	54.25	-0.39		-3.24	
	166		dark	54.50	-0.07		-3.34	
	167		dark	54.75	-0.41		-3.40	
	168		**light**	**55.00**	**-0.75**		**-2.34**	
	169		dark	55.25	-0.03		-2.51	
	170		dark	55.50	0.46		-2.83	
	171		light	55.75	-0.59		-3.06	
	172		**dark**	**56.00**	**-0.34**		**-2.44**	
	173		dark	56.33	0.27		-3.12	
	174		light	56.66	-1.33		-3.06	
	175		**dark**	**57.00**	**-0.32**		**-2.71**	
P2	176	1.22	dark	57.33	0.09	<±0.03	-3.34	<±0.03
	177		light	57.66	-0.42		-3.26	
	178		**dark**	**58.00**	**-0.37**		**-2.35**	
	179		light	58.33	0.23		-3.38	
	180		light	58.66	-0.11		-2.91	
	181		dark	**59.00**	**-0.41**		**-2.88**	
	182		dark	59.50	0.05		-3.46	
	183		**light**	**60.00**	**-0.33**		**-2.73**	
	184		dark	60.33	0.37		-3.26	
	185		dark	60.66	-0.14		-3.24	
	186		light	**61.00**	**-1.02**		**-2.31**	
	187		dark	61.33	0.04		-3.42	
	188		dark	61.66	-0.21		-3.50	
	189		**light**	**62.00**	**-1.19**		**-2.29**	
	190		dark	62.20	-0.07		-2.65	
	191		dark	62.40	0.14		-3.49	
	192		light	62.60	0.06		-3.05	
	193		dark	62.80	0.44		-3.24	
	195		**light**	**63.00**	**-0.81**		**-2.55**	
	196		dark	63.33	-0.10		-2.97	
	197		dark	63.66	-0.21		-3.45	
	198		**light**	**64.00**	**-0.10**		**-2.18**	
	199		dark	64.25	0.64		-3.22	
	200		dark	64.50	0.58		-3.35	
	201		light	64.75	-0.54		-2.72	

	202		**dark**	**65.00**	**0.97**		**-2.42**	
	203		dark	65.33	0.84		-3.27	
	204		light	65.66	0.09		-3.42	
	205		**dark**	**66.00**	**-0.40**		**-2.52**	
	206		dark	66.25	-0.06		-3.45	
	207		light	65.50	-0.11		-3.39	
	208		light	66.75	-0.45		-2.91	
P2	**209**	1.22	**dark**	**67.00**	**-0.48**	<±0.03	**-2.76**	<±0.03
	210		dark	67.33	-0.34		-3.63	
	211		light	67.66	0.00		-3.12	
	212		**dark**	**68.00**	**-0.23**		**-2.48**	
	213		dark	68.33	0.17		-3.31	
	214		light	68.66	-0.82		-3.26	
	215		**dark**	**69.00**	**-0.31**		**-2.56**	
	216		dark	69.33	-0.19		-3.42	

A2. Coral stable isotope data set ($\delta^{13}C$ and $\delta^{18}O$). Sample P2, Psalidha, Coral Site 1.3B, Coral Level 1, early Tortonian.

Coral	Identifier	Sampling interval (mm)	Growth band (reflected light)	Age model (years)	$\delta^{13}C$ (V-PDB)	$\delta^{13}C$ standard deviation (1σ)	$\delta^{18}O$ (V-PDB)	$\delta^{18}O$ Standard deviation (1σ)
P3	01	1	dark	0.28	-0.20	0.01	-3.14	0.02
	02	2	dark	0.42	-0.89	0.01	-3.35	0.01
	03	3	dark	0.56	-1.09	0.01	-2.98	0.02
	05	4	light	0.84	-1.67	0.01	-2.44	0.02
	06	**5**	**light**	**1.00**	**-1.13**	**0.01**	**-1.94**	**0.01**
	07	6	light	1.14	-0.23	0.01	-2.64	0.01
	08	7	dark	1.28	-0.01	0.01	-3.01	0.01
	09	8	dark	1.42	0.52	0.01	-2.80	0.01
	10	9	light	1.56	0.13	0.01	-2.63	0.01
	11	10	light	1.70	-1.25	0.01	-2.25	0.01
	12	11	light	1.84	-1.41	0.01	-1.98	0.02
	13	**12**	**light**	**2.00**	**-0.26**	**0.01**	**-1.75**	**0.02**
	1	13	dark	2.17	-0.08	0.02	-2.77	0.00
	16	14	dark	2.34	0.15	0.01	-3.02	0.01
	17	15	dark	2.51	-0.62	0.01	-2.72	0.01
	18	16	light	2.68	-1.13	0.01	-2.72	0.02
	19	17	light	2.85	-1.33	0.01	-2.11	0.02
	20	**18**	**light**	**3.00**	**-0.20**	**0.01**	**-1.93**	**0.03**
	21	19	light	3.20	0.29	0.01	-2.67	0.02
	22	20	dark	3.40	0.68	0.01	-2.92	0.02
	23	21	dark	3.60	-0.13	0.01	-2.89	0.02
	24	22	dark/light	3.80	-0.92	0.01	-2.74	0.01
	25	**23**	**light**	**4.00**	**-1.14**	**0.01**	**-2.11**	**0.02**

A3. Coral stable isotope data set ($\delta^{13}C$ and $\delta^{18}O$). Sample P3, Psalidha, Coral Site 1.3A, Coral Level 1, early Tortonian.

Coral	Identifier	Sampling interval (mm)	Growth band (reflected light)	Age model (years)	$\delta^{13}C$ (V-PDB)	$\delta^{13}C$ standard deviation (1σ)	$\delta^{18}O$ (V-PDB)	$\delta^{18}O$ standard deviation (1σ)
P4	01	1	dark	0.25	-0.61	0.01	-3.48	0.01
	02	2	dark	0.50	-0.63	0.00	-3.31	0.01
	03	3	light	0.75	-0.67	0.01	-2.85	0.01
	04	**4**	**light**	**1.00**	**-1.34**	**0.01**	**-2.14**	**0.02**
	05	5	light	1.20	-0.70	0.01	-2.80	0.02
	07	6	dark	1.40	-0.77	0.01	-3.37	0.01
	08	7	dark	1.60	-0.44	0.01	-3.42	0.01
	09	8	light	1.80	-0.96	0.01	-2.55	0.01
	10	**9**	**light**	**2.00**	**-1.24**	**0.01**	**-2.39**	**0.01**
	11	10	light	2.25	-1.57	0.01	-3.44	0.02
	12	11	dark	2.50	-0.86	0.01	-3.53	0.02
	13	12	dark	2.75	-0.23	0.01	-3.14	0.01
	14	**13**	**light**	**3.00**	**-0.79**	**0.01**	**-2.02**	**0.01**
	15	14	light	3.20	-0.95	0.01	-3.02	0.00
	16	15	dark	3.40	-1.23	0.01	-3.56	0.01
	17	16	dark	3.60	-0.69	0.01	-3.54	0.02
	18	17	light	3.80	-0.57	0.01	-2.86	0.02
	19	**18**	**light**	**4.00**	**-0.27**	**0.01**	**-1.85**	**0.01**
	20	19	dark	4.20	-0.37	0.01	-3.00	0.01
	21	20	dark	4.40	-0.62	0.01	-3.55	0.01
	22	21	dark	4.60	-0.08	0.01	-3.26	0.02
	23	22	light	4.80	-0.92	0.01	-2.64	0.02
	24	**23**	**light**	**5.00**	**-0.68**	**0.01**	**-2.39**	**0.02**
	25	24	light/dark	5.25	-0.70	0.01	-3.08	0.02
	26	25	dark	5.50	-0.28	0.01	-3.33	0.01
	27	26	light	5.75	-0.66	0.02	-2.70	0.01
	28	**27**	**light**	**6.00**	**-0.91**	**0.01**	**-2.57**	**0.02**
	29	28	light	6.50	-0.62	0.01	-3.19	0.01
	30	29	dark	7.00	-1.03	0.01	-2.74	0.01
	31	30	light	7.50	-0.47	0.01	-3.20	0.01
	32	**31**	**light**	**8.00**	**-1.39**	**0.01**	**-2.27**	**0.02**
	33	32	dark	8.20	-1.37	0.01	-2.70	0.01
	34	33	dark	8.40	-1.20	0.01	-3.36	0.03
	35	34	dark	8.60	-0.90	0.00	-3.42	0.01
	36	35	light	8.0	-1.58	0.02	-2.49	0.02
	37	**36**	**light**	**9.00**	**-1.18**	**0.01**	**-2.16**	**0.01**
	38	37	dark	9.25	-1.53	0.01	-3.33	0.01
	39	38	dark	9.50	-1.30	0.01	-3.55	0.02
	40	39	dark	9.75	-1.39	0.01	-2.73	0.02
	41	**40**	**light**	**10.00**	**-1.68**	**0.01**	**-2.28**	**0.02**
	42	41	light	10.20	-1.73	0.01	-3.31	0.02
	43	42	light	10.40	-0.99	0.01	-3.57	0.01
	44	43	dark	10.60	-0.68	0.01	-3.36	0.01
	45	44	dark	10.80	-1.01	0.01	-2.83	0.01
	46	**45**	**light**	**11.00**	**-1.43**	**0.01**	**-2.41**	**0.01**
	47	46	light	11.20	-0.56	0.01	-2.70	0.01
	48	47	dark	11.40	-0.85	0.01	-3.45	0.02
	49	48	light/dark	11.60	-0.50	0.01	-3.42	0.01
	50	49	light	11.80	-0.86	0.01	-2.79	0.02
	51	**50**	**dark**	**12.00**	**-1.14**	**0.01**	**-2.09**	**0.01**
	52	51	dark	12.20	-1.25	0.01	-3.30	0.01
	53	52	dark	12.40	-1.27	0.01	-3.66	0.02

A4. Coral stable isotope data set ($\delta^{13}C$ and $\delta^{18}O$). Sample P4, Psalidha, Coral Site 1.3A, Coral Level 1, early Tortonian.

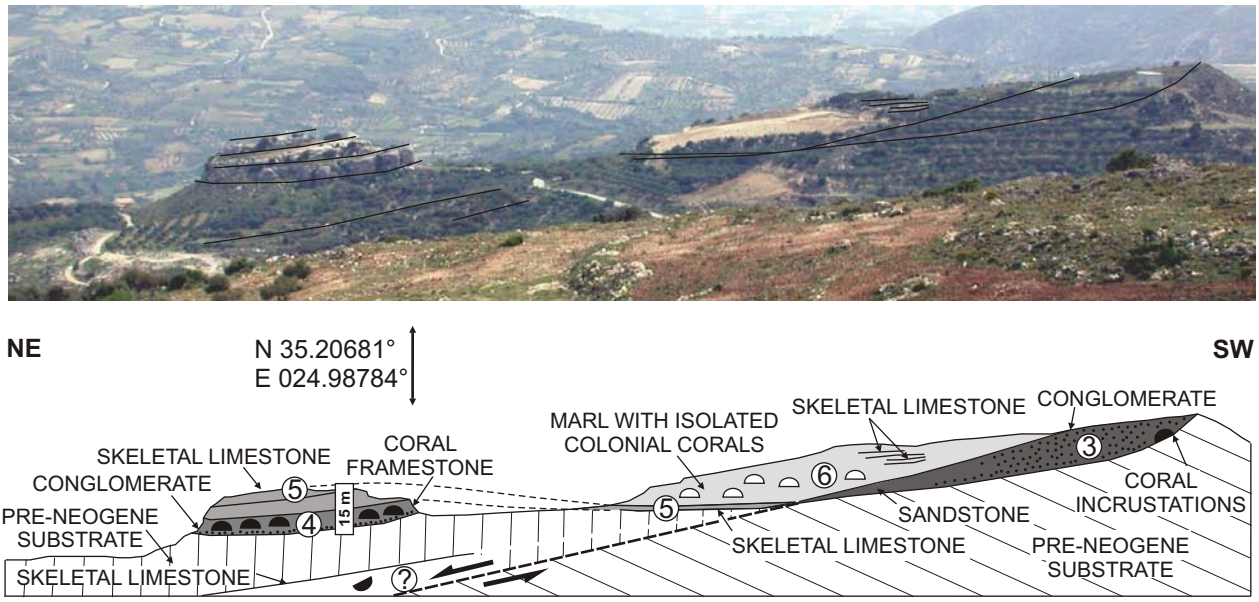

A5. Photo mosaic and line diagrame of transect Moni Gorgolaini-South at the western margin of Irakleion Basin showing stratal geometries and facies patterns of backstepping coastal sediment wedges. Numbers refer to depositional units in fig. 1.2 and are equivalent to coral levels in chapter 5. A wedge of skeletal limestone beneath the reef of Coral level 4 is not clearly assigned to a certain unit because of its stratigraphic isolation. Therefore it is not considered in fig.5.4. Probably, it represents the deepwater facies of Coral Level 3 or 4.

Unit (Fig. 2)	Geometry of sediment body	Lithofacies, depositional textures and bedding	Max. thickness (m)	Fossil content	Interpretation
3	wedge, pointing to the SW; covers pre-Neogene substratum.	brown sandstone; composed of coarse grained angular lithoclasts (pre-Neogene rocks) and quartz; to proximal coarsening into a grain supported, poorly sorted (pebbles to bolders) conglomerate with well rounded lithoclasts and *in situ* corals.	10	*Porites, Tarbellastrea* (*in situ*, massive growth forms), molluscs (e.g. pectinids, cardiids, *Conus*), *Clypeaster*	coastal sands; patch reef
4	sheet like reef body resting on a steep sided cape with plane surface build-up by pre-Neogene rocks from the Tripolitza Flysch	**coral reef: f**ramestone; matrix: bioclastic floatstone with isolated, well rounded lithoclasts (pebbles); at the basis: grain-supported, poorly sorted (pebbles to boulders) conglomerate with well rounded lithoclasts.	5,5	*Porites* (massive colonies, *in situ*), *Tarbellastrea* (ramose branching and massive colonies), bryozoans, molluscs, cidarid echinoids.	nearshore coral patch reef
5	low angle wedge pointing to the SW; drapes over Units 4.	bioclastic rudstone and skeletal floatstone with quartz sand and isolated well rounded lithoclasts (pebbles), massive beds	7.5	coralline red algae, celleporiform bryozoans, *Heterostegina*, pectinid bivalves	marine, shallow to-moderatly-shallow coastal clastics
6	wedge pointing to the SW; cover Unit 5	fossiliferous, bright grey, homogeneous marl with intercalated beds of skeletal limestone (floatstone) **limestone:** skeletals are mostly intact and embedded in a micritic matrix with no preference regarding to shape, size and orientation; massive beds;	>8	**marl:** coralline red algae, pectinids, cidarid echinoids, isolated *in situ* corals (massive *Porites* and *Tarbellastra* with ragged magins) **limestone:** *Heterostegina*, celleporiform bryozoans, coralline red algae, molluscs	marine; calm, moderately shallow environment
?	wedge; pointing to SW	skeletal limestone (rudstone and floatstone, homogeneous beds; intact and broken skeletals	8	coralline red algae, celleporiform bryozoans, echinoids, molluscs, coral fragments (*Porites*, *Tarbellastrea*)	marine, moderatley-deep, input of skeletals from a shallow source area

A6. Transect Moni Gorgolaini-South. Stratal geometries, facies, stratigraphic thickness and fossil content.

Coral Site	GPS	Coral Level	Setting	Preservation	Sample	Growth rate (mm/yr)	Mean growth rate (mm/yr)	Standard deviation (1σ)
1.1	N 35.12128° E 024.96757°	1	nearshore, biostrome, *in situ*	calcite calcite calcite	coral 1 coral 2 coral 3	1.85 3.77 2.07	2.56	1.05
1.2	N 35.08452° E 024.96611°	1	nearshore, biostrome, *in situ*	calcite calcite calcite calcite calcite calcite	coral 1 coral 1 coral 1 coral 1 coral 2 coral 2 coral 3 coral 4 coral 5 coral 6	1.50 2.10 2.50 1.73 1.67 2,29 2.63 2.00 2.10 2.14	2.07	0.36
1.3	N 35.08424° E 024.96094°	1	nearshore, biostrome, *in situ*	calcite aragonite aragonite aragonite aragonite aragonite aragonite aragonite aragonite	coral 1 coral 2 coral 2 coral 2 coral 2 coral 3 coral 4 coral 5 coral 6 coral 7 coral 8 P1 P4	5.20 4.40 3.37 3.50 3.88 4.55 4.19 5.20 4.56 5.13 4.08 4.40 4.77	4.30	0.58
2.1	N 35.20568° E 024.97339°	2	nearshore, patch reef, *in situ*	calcite calcite calcite	coral 1 coral 2 coral 2 coral 3	1.75 2.00 2.25 2.29	1.78	0.36
3.1	N 35.20568° E 024.97339°	3	nearshore, patch reef, *in situ*	calcite calcite calcite	coral 1 coral 2 coral 2 coral 3	1.75 2.00 2.25 2.29	2.07	0.25
3.2	N 35.20364° E 024.98722°	3	nearshore, patch reef, *in situ*	calcite calcite calcite calcite calcite	coral 1 coral 2 coral 3 coral 3 coral 3 coral 4 coral 5 coral 5 coral 5	1.83 2.87 2.38 2.53 3.00 2.60 1.96 1.40 1.75	2.26	0.55
4.1	N 35.20535° E 024.98190°	4	neashore, non-framework, *in situ*	all samples: calcite with aragonite relicts	coral 1 coral 1 coral 2	2.31 2.25 1.92	2.16	0.21

4.2	N 35.20270° E 025.01148°	4	offshore, fringing reef, reworked	calcite calcite calcite calcite	coral 1 coral 1 coral 1 coral 2 coral 2 coral 3 coral 3 coral 4	4.00 4.67 3.86 2.27 2.33 4.38 3.85 2.50	3.48	0.96
4.3	N 35.20681° E 024.98784°	4	nearshore, patch reef, *in situ*	calcite calcite calcite calcite	coral 1 coral 1 coral 2 coral 2 coral 3 coral 4	2.57 2.80 2.86 2.17 2.22 4.86	2.91	0.99
5.1	N 35.17075° E 025.00845°	5	offshore, non-framework, *in situ*	calcite calcite calcite calcite	coral 1 coral 1 coral 2 coral 3 coral 4	2.17 1.42 2.75 2.50 2.50	2.27	0.52
5.2	N 35.20260° E 024.97421°	5	nearshore, patch reef, *in situ*	calcite	coral 1 coral 1 coral 1 coral 1 coral 1 coral 1	6.07 3.75 4.00 3.60 5.00 4.50	4.49	0.93
5.3	no coordinates	5	offshore, fringing reef, reworked	calcite calcite	coral 1 coral 1 coral 1 coral 2	3.08 3.27 2.78 3.18	3.08	0.22
6.1	no coordinates	6	nearshore non-framework, i*n situ*	calcite calcite calcite calcite calcite calcite calcite	coral 1 coral 2 coral 2 coral 3 coral 4 coral 4 coral 5 coral 6 coral 7	1.58 1.60 1.55 1.75 2.10 2.25 1.40 1.52 2.82	1.84	0.46
7.1	N 35.20535° E 024.98190°	7	nearshore, debrite, reworked	aragonite	coral 1 coral 1 coral 1	4.38 4.00 3.75	4.04	0.32
7.2	N 35.20535° E 024.98190°	7	nearshore, debrite, reworked	aragonite aragonite	coral 1 coral 1 coral 2 coral 2 coral 2	1.82 2.03 3.86 4.23 4.37	4.15	0.26
7.3	N 35.20535° E 024.98190°	7	nearshore, reworked, debrite	aragonite aragonite	coral 1 coral 2	4.22 4.28	4.25	0.04

A7. Annual growth rates of corals in coral sites analysed in chapter 5.